DISRUPTION OF MICROORGANISMS DUE TO AGITATION IN SLURRIES OF FINE PARTICLES

A thesis submitted to the
UNIVERSITY OF CAPE TOWN
in fulfillment of the requirements
for the degree of
MASTER OF SCIENCE IN ENGINEERING

by
SARA JANE AMANDA PEARCE B. Sc. (Chem. Eng.) (U.C.T)

Department of Chemical Engineering
University of Cape Town
Rondebosch, 7700
South Africa

December 1993

ACKNOWLEDGEMENTS

The author would like to extend her thanks to the following people who assisted with the work presented in this thesis:

Dr Susan Harrison and Professor Geoffrey Hansford for their guidance, advice and support for the duration of this research. I wish to acknowledge Dr. Harrison's interest and direction during this research. The advice and assistance provided by Professor Hansford have been invaluable.

Mr Tony Barker and Mr Peter Dobias, as well as Mr Bill Randall, for assisting in the design and construction of the torque measurement system.

The secretarial staff, Mrs Linda Harrower, Mr Jeremy Tucker, Miss Shenaaz Moosa, Mr Granville De La Cruz, Mrs Maria Josias and other colleagues and staff for their general assistance whenever it was required.

My parents for the support and encouragement they have given me throughout my university studies.

Richard Fraser-Mackenzie who has given me endless encouragement and support and has always been there when needed.

I wish to acknowledge the financial support I have received from the FRD in the form of studentships.

SUMMARY

This dissertation presents the results of an investigation into the disruption of microorganisms when agitated in slurries of fine particles in a stirred tank.

The most widely used industrial process involving agitation of microorganisms in slurries of particles in stirred tanks is the biooxidation process. Mixed cultures of thiobacilli are used in stirred tank reactors for the biooxidation of sulphide minerals.

In addition to operating conditions, the efficiency of biotechnological processes is dependent on the growth and metabolism of the microorganisms. The microorganisms are sensitive to the hydrodynamic conditions generated in the processes. In response to adverse hydrodynamic conditions there may be changes in the growth rate of the microorganisms, the nutrient uptake rate, the product formation rate and morphology of the microorganisms. Under extreme conditions cell damage and disruption may ensue. The presence of particulates in bioprocesses, in the form of solid substrates or support systems for attached growth, further complicate the hydrodynamic conditions. The knowledge of the effect of particulates on microorganisms is an important priority.

Saccharomyces cerevisiae (Bakers' yeast) was chosen as a model microorganism with which to investigate cell disruption on agitation with particulates. Particulates investigated included silica, activated carbon, chromite and pyrite. The experimental apparatus included a 1 dm^3 stirred tank with agitation produced by an overhead motor equipped with a Rushton turbine. A torque measuring device was attached to the motor to allow measurement of torque and subsequent calculation of power consumption.

The disruption of yeast was measured in terms of the soluble protein release and the release of the wall-associated enzyme, invertase. The kinetics of cell disruption were modelled by first order kinetics.

In Chapter 4 the disruption of yeast was quantified at operating conditions of impeller speeds in the range 150 rpm to 1090 rpm at volume fractions of solid particles in the range 0.05 to 0.40. The effects of particle size (range of sizes studied: 114 μm to 1245 μm) and particle density (1600 kg m^{-3}, 2700 kg m^{-3} and 4500 kg m^{-3}) on the cell disruption were also investigated. In addition,

the effect of the concentration of the yeast suspensions in the range 20 kg m^{-3} to 130 kg m^{-3} on cell disruption was studied. Disruption of Bakers' yeast occurred upon addition of particulates to a stirred tank reactor. The disruption rate constant of yeast cells was found to be dependent on the concentration of solid particles, impeller speed and the size of the particles.

Analysis of the results included modelling of the dependency of the disruption rate constant on the concentration of solids, the impeller speed and the particle size. The dependency of the disruption rate constant on the impeller power input was established. The extent of disruption was found to be dependent on the energy input. The mixing intensity in the stirred tank altered with varying impeller speed. The nominal suspension of particulates at impeller speeds of less than 380 rpm (equivalent tip speed of 1.1 m s^{-1}) was reflected by the low extents of disruption. The extents of disruption at low speeds were attributed to partial damage due to the lack of suspension of the particulates.

The effects of pyrite and silica particles on the growth of thiobacilli were investigated in a very preliminary study. This work formed a minor part of the whole study. Due to the preliminary nature of the investigations it was not possible to draw firm conclusions.

TABLE OF CONTENTS

LIST OF TABLES

LIST OF FIGURES

NOMENCLATURE

Abbreviations:

ABTS	di-ammonium 2,2-azino-bis(3-ethylbenzothiazoline-6-sulfonate)
BCA	Bicinchoninic acid assay for soluble protein determination
CMC	carboxymethyl cellulose gum
DNA	deoxyribonucleic acid
Eh	redox-potential of solution relative to standard hydrogen electrode, mV
k_La	mass transfer coefficient
m/v	mass solids by total volume reactor
OTR	oxygen transfer rate
OUR	oxygen utilization rate
RNA	ribonucleic acid
T/D	tank to impeller diameter ratio
vvm	volume air flow/volume of suspension/minute
w/v	weight solids per total volume reactor

Symbols:

A	constant associated with calculation of average shear rate in stirred tank	
A_{sample}	absorbance of glucose sample at 620 nm	
$A_{standard}$	absorbance of glucose standard at 620 nm	
a_{H+}	activity of the hydrogen ion in redox reactions	
B	free bacterial population in solution	no. cells m^{-3}
B	impeller blade length	m
c	glucose concentration	mmol l^{-1} or mg/100 ml
c_v	volumetric solid concentration	
C	clearance of impeller above tank bottom	m
C_R	protein content of one cell	
C_E	enzyme content of one cell	
d_{50}	50% of the mass of particles in the distribution have diameters less than this value (median size in range)	μm
d_{y50}	median size of yeast cells	μm

d_{10}	10% of the mass of particles in the distribution have diameters less than this value	μm
d_{90}	90% of the mass of particles in the distribution have diameters less than this value	μm
d_{ave}	geometric mean diameter of the particles in the distribution ($\sqrt{d_{10} * d_{90}}$)	μm
d_{yave}	geometric mean diameter of yeast cells	μm
d_p	particle diameter	m
D	tank diameter	m
D	impeller diameter	m
D_i	impeller diameter	m
D_R	reactor diameter	m
D_T	turbine diameter	m
E	dissipation rate of turbulence	
E	energy input per unit volume	W s m^{-3}
E	variation of standard reduction potential with hydrogen ion activity in the Nernst equation	mV
E^o	standard reduction potential	mV
E_{ff}	efficiency of bead mill	W kg cells/s
E	enzyme released	units/g cell
E_m	maximum enzyme release	units/g cell
F	function of equilibrium constants of half-reactions involved in redox reaction	
g	acceleration due to gravity, 9.81 m^2 s^{-1}	
g_c	gravitational constant, 1 for SI units	
H	height of liquid in stirred tank	m
k	first order disruption rate constant	min^{-1}
k_E	first order rate constant for release of enzyme	min^{-1}
k_m	logistic rate constant	
k_{max}	maximum value of disruption rate constant	min^{-1}
k_{min}	minimum value of disruption rate constant	min^{-1}
K	function of impeller Reynolds' number and Froude number	
K	fluid consistency index in power law	
k_a	rate constant of bacterial attachment	
k_d	rate constant of bacterial detachment	
L	Kolmogorov length scale	m
M	torque	N m
n	flow behaviour index in power law fluid	
n	number of impellers	

Greek symbols:

ϵ_M	impeller power input	W kg^{-1}
ϕ	volume fraction of solids	
ϕ	volume fraction of cells	
ρ	liquid density	kg m^{-3}
ρ	fluid density	kg m^{-3}
ρ	density of particle	kg m^{-3}
ρ_l	liquid density	kg m^{-3}
ρ_f	fluid density	kg m^{-3}
ρ_p	density of particle	kg m^{-3}
ρ_s	solids density	kg m^{-3}
ρ_{sl}	slurry density	kg m^{-3}
μ_f	fluid viscosity	Pa s
μ	fluid viscosity	Pa s
μ	liquid viscosity	Pa s
μ_l	liquid viscosity	Pa s
μ_{sl}	slurry viscosity	Pa s
ϑ	surface of mineral covered with attached bacteria	
γ	average shear rate	s^{-1}
γ_{ave}	linear average shear rate	s^{-1}
ω	turbine angular velocity	s^{-1}
υ	kinematic viscosity of fluid (μ/ρ)	m s^{-2}

CHAPTER 1
INTRODUCTION

The processing of biological materials such as microorganisms, enzymes and antibodies are the fundamental spheres of biochemical engineering. These biological materials have been used by mankind for millennia. Fermentation for wine making and beer brewing was utilized by the ancient Greeks and Babylonians. Fermented foods such as cheese, bread and yoghurt have been part of mankind's diet for hundreds of years. In this era biochemical engineering processes are used for the production of a wide range of products, including antibiotics, steroids, vaccines and feedstocks. In addition the processes of brewing and wine fermentation are still universal. The use of microorganisms in waste water treatment and the bioremediation of soils is widespread.

The cultivation of microorganisms in stirred tank fermenters is a common industrial process. The microbial mass in fermenters may appear as films, flocs or unicellular culture. Films occur when the microorganisms become attached to the surface of a solid particle or a reactor part. The solid particles found in fermenters are either support particles for attached growth or substrate required for cell metabolism. Microbial flocs occur when the microorganisms aggregate to form clusters of cells. Unicellular cultures occur when the microorganisms remain separate and free in solution. The hydrodynamic conditions, produced by agitation, of the liquid media in stirred tanks are complicated by the presence of solid particles and flocs. Due to the sensitivity of microorganisms to adverse hydrodynamic forces, it is important to discern the consequence of the presence of solid particles in the fermenter. This dissertation presents the results of an investigation into the disruption of microorganisms when agitated in slurries of fine particles in a stirred tank.

One of the most widely used industrial processes involving growth of microorganisms on solid substrates is the biooxidation of sulphide minerals in stirred tank reactors. Mixed cultures of the bacteria thiobacilli are used for the biooxidation of sulphide minerals in the treatment of gold ores. It was recognised early in this study, after a literature survey, that there existed difficulties in enumerating thiobacilli, due to their size (1 μm) and their adhesion to particles, as well as difficulties in determining the release of intracellular products. On account of these complications, a model

microorganism was chosen to investigate the cell disruption due to agitation in slurries of particles.

Saccharomyces cerevisiae (Bakers' yeast) was chosen as the model microorganism because it is a large microorganism (5-10 μm) and therefore easy to observe microscopically. The release of soluble protein and wall-associated proteins from the disruption of yeast is readily evaluated. In addition to these obvious advantages, yeast was available in reproducible batches from Anchor Yeast, Cape Town. Silica particles were used as model particles in the bulk of the investigation instead of sulphide containing ore particles. The silica was readily available, furthermore it is an inert and uniform solid.

The aim of this research project was to provide a study of the disruption of microbial cells when agitated in slurries of particles in stirred tanks. Primarily, it was necessary to determine whether the presence of particulates during agitation caused cell disruption. If cell disruption occurred due to the presence of particulates, the effect of changes in the physical parameters of the particles, such as the particle size, particle density and concentration of particles, required investigation.

Chapter 2 provides a literature review of the biotechnological processes where solid particles are present. These include mechanical cell disruption by bead milling, the growth of aggregated and attached microorganisms, the biooxidation process and stirred tank bioreactors.

The experimental apparatus and methods are described in Chapter 3. This is followed by the results and discussion, Chapter 4, of the investigations into the disruption of Bakers' yeast in the presence of particulates during agitation in a stirred tank. The results are presented in terms of the disruption rate constant, determined from first order kinetics, and the extent of disruption. Chapter 5 includes analysis and further discussion of these results. The analysis includes studies of mathematical modelling of the effects of particle parameters on the first order disruption constant. Furthermore investigations into the effect of impeller power input on the yeast cell disruption is discussed. Finally, the degree of suspension of solids is investigated and discussed.

A very preliminary study on the effect of particulates on the metabolism of thiobacilli is presented in Chapter 6.

Chapter 7 concludes the dissertation by presenting the findings of the research project. Recommendations on operating conditions favourable for protein release by cell disruption are included. Finally areas of further work relating to the subject are suggested.

CHAPTER 2
LITERATURE REVIEW

2.1 INTRODUCTION

Despite the lack of rigorous study, it has long been recognized that microorganisms are sensitive to hydrodynamic forces. These forces may be generated in high pressure disruption devices, bead mills, bioreactors or flow through pipes and pumps (Engler and Robinson, 1980; Keshavarz Moore *et al.*, 1990; Toma *et al.*, 1991). The hydrodynamic conditions in the system may cause changes in cell growth rate, morphology, nutrient uptake and product formation. Cell damage or disruption may also occur (Logan and Dettmer, 1990; Smith *et al.*, 1990; Toma *et al.*, 1991).

Agitated systems which include non-microbial particulates are found in various biotechnological processes, such as high speed bead mills for intracellular product liberation, immobilized cell systems and solid substrate processes.

In bead mills, where the cell suspension is mixed at high rotational speeds in the presence of a high volume of glass beads, the microorganisms do not attach to the particulates. Agitation of the microorganisms with the beads results in the disruption of the cells and the consequent harvesting of the intracellular products (Kula and Schutte, 1987).

Animal cells are often cultivated on microcarriers in stirred tank systems. The cells attach to the microcarriers and grow as an attached system or biofilm. Cell disruption may occur by several mechanisms including collisions between the microcarriers and turbulence within the culture (Croughan *et al.*, 1987; Lakhotia and Papoutsakis, 1992).

Immobilized microbial suspensions are also in use, for example, in the mediation of biotransformations. In waste-water treatment the cells attach themselves to the solid particles, usually a substrate source, and form a biofilm. Removal of this biofilm is caused by fluid shear forces acting on the attached cells (Logan and Dettmer, 1990; Li and Ganczarczyk, 1990). In the biooxidation process, a solid substrate, such as mineral ore, is suspended in the leach liquid containing bacteria. A portion of the bacteria attach themselves to the solid particles and use the ore as an energy source for metabolism (Torma, 1977).

The following spheres of the literature concerning biochemical processes have been included in this review:

- the structure of the cell wall,
- cell disruption methods,
- attached and aggregated cell cultures,
- the biooxidation process,
- stirred tank fermenters and
- the analysis of cell viability.

2.2 CELL STRUCTURE

The cell is the basic unit of organisation in a living organism. There are two basic types of cell: prokaryotic and eukaryotic. A fundamental difference between the two types of cell is that eukaryotic cells possess membrane-bound organelles, including a membrane-bound nucleus whereas this is absent in prokaryotic cells (Atlas, 1984). Bacteria are prokaryotic cells whilst plants, animals, protozoa, algae, and fungi consist of eukaryotic cells (Atlas, 1984). The cytoplasmic membrane which surrounds the cell contents and forms the biological boundary is composed of phospholipid. Most membranes consist of two phospholipid layers, although the specific structures of the phospholipids vary from organism to organism.

Most prokaryotic cells and many eukaryotic cells are surrounded by a cell wall which provides structural strength protecting the cell against osmotic shock. The cytoplasmic membrane, situated within the cell wall, is unable to protect the cell from osmotic pressure. The cell wall is relatively permeable and allows the flow of small molecules through it (Atlas, 1984).

Bacterial cell walls consist of a rigid matrix composed of peptidoglycan which is a network of glycan chains cross-linked by short peptides. Bacteria are separated into two major groups, Gram-positive and Gram-negative. In Gram-positive bacteria the cell walls are relatively thick (approximately 15-50 nm) and contain 90% peptidoglycan. Gram-negative cells have a much thinner peptidoglycan layer in the region of 1.5-2 nm which is surrounded by an outer membrane or envelope (Atlas, 1984; Engler, 1985).

Fungal cell walls are very diverse and there are few for which detailed information is available, however the constituents of most fungi cell walls are known to be polysaccharides with some proteins and lipids (Engler, 1985; Kula and Schutte, 1987). Yeasts are an important subgroup of fungi. Hunter and Asenjo (1988) described a yeast cell wall as one of the most tough and rigid of all microbial cell walls. The cell wall is approximately 70 nm thick and is made of glucans, mannans and proteins. Glucans make up 50-60% of the wall and the remainder is a mannan-protein complex. Wall-linked and periplasmic glycoproteins are also present in the cell wall. Mannan and proteins are always found together in the outer layer of the cell wall. The structure of the yeast cell wall is shown in Figure 2.2.1. The cell wall is represented by a two layer structure. The inner layer consists of glucan units. The outer layer consists of mannan-protein, cross-linked by disulfide bonds and interchain hydrogen bonding. This layer allows small molecules to pass through but does not allow the passage of enzymes (Hunter and Asenjo, 1988). The enzymes in the outer layer form complexes with the mannans (Engler, 1985). The outer layer was found to be removed by autoclaving, treatment with thiols, alkaline extraction and proteolysis (Hunter and Asenjo, 1988). Andrews *et al.* (1990) investigated differential product release from yeast cells. They found that invertase was a wall-associated enzyme and could be extracted by wall disruption leaving intact spheroplasts. Follows *et al.* (1971) reported that invertase was found predominantly outside the cell membrane.

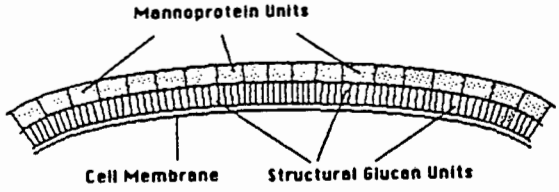

Figure 2.2.1 Yeast cell wall illustrating the mannoprotein (where wall associated enzymes are found) layer and the glucan layer, surrounding the cell membrane (Hunter and Asenjo, 1988)

Bacterial cells are usually less than 2 μm in size, whilst yeast cells are 5-10 μm. Animal cells do not have a cell wall surrounding their cell membrane and are much larger (in the region of 20 μm) than bacterial cells .

2.3 CELL DISRUPTION

Microorganisms are an important source of proteins with catalytic or enzymatic properties. These proteins are used for the commercial production of chemicals, antibiotics and enzymes. Some proteins used industrially are produced within the microorganisms and excreted into the environment. In addition, there are many intracellular proteins not excreted by the microorganisms, which have potential industrial application. The release of these intracellular proteins is the primary unit operation in their isolation from the remainder of the microorganisms. The optimal cell disruption technique exposes the cell walls to high shear forces but minimizes the exposure of the solubilised proteins to avoid protein denaturation and excessive fragmentation of the cell occurring. The resulting small cell fragments cause many difficulties in the subsequent separation processes (Chisti and Moo-Young, 1986, Harrison, 1991).

2.3.1 Cell disruption methods

Using non-mechanical methods, the intracellular proteins may be released by physical, chemical or enzymatic lysis. Physical methods of cell disruption include cavitation (ultrasonic or hydrodynamic), desiccation, osmotic shock and temperature extremes. Chemical disruption methods include the use of pH extremes, chaotropic agents, detergents, ethylenediaminetetraacetic acid (EDTA) and solvents (Harrison, 1991).

The three main enzymes used for enzymatic lysis of bacteria are glycosidases, acetylmuramyl-L-alanine amidases and endopeptidases (Harrison, 1991). Glycosidases achieve lysis by splitting the polysaccharide chains of the peptidoglycan backbone. An example of a glycosidase is lysozyme, which has been used successfully to solubilize the cell wall of yeast by Hunter and Asenjo (1988). The acetylmuramyl-L-alanine amidases break the polysaccharide-polypeptide junction. Endopeptidases split the polypeptide chains within the peptidoglycan. Enzymatic lysis is specific in its disintegration process and also occurs under mild operating conditions and thus causes minimum damage to the

product. It is not used widely due to the cost of the enzymes and their limited availability (Harrison, 1991).

The lysis of the cells by their own enzymes is termed autolysis. Autolysis is another means of cell disruption. It occurs when the enzymes within the microorganisms, which normally hydrolyse the polymeric structures of the cell wall to allow growth, are overproduced. This can be manipulated by culture conditions and genetic mutation (Harrison, 1991).

The two most common mechanical methods of cell disruption are bead milling and high pressure homogenization. The mechanism causing disruption in bead milling involves solid shear forces. According to Kula and Schutte (1987) differential velocity profiles are formed due to the movement of the grinding elements. High shear forces result from these velocity profiles and are responsible for the disruption of the cells. The frequency and momentum of collisions between the beads are also factors in the disintegration process. Cell disruption is achieved in high pressure homogenization by passing the cell suspension through a restricted orifice discharge valve under high pressure (Engler, 1985). The mechanisms involved in the disruption include turbulence, impingement, rate of pressure release, cavitation and liquid shear (Keshavarz Moore *et al.*, 1990; Harrison, 1990).

2.3.2 Bead mills

Cell disruption in bead mills is considered one of the most efficient industrial methods. A bead mill consists of a horizontally or vertically orientated chamber with a motor driven central shaft. Attached to the shaft, either centrically or eccentrically, are a number of agitator discs or pins. The grinding elements are either steel or ballotini glass beads. The optimal construction favours maximum transport of kinetic energy from the discs to the beads. The beads are retained within the chamber by use of sieve plates or by a coaxial ring slot which is integrated into the bearing housing. The mills are usually run continuously requiring an entry and exit port. A cooling jacket is required due to most of the energy input being dissipated as heat. In some designs the agitator shaft and discs are hollow to allow circulation of cooling liquid. The optimal diameter and length of the grinding chamber are in the ratio 1:2.5 up to 1:3.5. Commercially available mills vary from 50 cm^3 up to 0.1 m^3 in volume. Further scale up is

limited by the heat removal required (Chisti and Moo-Young, 1986 and Kula and Schutte, 1987).

The efficiency of bead milling is dependent on many variables including: agitator speed; feed rate of cell suspension; size and concentration of beads; bead density; concentration of cells; temperature; design of stirrer and the geometry of the grinding chamber (Kula and Schutte, 1987).

Agitator speed

The source of energy input to the grinding elements in the mill is the agitator (Kula and Schutte, 1987). The effect of agitator speed was investigated by several researchers, including Currie *et al.* (1972), Limon-Lason *et al.* (1979) and Marffy and Kula (1979). The working range of agitator speeds was reported as 5 to 15 m s^{-1} with an optimal range of 10 to 15 m s^{-1} reported by Limon-Lason *et al.* (1979). The working volumes of the mills ranged from 0.6 to 20 dm^3. The rate of cell disruption was found to increase with increasing tip speed (Currie *et al.*, 1972; Marffy and Kula, 1974; Mogren *et al.*, 1974; Limon-Lason *et al.*, 1979; Schutte *et al.*, 1983; Kula and Schutte, 1987).

An additional effect of increased agitator speed was an increase in temperature (Kula and Schutte, 1987).

Feed rate of cell suspension

Increased flowrate of cell suspension was observed to decrease the disruption of cells (Currie *et al.*, 1972; Marffy and Kula, 1974; Rehacek and Schaefer, 1977). In addition, an increase in power consumption was observed upon increasing the flowrate (Mogren *et al.*, 1974).

Design of the agitator and mixing behaviour of the mill

The agitator is responsible for transmitting kinetic energy from the beads to the cell suspension (i.e creating velocity profiles and shear forces) and therefore their design is very important. The agitators are also responsible for mixing the

suspension. The design of the mill and agitators should aim at minimizing axial back mixing, dead zones and channelling (Kula and Schutte, 1987).

A helical arrangement of circular discs has been used to accelerate the beads in both the centrifugal and centripetal directions (Currie *et al.*, 1972; Schutte *et al.*, 1983). The movement of beads in the opposite direction to flow of suspension prevents compaction.

Size of the glass beads

Lead free glass beads, less than 1.5 mm in diameter, were used for cell disintegration (Kula and Schutte, 1987). Smaller glass beads increased the frequency of collision of the beads due to their greater number. As the agitator speed was increased the energy content of the beads was increased. The size of the bead was limited by the tendency of very small beads (0.1 mm) to float. An advantage in larger beads was their higher kinetic energy due to their higher mass. This led to larger differences in the velocity profiles of the beads which subsequently increased the shear forces.

The optimal size of the bead was determined by the size of the microorganism. Experimental findings have defined that yeast cells are more efficiently disrupted using beads with diameters in the range 0.55 to 0.85 mm whilst bacterial disruption is favoured by using beads of less than 0.5 mm diameter. Furthermore, it has been found that larger beads are more efficient at solubilizing enzymes found in the periplasmic space than those found in the cytoplasm. In addition, abrasion of the glass beads did not exceed 3% in 100 hours of use (Kula *et al.*, 1983; Kula and Schutte, 1987; Marffy and Kula, 1974).

Beads of diameters ranging from 0.42 to 2.8 mm were used to disrupt *Saccharomyces cerevisiae* (Currie *et al.*, 1972; Limon-Lason *et al.*, 1979; Mogren *et al.*, 1974). The effect of bead size differed with yeast concentration. Small beads (0.5 to 1 mm) favoured disruption of a 30% yeast slurry. Their advantage was reduced at a concentration of 60% yeast owing to a large tendency to float at high yeast concentrations.

Concentration of beads

The concentration of the beads is usually expressed as volume percentage relative to the free volume of the grinding chamber (Kula and Schutte, 1987).

Using beads of 0.50-0.85 mm the highest release of soluble protein from bakers' yeast was achieved with a concentration of beads of 80% (Currie *et al.*, 1972; Schutte *et al.*, 1983). The temperature of the suspension and the power consumption of the system increased with increasing concentration of beads. These increases in temperature and power consumption were confirmed by Rehacek and Schaefer (1977). They found that with a mill only cooled by a cooling jacket it was not advisable to use a concentration greater than 85% as the temperature increased to 40 - 50 °C for higher concentrations.

Bead density

Kula and Schutte (1987) discussed the density of the grinding agents. Glass beads in the range 2500 to 2900 kg m^{-3} and ceramic beads, made of a mixture of zirconium oxide, in the range of 3800 kg m^{-3} and 5400 kg m^{-3} were used. These beads were investigated in a Dyno-Mill of 0.6 dm^3 volume for disintegration of the bacterium *Bacillus cereus*. Disintegration did not improve with increasing density, however the price of beads increased significantly. Beads of high density were found successful in disintegrating cells in highly viscous suspensions (Kula and Schutte, 1987). Glass beads are commonly used as their availability in a range of sizes is advantageous for disrupting different organisms.

Concentration of the cell suspension

The effect of cell concentration on the degree and rate of disintegration has been reported (Mogren *et al.*, 1974; Schutte *et al.*, 1983). Observations of disintegration of yeast cell dry weight concentrations of 4 to 20 percent showed no effect on the degree of disintegration (Mogren *et al.*, 1974). An optimum yeast cell concentration of 30 to 50 percent was reported by Schutte *et al.* (1983).

The decrease in the disruption rate constant observed by Limon-Lason *et al.* (1979) was attributed to the difficulty in mixing more concentrated suspensions, especially upon moving away from the impeller region. They also observed that at very low concentrations (and thus low viscosity) the yield of protein was very low as the energy from the impeller dissipated very rapidly, thereby diminishing the region of high shear.

Temperature

The microorganisms are temperature sensitive with protein denaturation occurring at elevated temperatures. During disruption the temperature of the cell suspension increases due to the conversion of kinetic energy from the agitator to heat energy. Thus a cooling system is necessary.

A decreased rate of disruption at increased temperatures in the range 40°C to 50°C was reported (Currie *et al.*, 1972; Limon-Lason *et al.*, 1979). Over a temperature range of 5°C to 20°C, the decrease in protein released was 2%. Marffy and Kula (1974) found that even at operating temperatures below 5°C enzymes were detectably inactivated in the disruption process. Apparently this denaturation is caused by shear or other mechanical effects, and is not temperature related.

Kinetics of cell disintegration

The rate of cell disruption can be represented by a first order process with respect to the number of whole cells. This rate equation can be expressed as:

$$-dN/dt = k\,N \qquad \text{Eqn. 2.3.1}$$

which can be integrated to

$$\ln N_o/N = k\,t \qquad \text{Eqn. 2.3.2}$$

where: t = time
N_o = number of cells at time = 0
N = number of cells at time = t

Similarly, this equation can be expressed in terms of soluble protein release from the cells as shown by Limon-Lason *et al.* (1979):

$$dR/dt = k (R_m - R) \qquad \text{Eqn. 2.3.3}$$

where: R = mass of protein released per unit mass of yeast cells
R_m = maximum measured protein release
k = first order rate constant

On integration between the limits of $t=0$ and $t=t$, the following is obtained:

$$\ln \{ R_m / (R_m - R) \} = k t \qquad \text{Eqn. 2.3.4}$$

(Currie *et al.*, 1972; Kula and Schutte, 1987; Schutte *et al.*, 1986)

The first order rate constant has been shown to be a function of several operating parameters including design and speed of impeller, bead loading, bead size, cell concentration and temperature.

A similar first order expression can be used for the solubilization of enzymes (Kula and Schutte, 1987; Marffy and Kula, 1974).

Energy consumption and efficiency of disruption

The major source of power consumption of the mill is in the drive to the impeller. Hence the consumption is dependent on agitator speed, concentration of beads, flowrate of cell suspension and agitator design (Engler, 1985).

The power consumption of the mill was dependent on agitator speed, concentration of beads and feed rate (Engler, 1985). Increased flowrates and increased agitator speed caused an increase in power consumption (Mogren *et al.*, 1974; Schutte *et al.*, 1986).

2.4 ATTACHED AND AGGREGATED CELL CULTURES

2.4.1 Introduction

The attachment of cells to solid surfaces is termed cell immobilization. Cell aggregation occurs when cells form a cell clump and these cell clumps are known as flocs (Black *et al.*, 1984).

The immobilization of cells to solid surfaces or particles is used to produce high cell concentrations within reactors. Passive immobilization occurs when films or flocs of cells form naturally on, around, or within solid surfaces or particles. Active immobilization of cells requires the production of cells which are mixed with chemical agents and are then immobilized by chemical or physical means (Black *et al.*, 1984).

Cell attachment and cell aggregation occur in several types of bioreactors. Bioreactors may be classified according to whether the microbial mass appears as films, flocs or unicellular cultures. Microbial films may be made up of either a single or a multiple layer of cells of one or several types of microorganisms. Microorganisms attach themselves in films to various surfaces including suspended particles, rising bubbles and fixed surfaces. Microbial attachment alters the fluid environment of a microorganism. Unattached bacteria must move with the bulk fluid whilst attached bacteria remain in one place. In this stationary position the bacteria are subjected to the advective flow of the passing fluid and may increase their nutrient uptake (Atkinson and Fowler, 1974).

Solid surfaces offer a beneficial environment for the microorganisms as nutrients concentrate at the surface. Coupled with this concentration of organic matter is the breakdown of large molecules in this region, resulting in forms more easily assimilable by heterotrophic organisms. The retardation of diffusion of metabolites and exo-enzymes from the interstices between the cell and the surface may be a further advantage to the adjacent cells. These interstices may also aid the production of optimum oxidation-reduction or other physico-chemical conditions, as well as providing protection from Brownian movement or other hydrodynamic forces. Adhesion may be increased by the microbial film by the formation of a slime film or the secretion of cement-like materials, some of which show considerable chemical resistance (Atkinson and Fowler, 1974; Logan and Dettmer, 1990).

2.4.2 Flocs and biomass support particles

Li and Ganczarczyk (1990) found that there was an absence in uniformity in the structure and distribution of microorganisms in activated sludge flocs. Water gaps of various sizes within the flocs were observed. They hypothesised that water was able to flow freely through the flocs via the water gaps. Models predicting advective flow through individual flocs have been presented by Logan and Hunt (1988). They reported that the floc permeability is a function of porosity. Logan and Dettmer (1990) observed that fluid shear and therefore fluid mixing intensity did not increase substrate uptake by bacteria suspended in a laminar shear field. However fluid flow past attached bacteria did increase bacterial uptake

The attachment of yeast cells to biomass support particles was investigated by Black *et al.* (1984). The concept of porous biomass support particles involved the provision of an environment free of high shear forces. Weak adhesion or flocculation was sufficient for yeast cells to be retained within the biomass support particle. Yeast cells did not form robust biofilms nor did attachment occur easily. However, particles of the type described by Atkinson *et al.* (1979) (wire mesh lattice particles) were successfully employed for attachment of yeast cells. Particles prepared from stainless steel wire mesh crushed into 6 mm diameter spheres of about 80% porosity were found to be satisfactory for growth of biomass within the lattice structure in an environment of low shear. Andrews and Przezdziecki (1986) discussed adsorptive particles such as activated carbon. The pores in activated carbon were too small for microorganisms but substrates and products were adsorbed. Provided that the adsorbent particle contained more substrate than in the fluid, the substrate desorbed from the particle and fed the bottom layer of the biofilm.

2.4.3 Biofilms

Biofilms are beneficial in certain waste-water treatments, natural stream purification and specific fermentation processes (Bryers and Characklis, 1982). The formation of biofilms has been attributed to the following mechanisms. Dissolved organic materials are adsorbed to the surface which is then followed by the transportation, via the turbulent flow stream, of the microorganisms to the surface. The cells then adhere to the solid surface and begin to produce biomass. The term biofilm accumulation refers to the net accumulation of

attached material due to cellular reproduction and production of extracellular polymers. Finally portions of biofilm peel away from the surface. Detachment is not identical to sloughing off of biofilm. Detachment is a continual process of biofilm removal whereas massive amounts of biofilm are removed during sloughing off (Bryers and Characklis, 1982).

The thickness of the biofilms on the solid surface are dependent on the type of fermenter in which they are grown. In summary, the thickest films are those made up of mixed populations of microorganisms such as those involved in waste-water treatment. These populations are usually zoogleal in character. An uncontrolled film of this nature may grow to a thickness of between 0.2 and 0.4 mm, whereas one subject to mechanical or hydrodynamic control may only grow to between 0.07 and 0.2 mm thick. In a continuous stirred tank fermenter, a pure culture may develop films of between 0.001 and 0.01 mm thickness (Atkinson and Fowler, 1974).

2.4.4 Fluidised reactors

Fluidised beds have become more versatile and their advantages as fermenters are numerous. Cell wash out will not occur unless the fluid velocity is high enough to approach plug flow. Fluidised beds provide isothermal conditions with high heat and mass transfer rates (Andrews and Przezdziecki, 1986).

Shieh (1980) studied a fluidised bed biofilm reactor kinetic model. The parameters which affected the performance of the fluidised bed biofilm reactor included size and density of the media particle and the biofilm thickness. The use of small particles led to excessive bed expansion which caused a decrease in biomass concentration. The biofilm is sloughed off by the upward movement of the particles during bed expansion. Heavier particles allowed for less bed expansion and thus more biomass concentration however the heavier particles increased the energy requirements.

Andrews and Przezdziecki (1986) emphasized the importance of the type of particle used in the fluidised bed bioreactor. The size and density of the particles and biofilm thickness were important variables and determined the height, diameter and thus volumetric productivity of the fermenter. The size of particles used depended on the type of biomass film attached to the particles. Cohesive rapidly growing aerobic films were not susceptible to wash-off caused by

increased shear stress at the particle surface. Large particles which are associated with high particle Reynolds' number and high shear stress at the surface were found to be suitable for this type of biofilm growth. Biofilms which were susceptible to wash-off required smaller particles with lower particle Reynolds' numbers (Andrews and Przezdziecki, 1986).

2.4.5 Cell damage in microcarrier cultures

Microcarrier cultures are attached animal cell cultures. Animal cells do not possess a cell wall and are larger in size than bacterial cells and are thus more susceptible to damage. Animal cells are being produced on a large scale for the production of biochemicals such as hormones, interferons, enzymes and antibodies. The growth of cells attached to microcarriers offers advantages including high growth surface to reactor volume ratios, simple separation of liquid media and cell, a readily assessed and controlled homogeneous environment and often allows for reduced media requirements (Croughan *et al.*, 1987).

Croughan *et al.* (1987) reported that the anchorage of animal cells may contribute to their vulnerability, as the attached cells could not rotate or translate freely in the fluid flow. Due to their immobility they were unable to reduce the total force and torque acting on the cells when the culture was exposed to excessive hydrodynamic forces. Moderate fluid shear led to increased cell permeability and increased cell secretion of proteins. Agitation was required to suspend the microcarriers and to allow for mass and heat transfer.

Croughan and Wang (1989) investigated the inhibition and enhancement of cells due to hydrodynamic conditions. They postulated that high agitation intensities inhibited cell growth through affecting the biosynthetic capability required for cell growth and the replication of the cells. The authors investigated whether cell death occurred before, after or during removal of cells from microcarriers and if cell death eventually led to lysis and disintegration. They used the release of DNA to assess cell death. It was observed that cells were removed from the microcarriers and inhibited from maximum growth upon increasing agitation speed. Lysis and disintegration of the cells also occurred at elevated agitation rates. Furthermore, fluid shear appeared to have an effect on cell shape. It was observed that cells exposed to fluid shear developed mechanical stiffness and were non-spherical. By staining of the cells with Trypan blue it was shown that

the attached cells were viable, whilst cells in suspension were non-viable. These results indicated that cells which detached were killed.

The role of eddies in the turbulent regime in a microcarrier culture has been reported in several studies (Cherry and Papoutsakis, 1988; Cherry and Kwon, 1990; Croughan *et al.*, 1987; Dunlop and Ye, 1990; Lakhotia and Papoutsakis, 1992). Eddies of a range of sizes exist in a turbulent liquid. The minimum size of the eddy is limited by the viscous dissipation regime. Below this minimum size the kinetic energy of the eddies is rapidly dissipated. Croughan *et al.* (1987) reported that the relationship between eddy size and particle size was important. An eddy that was larger than a microcarrier particle entrained the microcarrier particle. The microcarrier was then translated and rotated with the fluid and thus the net forces acting on it were minimised. However, if the eddy which formed was smaller or the same size as the microcarrier, the microcarrier was not entrained and the eddy forces acted upon the surface of the microcarrier. The small energy-containing eddies are called Kolmogorov eddies (Cherry and Papoutsakis, 1988; Cherry and Kwon, 1990; Croughan *et al.*, 1987; Lakhotia and Papoutsakis, 1992). Croughan *et al.* (1987) reported that when using microcarriers of 185 μm, detrimental effects on the cells were observed when eddies of 100 μm and below were present in the fluid.

Three potential cell damage mechanisms have been identified (Cherry and Papoutsakis, 1988; Lakhotia and Papoutsakis, 1992). Damage to microcarrier cells has been attributed to collisions between cell-covered microcarriers, collisions between the microcarriers and the impeller or other parts of the reactor and interaction with the turbulent Kolmogorov eddies. The energy of bead-bead collision was estimated by the kinetic energy of a bead moving at the same velocity as the eddies of bead size. Some of the collision energy was dissipated by the expulsion of fluid in the inter-bead space. Therefore, the spacing between beads and the input energy to the beads by fluid dynamics were critical to the amount of collision energy. Collisions between the beads and the impeller were observed to contain more collision energy.

Cherry and Papoutsakis (1988) found that growth rate of cells could not be correlated with impeller collision severity which led to the conclusion that collisions between beads and impeller were not the primary cause of cell damage. They proposed that there was a more complex mechanism than collisions or shear forces. The physical connection between two beads was termed bridging and there were several steps in the formation and destruction of bridges. The

first step was the collision of two beads covered with cells followed by a physical connection formed by the adhesion of cells to both beads. These bridge cells then continued to grow on both beads, strengthening the bridge and finally the beads were torn apart by environmental forces such as impeller collisions, bead collisions and eddy interactions. They observed that the rate of bridge formation was a function of the frequency of collisions, the number of cells attached to the beads and the efficiency of bridging during each collision. A bridge destruction rate was found to be dependent on bridge concentration and strength. As the bead clumps were larger they were subjected to more eddies and thus eddy interactions were thought to be important in the destruction of bridges. Due to their larger size, bead clumps contain more momentum and therefore collisions with the impeller were more damaging than for single beads. In conclusion they stated that they were unable to distinguish conclusively which damage mechanism was most effective.

The effect of media viscosity on cell injury was reported by Lakhotia and Papoutsakis (1992). Their results suggested that high viscosity media suppresses the cell death rate. The magnitude of the protective effect of viscosity seemed to depend on agitation intensity as less cells were damaged at higher agitation rates. This indicated that there was a cross-parametric effect of media viscosity and agitation rate.

Microcarrier concentration was investigated by Croughan *et al.* (1988) to determine whether there were positive or negative effects due to bead concentration and whether there were any other damage mechanisms involving bead-bead interactions besides collisions. They observed long lag phases of cell growth and decreased growth rates when microcarrier concentration was high. It was observed that at low agitation speeds increased microcarrier concentrations had no effect on cell growth but at high agitation speed increased microcarrier concentration was detrimental. They identified a mechanism between beads (not collision) that was due to viscous forces and pressure fluctuations generated by eddies throwing two beads together. For low microcarrier concentration it was observed that cell damage from direct eddy bead interaction was predominant but at higher microcarrier concentrations the bead-bead collisions and the mechanism described above became more crucial.

2.5 BIOXIDATION PROCESSES

2.5.1 Introduction

Biooxidation is an application of a solid substrate process requiring the growth of microorganisms in the presence of an agitated, aerated particulate ore slurry. Bacterial oxidation has existed for centuries. The practise of dump leaching was common in America, Peru, Canada, Africa and other countries, however the role of microorganisms went unnoticed. The earliest report of microbiological leaching was reported in 1922, however the microorganism was not identified. In 1947, the species *Thiobacillus ferrooxidans* was isolated from acid mine drainage of bituminous coal mines. *Thiobacillus ferrooxidans* can be found where an acidic environment is maintained in the presence of sulphide minerals. The bacteria convert the energy released from the oxidation of the inorganic substances to adenosine triphosphate (ATP) by oxidative phosphorylation. The following simplified equation illustrates the oxidation process.

$$MS + 2O_2 \xrightarrow{\text{microorganisms}} MSO_4$$

where M is a bivalent metal (Torma, 1977).

The bacteria may be autotrophic or heterotrophic. Autotrophs eg. *T. ferrooxidans* are able to grow on inorganic substances only and use carbon dioxide as their main source of carbon.

2.5.2 The microorganisms and metabolism

Thiobacillus ferrooxidans is a Gram-negative, rod-shaped (0.3 to 0.8 by 0.9 to 2 μm) bacterium which occurs singly or occasionally in pairs. The bacteria achieves movement by use of a single polar flagellum and pili have been observed on some species of thiobacilli, which are thought to aid in attachment of cells to solid surfaces. The cell wall consists of an external membrane which is 7.5 to 8 nm thick and a peptidoglycan layer which is about 3.5 nm thick. The cytoplasmic layer consists of two electron-dense lipid layers each about 3 nm thick, in between which is an electron-transparent layer of a similar size. Biooxidation is frequently attributed to *T. ferrooxidans* but involves a mixed culture. The fundamental difference between *T. ferrooxidans* and *Thiobacillus*

thiooxidans is the inability of *T. thiooxidans* to oxidise ferrous iron and insoluble metal sulphides (Torma, 1977). Barrett *et al.* (1993) include the microorganism *Leptospirillium ferrooxidans* in the list of common autotrophs involved in biooxidation. *Thiobacillus ferrooxidans*, *Thiobacillus thiooxidans* and *Leptospirillium ferrooxidans* are known collectively as thiobacilli and are all three responsible for biooxidation.

Thiobacilli oxidise various forms of iron (II) to iron (III). Pyrite (FeS_2) is one of the most important sources of iron (II). The following equations denote the oxidation reactions occurring (Pronk and Johnson, 1992).

$$2FeS_2 + 7.5O_2 + H_2O \text{ ---> } Fe_2(SO_4)_3 + H_2SO_4$$
$$FeS_2 + 7Fe_2(SO_4)_3 + 8H_2O \text{ ---> } 15FeSO_4 + 8H_2SO_4$$
$$4FeSO_4 + 2H_2SO_4 + O_2 \text{ ---> } 2Fe_2(SO_4)_3 + 2H_2O$$

It is necessary to apply new methods, such as biooxidation, to the recovery of low grade ores and to seek processes which are economic, energy efficient and pollution free. Gold occurs in minerals such as arsenopyrite, pyrite, pyrrhotite and chalcopyrite. The conventional methods of liberation are roasting and pressure leaching (Barrett *et al.*, 1993). Bacterial oxidation has been applied to dump and heap leaching of base metals. It is now finding approval in treatment of gold-containing refractory ores in both vat and heap processes (Lindstrom *et al.*, 1992). Biological leaching of pyrite and arsenopyrite ores involve many redox reactions and the formation of sulphuric acid and other toxic side products. The bacteria adapt to the arsenic in high arsenic content ores and oxidise the ores even though the soluble arsenic may exceed 10 mg ml^{-1} (Harris and Brierly, 1989).

2.5.3 Reactor design

Bacterial oxidation is carried out in four general environments: agitated reactors, prepared heaps, dumps, and *in-situ.* Reactor leaching apparatus vary from laboratory scale shake flasks to stirred tanks and pachuca reactors (Lindstrom *et al.*, 1992). Aeration, pH and agitation require operational control for optimum results and stirred tanks provide an opportunity for this control. Stirred tanks can be easily scaled up and can be operated in either batch or continuous mode. The following are the most important factors affecting biooxidation: quantity of sulphide material (includes suspension density and particle size distribution);

aeration; acidity; temperature; nutrient supply and culture growth (Barrett *et al.*, 1993). The concentration of solids, impeller speed and impeller design are critical for optimum operation. A major limitation on the concentration of solids in these reactors is the oxygen transfer rate.

2.5.4 The concentration of solids

Concentrations of solids used in the bioleaching process have been limited to 18 to 20% (mass/volume) solids (Hansford and Bailey, 1993). The proposed reasons for this limitation included oxygen and carbon dioxide availability, bacteria to solid ratio, mechanical stress to the bacteria and build up of toxic products. Oxygen transfer limitations as a function of the concentration of solids appeared to be dependent on the sulphide content of the ores. The oxygen transfer rate is the product of oxygen transfer coefficient and the difference between the saturated and actual dissolved oxygen concentrations. The oxygen utilization rate is the oxygen demand of the bacteria. A critical dissolved oxygen concentration of between 0.5 and 1 mg ml^{-1} has been documented by Barrett *et al.* (1993). If the oxygen level in the reactor falls below this level the bacteria revert to the lag phase.

The oxygen transfer rate (OTR) and oxygen utilization rate (OUR) converged at a concentration of solids of about 15% (m/v) for pyrite ores containing 28% sulphur, which indicated that above this concentration of solids the biooxidation rate was limited by oxygen availability (Hansford and Bailey, 1993). The OTR and OUR did not converge when ores with low sulphur content (1%) were used, which indicated that oxygen transfer was not the limiting factor at high concentrations of solids.

The concentration of solids should be maximised for economic reasons, however it has been found that concentrations of solids above 20% (m/v) cause a decrease in the bioleaching rate (Gormely and Branion, 1989). Torma *et al.* (1970) found that the bacterial extraction of zinc increased up to a concentration of solids of 16% (m/v) but decreased as the concentration of solids rose above 20% (m/v). This decrease was attributed to CO_2 limitations. In a CO_2 enriched process, levelling off of the bioleaching rate only occurred at a concentration of solids of about 24% (m/v) (Torma, 1972). Bioleach rates at different concentrations of solids were investigated in shake flasks by Pinches (1975). The bioleach rate increased with increasing concentration of solids, however the

rate of increase decreased between concentrations of solids of 10 and 20% (m/v).

The influence of the concentration of solids on the pyrite biooxidation of coal in an airlift reactor and a stirred tank was investigated by Beyer *et al.* (1986). The bacterial population consisted mainly of *T. ferrooxidans* and other acidophilic heterotrophic microorganisms. Sulphur-oxidising organisms were not identified separately. The stirred tank reactor was operated at an agitation rate of 400 rpm and an aeration rate of 1 vvm (volume of air flow/ volume of suspension/ minute). Concentrations of solids in the range 20% (m/v) to 50% (m/v) were used. Redox potential, pH and cell number were monitored. In the airlift reactor, pyrite oxidation was retarded at a concentration of solids of 10% (m/v) and completely inhibited at a concentration of solids of 20% (m/v). This was also observed in the stirred tank reactor and was accompanied by a decrease in the number of viable cells.

2.5.5 Shake flask growth of thiobacilli

Thiobacillus ferrooxidans was inhibited by the presence of particulates such as sulphur flowers, fluorapatite, glass beads and pyrite according to Dispirito *et al.* (1981). Experiments were carried out in shake flasks and soluble iron (Fe^{3+}) was monitored as a measure of oxidation rate. Concentrations of particles ranged from 0.1 to 5% (mass/volume). Pyrite and flowers of sulphur were found to be the most inhibitory substances. Pyrite concentrations of above 1% caused complete inhibition. Concentrations of 1 to 4% glass beads decreased the oxidation rates, whilst 5% glass beads caused complete inhibition. Furthermore it was found that the bacteria sorbed to the glass flasks and to the solid particles and could not be completely removed by rinsing. Experiments were also conducted on the effect of pH on the inhibition of thiobacilli and pyrite was found to be inhibitory at all pH values. Glass beads and fluorapatite at 1% concentration were no longer inhibitory at pH 2 and above.

Liu *et al.* (1988) confirmed this observation after completing a set of oxidation experiments carried out in shake flasks. Inert glass beads (particle diameter 65 μm) suspended in concentrations from 0.25 to 5% (by weight) were used in oxidation experiments. The authors found that oxidation decreased between concentrations of solids of 0.5 and 1% (m/v) and ceased at 5% (m/v) concentration. The conclusion from these experiments was that the gyratory

motion of the shaker was detrimental to cell growth when solid particles were present.

2.5.6 Attachment of thiobacilli

DiSpirito *et al.* (1983) discussed the sorption of *T. ferrooxidans* to solid particles. The biomass was monitored by the determination of protein concentration. The results showed that the bacteria sorbed rapidly to glass beads, fluorapatite and pyrite with over 25% of the bacteria being sorbed in the first fifteen minutes. Sorption was complete after one hour. It was also shown that at pH values of 1 and 2 sorption was higher for glass bead suspensions than at pH values of 3 and 4. The adsorption of *T. ferrooxidans* on solid particles was investigated by Myerson and Kline (1983). The population of the bacteria in solution and attached to the particles was determined by measurement of total protein concentrations. Two types of solids were used, namely crushed coal (containing sulphur) and controlled pore glass particles. Their results suggested that complete and irreversible sorption of bacteria to the coal occurred after 30 minutes. Irreversible adsorption to the porous glass particles was not complete after 30 minutes. The rapid initial rate observed by DiSpirito *et al.* (1983) is confirmed by Myerson and Kline (1983) who report that 90% of the bacteria adsorbed to the coal in the first 5 minutes.

The growth of free and attached *T. ferrooxidans* in ore suspensions is discussed by Espejo and Ruiz (1987). Shake flask experiments were carried out with pyrite, chalcopyrite and bornite ores. The total number of bacteria was determined by microscopic counting. Viable bacteria were counted by plating in a two-layer gel of pH 2.5. Attached cell numbers were estimated by plating of cell suspension after washing 3 times by centrifugation. Their experiments showed that the total activity associated with attached bacteria in a copper-containing ore suspension was between 1 and 10% of the total activity. They did not detect adsorption of large numbers of bacteria to glass as reported by other authors. This low level of attachment may be a function of the analytical method as it is well known that bacteria are not readily removed from the ore surface. In contrast to this work, Roy and Mishra (1981) reported 98 to 99% attachment of *T. ferroxidans* to pyrite ore in shake flask oxidation tests.

According to Barrett *et al.* (1993) a dynamic equilibrium between free and attached cells almost certainly exists. The adaptation of *T. ferrooxidans* to the

sulphide substrate plays an important role in the length of time taken for the cells to adhere to the surface of the substrate. Cells which were already adapted to the substrate established an equilibrium between attached and free cells after 1 to 5 hours, whereas non-adapted cells required 120 to 300 hours.

The process of attachment and detachment has been modelled using the Langmuir approach which considers the attachment to be an adsorption process (Barrett *et al.*, 1993). The symbol ϑ represented the surface of the mineral already covered with bacteria and thus $1-\vartheta$ was the available surface for attachment. If B was the bacterial population in the solution, the rate of attachment could be written as:

$$\text{Rate of attachment} = k_a B(1-\vartheta) \qquad \text{Eqn. 2.5.1}$$

where k_a is the rate constant of the attachment process. Similarly the rate of detachment could be written as:

$$\text{Rate of detachment} = k_d \vartheta \qquad \text{Eqn. 2.5.2}$$

where k_d is the rate constant for the detachment process. When the bacterial attachment and detachment have reached equilibrium these two expressions are equal, giving the following expression:

$$\vartheta = k_a B/(k_a B + k_d) \qquad \text{Eqn. 2.5.3}$$

It is understood that the establishment of the equilibrium stage illustrated above is sufficiently rapid for the attachment process not to be rate determining. However, a low bacterial population in the fluid may be rate determining (Barret *et al.*, 1993).

2.5.7 Mixing characteristics

The mixing characteristics are as important in bioleaching processes as in any other fermentation. The power consumption, energy flow and shear stresses of different types of impeller require consideration. In solid-liquid bioreactor slurries, the impeller must provide adequate flow patterns to ensure uniform solid suspension. In addition, there must be sufficient fluid shear to provide adequate oxygen transfer. The impeller should also be energy efficient. Two types of

impeller are used in bioleaching stirred tanks: the Rushton turbine and the axial flow impeller. The Rushton impeller has high energy consumption but produces high shear fields and is thus preferred for oxygen transfer. The axial flow is less energy consuming and produces less shear (Hackl *et al.*, 1989). Pilot tests (170 dm^3 tanks, capacity of 15-50 kg day^{-1}) performed by Hackl *et al.* (1989) showed that bioleach rates decreased when using a Rushton turbine at high rotational speeds (equivalent tip speed 5.3 m s^{-1}). The bioleach rate recovered when the tip speed was decreased to 3.3 m s^{-1}. Axial impellers employed at the same high rotational speed did not cause a decrease in biooxidation rate. These results indicate that the bacteria may be affected by excessive shear.

2.6 STIRRED TANK FERMENTERS

2.6.1 Introduction

Stirred tank fermenters are used for the cultivation of many types of microorganisms including bacteria, yeast and other fungi and single cell colonies such as animal and plant cells. Cultivated microorganisms and most desired products are sensitive to temperature, pH and shear stress. While the temperature and pH are controlled readily, shear stress is more complex. The rotating impeller causes the shear stress and thus the impeller design and speed are vitally important (Mersmann *et al.*, 1990). This section includes a review of impeller types and the flow produced by these impellers. Furthermore, the effects of impeller type and agitation intensity on the growth of microorganisms is reviewed. The methods of determining power consumption, energy dissipation and average shear rates are reviewed. Finally the kinetics of cell damage in stirred tanks are discussed.

2.6.2 Impeller types, velocity profiles and mixing

Impellers are classified into two general types: axial flow impellers with which the principal flow occurs parallel to the impeller shaft and radial flow impellers which

causes fluid flow to be discharged along the impeller radius in distinct patterns (Bates *et al.*, 1966; Oldshue, 1983).

Oldshue (1983) described seven basic impeller designs in common use: the flat blade turbine (Rushton turbine), the bar turbine, the anchor impeller, the three blade propeller (marine propeller), the four blade axial impeller, the three blade axial impeller and the double spiral impeller (Figure 2.6.1). The Rushton or flat blade turbine is a radial flow impeller and is generally used in situations which require high shear or turbulent mixing. The flat disk on which the blades are mounted is found to be of particular use in gas-liquid systems. Gas introduced via a sparger below the disk is forced by the disk along a path of maximum contact with the fluid instead of the gas travelling directly up between the blades. The bar turbine has blades consisting of square bars and produces the highest shear rates of basic impellers. The anchor impeller is of particular use in systems containing high viscosity fluids. The marine propeller produces a downward pumping action. These propellers have been found to be the best flow producers in an environment where there are large distances between the propeller and the boundaries of the system. The axial impellers are designed to perform in the same manner as the marine propeller but are more versatile due to their lighter weight, lower expense and ability to be taken apart for installation. The double spiral impeller is designed for very viscous materials and is constructed with an inner and outer spiral. The inner spiral produces downward flow and the outer produces upward flow.

Nienow (1992) compared new types of agitators with Rushton turbines for stirred bioreactors. The flat blade and disk of the Rushton turbine led to two low pressure trailing vortices at the rear of each of the six blades (Figure 2.6.2). A high power consumption was produced by this profile and thus a change in the shape of the blade was suggested. The flat blade was replaced by a blade with a parabolic cross section (Figure 2.6.3). This eliminated the trailing vortices and a lower power number was obtained for the system.

Number	Name	Description	
R-1	Flat blade	Vertical blades bolted to support disk	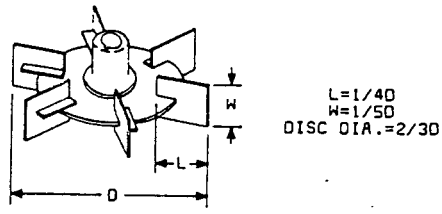
R-2	Bar turbine	Six blades bolted/welded to top and bottom of support disk	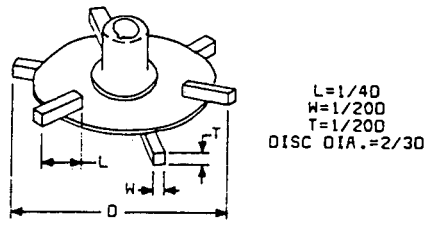
R-3	Anchor	Two blades with or without cross arm	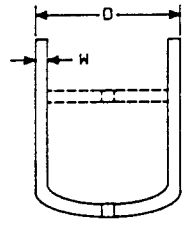
A-1	Propeller three blades	Constant pitch, skewed-back blades	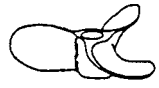 1.5 PITCH RATIO
A-2	Axial flow four blades	Constant angle at 45°	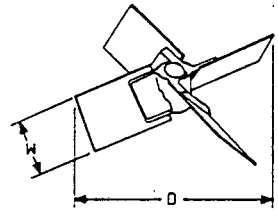
A-3	Axial flow three blades	Variable blade angle, near constant pitch	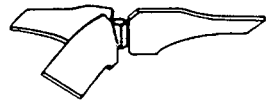 BLADE ANGLE AND WIDTH DECREASES HUB TO TIP
A-4	Double spiral	Two helical flights, pitch = $\frac{1}{2}D_0$	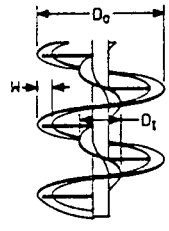

Figure 2.6.1 The seven basic impellers (Oldshue, 1983)

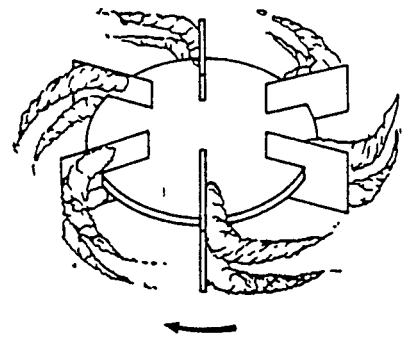

Figure 2.6.2 Flow patterns from flat blade turbine (Nienow, 1992)

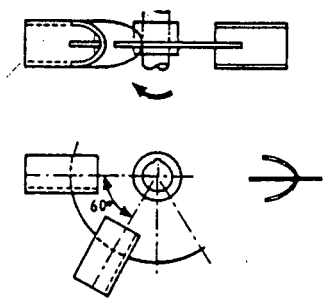

Figure 2.6.3 Parabolic shaped turbine (Nienow, 1992)

Davies (1972) discussed flat-bladed impellers. Most of the input energy was dissipated by the impeller and in the impeller stream. The impeller stream was a submerged jet which spread out as the liquid moved away from the tips of the blades. This resulted in an increase of jet width from the height of the blades to double this height at the walls of the vessel.

Flow patterns were investigated by Hooker *et al.* (1990) in a stirred tank by visually monitoring the movement of ceramic beads (simulating clumps of plant cells) in the vessel. They observed that the flow pattern followed that of a typical turbine-agitated, baffled vessel. The fluid was forced radially to the vessel wall where the flow separated into a portion which travelled up the wall and then returned to the impeller zone while the remainder travelled down along the sides

of the vessel to the bottom of the tank (Figure 2.6.4). In contrast, the flow patterns produced by an axial flow impeller is shown in Figure 2.6.5. The fluid is pumped directly down from the impeller to the bottom of the tank and then returns up the side of the tank and down parallel to the impeller shaft (Oldshue, 1983).

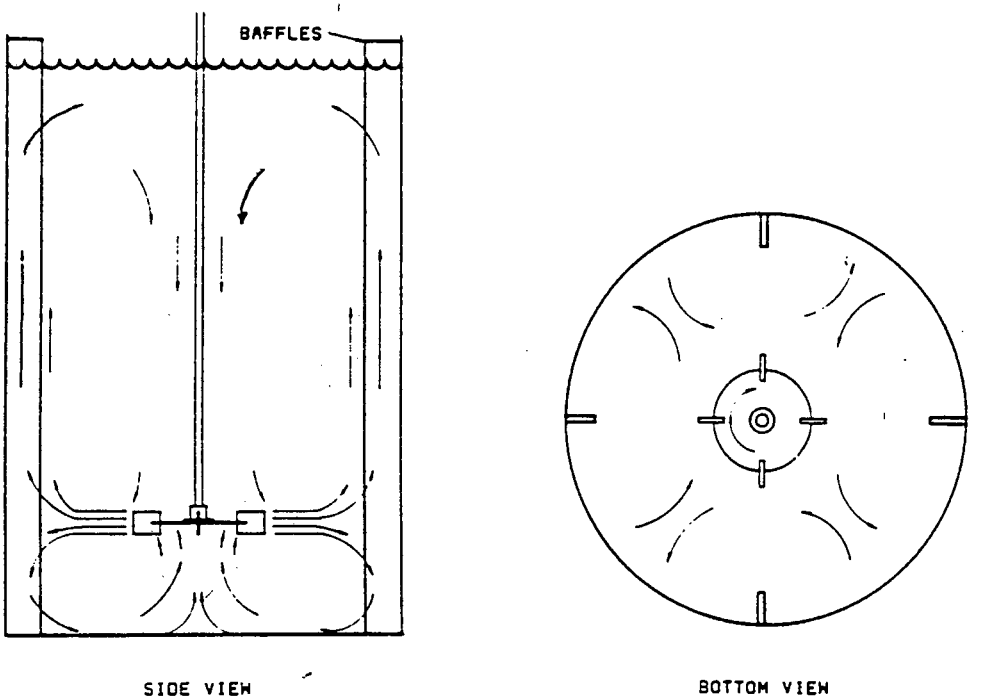

Figure 2.6.4 Baffled radial-flow turbine flow pattern (Oldshue, 1983)

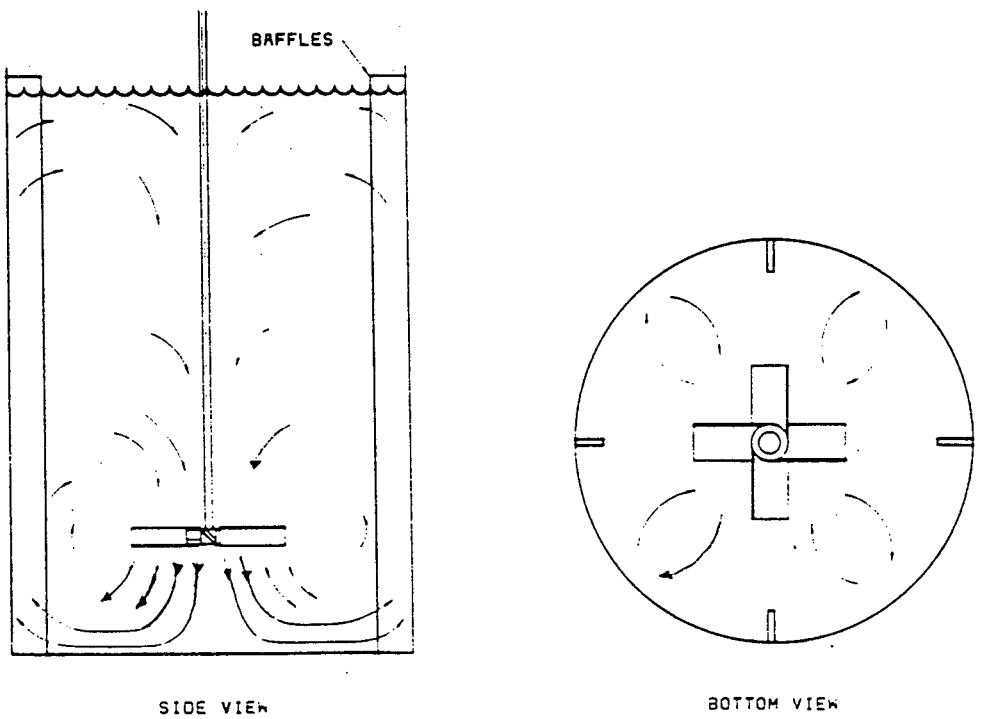

Figure 2.6.5 Flow pattern of baffled axial-flow impeller (Oldshue, 1983)

2.6.3 The effect of impeller type and agitation intensity on cell growth

The design of the impeller was discussed by Peillex *et al.* (1988) in their study of the influence of agitation on the growth of *Methanococcus thermolithotrophicus.* They investigated an impeller with straight blades as well as a Rushton impeller. They found that the Rushton impeller generated more radial movement of the liquid and increased the residence time of the gas in the liquid. It was also observed that the Rushton impeller increased the biomass production and concluded that the best results were obtained with the Rushton impeller. Gusek *et al.* (1991) used Rushton disk impellers with six flat rectangular blades and marine propellers. They also modified the Rushton impellers by coating the impeller blades with tight-fitting Tygon tubing. Using these modified impellers significantly improved cell biomass yield. Replacing these modified blades with marine propellers did not significantly improve biomass yield.

Hooker *et al.* (1990) investigated the effect of impeller design on the cultivation of plant cells. They used three types of impeller, the first was a regular flat-bladed impeller, the second was a large flat-bladed impeller and the third was a sail impeller with blades made of nylon cloth. They observed that the use of the large blades as opposed to the regular blades caused a decrease in shear with an increase in agitation. The velocity profile of a regular blade impeller was parabolic in shape, with the highest observed velocity occurring at the centerline of each blade. The resultant velocity decreased rapidly as the distance from the centerline increased and the rapid velocity change created a region of high shear. As the blade width or height increased (causing an increase in width to diameter ratio) the velocity profile became less parabolic and yielded a lower amount of shear due to a more gradual velocity gradient. The large blades however created more agitation due to their large surface area. The shear was again reduced using the sail impeller however the agitation was not sufficient and thus it was concluded that higher amounts of shear could be tolerated for the sake of more agitation.

The effect of the impeller speed is discussed in many studies. Gusek *et al.* (1991) investigated the effect of increased agitation on microbial growth and protease production by *Thermomonspora fusca*. Using a Tygon-coated Rushton impeller the impeller speed was increased from 300 to 500 rpm and it was found that the biomass and protease production were depressed by 85% thus indicating that the shear forces were excessive. Peillex *et al.* (1988) observed that using a straight blade impeller and increasing the speed from 320 to 660 rpm and then to

1015 rpm the *Methanococcus thermolithotrophicus* (a thermophilic methanogenic bacterium) biomass and CH_4 productivity increased with increasing impeller speed. Similar results were obtained when a Rushton impeller was used.

Smith *et al.* (1990) investigated the effect of agitation on the morphology and penicillin production of *Penicillium chrysogenum*. They found that the rate of decrease on the mean effective hyphal length was more rapid at speeds of 1000 rpm and 1200 rpm than at 800 rpm. In addition the rate of penicillin production was lower at the elevated speeds than at 800 rpm. Hooker *et al.* (1990) observed that tip velocity was a more reliable scale-up criteria than rotational rate as tip speed was dependent on the size of the impeller. The studies documented above indicated that the type of cell had an effect on the reaction to agitation rate. Reuss (1988) in his study of the influence of mechanical stress on the growth of *Rhizopus nigricans* stated that tip speed of the impeller was not suitable for a satisfactory comparison of different geometries and different systems. Energy or power dissipation rate was suggested as a better parameter for comparison of different systems.

2.6.4 Macromixing and Micromixing zones

Yu and Bajpai (1986) studied the role of mixing in stirred tanks and attempted to couple the mixing characteristics with microbial kinetics. The reactor volume was split into a highly turbulent impeller region (micromixer) and a non-impeller region (macromixer) through which the liquid continuously recirculated. Gusek *et al.* (1991) reported that the pseudoplastic non-Newtonian broth resulting in *Thermomonospora fusca* fermentation exhibited a nearly perfect mixing zone near the impeller, termed the micromixing region and a minimal mixing region in the remainder of the stirred tank, the macromixing zone. Intense agitation was required to activate the macromixing region in order to promote oxygen transfer, however this intense agitation could also damage the cells. Dunlop and Ye (1990) used the term micromixing to describe mixing on a molecular level and not as mentioned above. They reported on the decreasing size of microscale turbulence with increasing agitation rate and the role of energy containing Kolmogorov eddies in mass transfer.

2.6.5 Power consumption and energy dissipation

Agitation is required in bioreactors to effect adequate mass and heat transfer. The power required to operate the agitation apparatus, usually an impeller system, has been investigated fairly extensively. Fluids of Newtonian and non-Newtonian nature have been investigated due to the dependence of the power consumption on the rheological nature of the fluid.

Studies by Rushton *et al.* (1950), Metzner and Otto (1957), Calderbank and Moo-Young (1959) and Metzner *et al.* (1961) form the basis of most correlations used to predict power consumption in stirred tanks with various types of impeller. Rushton *et al.* (1950) documented correlations of the power number versus Reynolds' number for various types of impeller in various stirred tank configurations. Their work was mostly concerned with the dependence of power consumption on geometric, kinematic and fluid properties of the system. The rates and quality of mixing in stirred tanks were discussed by Metzner and Otto (1957). Their investigations dealt with non-Newtonian fluids. The flow in the impeller region was compared to the flow patterns around a sphere and around a flat plate. It was assumed that the flow in the impeller region could be characterised by an average shear rate which was linearly related to the impeller speed. The power number was correlated with the Reynolds' number for various non-Newtonian fluids (pseudoplastic fluids CMC and carbopol 934 and Bingham plastic fluid Attasol clay suspension) and the data was found to fall in the same range as that of Rushton *et al.* (1950). Due to this agreement, the authors concluded that their assumption of relating the average shear to the impeller speed was valid. The power number is expressed as:

$$N_P = P/(N^3 D^5 \rho) \qquad \text{Eqn. 2.6.1}$$

where P = power, W
N = impeller speed, rps
D = impeller diameter, m
ρ = fluid density, kg m^{-3}

The impeller Reynolds' number is expressed as:

$$N_{Rei} = \rho N D^2/\mu \qquad \text{Eqn. 2.6.2}$$

where μ = fluid viscosity, Pa s

Calderbank and Moo-Young (1959) adopted the same experimental procedure as Metzner and Otto (1957) and investigated the power required to operate various types and sizes of impellers in a baffled tank. Measurement of power was determined by torque measurement. A coaxial cylinder viscometer was used to determine the rheological behaviour of the fluids. The assumption that the average shear rate was linearly dependent on the impeller speed was used. The power number as a function of the Reynolds' number for various fluids was determined. It was found that for pseudoplastic and Bingham plastic fluids the average shear rate was independent of impeller size or tank diameter to impeller diameter ratio. However the average shear rate was influenced by the tank diameter to impeller diameter ratio for dilatant fluids.

Metzner *et al.* (1961) expanded the previous work on power consumption in agitation of non-Newtonian fluids. The effect on dilatant fluids observed by Calderbank and Moo-Young (1959) was confirmed. Experiments were carried out using different impeller types and configurations The measurement of power consumption in Newtonian fluids was extended to systems which included two turbines. The linear relationship between average shear rate and impeller speed was confirmed for flat-bladed turbines, fan turbines and marine impellers. Their results showed that the fan turbine produced better agitation for the same power consumption than the flat-bladed turbine at low agitation rates, however at high agitation rates this advantage was not predicted. In the non-Newtonian systems the turbines appeared to be more efficient than the marine propeller.

Hooker *et al.* (1990) monitored the power input required by each impeller. They calculated power consumption from torque measurements obtained using a laboratory torsiometer. The results were presented as the power number, N_P, as a function of the impeller Reynold's number, N_{Rei}. It was observed that at a constant Reynold's number the power consumption increased as the width of the impeller increased and then reached a constant value. This was attributed to the higher availability of surface area for agitation with wider impellers. The increase in agitation caused an increase in power consumption, however, after a critical value of impeller width has been exceeded, only the impeller region near the edges of each blade would be utilized in agitation. This caused the power consumption to become constant, regardless of increasing impeller width. Finally they found that the position of the impeller relative to an air-liquid interface had a negligible effect on power consumption until the interface itself was approached.

Whitton and Nienow (1993) investigated mass transfer in stirred tanks. The torque of the impeller was measured using calibrated strain gauges mounted on the agitator shaft below the lower gearbox bearing. The power consumption of the impeller was calculated by the following:

$$P = 2 \pi N M \qquad \text{Eqn. 2.6.3}$$

where P = power draw of impeller in W
N = impeller rotational speed in rps
M = torque in Nm

The impeller power input per unit mass of liquid was calculated from:

$$\epsilon_M = P/(\rho V_L) \qquad \text{Eqn. 2.6.4}$$

where ϵ_M = impeller power input in W kg^{-1}
ρ = liquid density in kg m^{-3}
V_L = liquid volume in m^3

The following correlation was used by Reuss (1988) for the growth activity of *Rhizopus nigricans* as a function of the energy input per unit volume in a stirred tank fermenter. The following represented the energy input:

$$E = P/(V_{susp}\, c_V) \qquad \text{Eqn. 2.6.5}$$

where E = energy input per unit volume, J m^{-3}
P = power input, W
V_{susp} = flowrate of suspension, m^3 s^{-1}
c_V = volumetric solid concentration

When the above was applied to bioreactor studies the volumetric concentration of the cells (*i.e.* the solids) was neglected. It was assumed that the energy was dissipated in the bulk fluid. The flowrate of the suspension was expressed as:

$$V_{susp} = V/t \qquad \text{Eqn. 2.6.6}$$

where V = reaction volume, m^3
t = average circulation time, s

The energy input per unit volume of bioreactors was then reported as:

$$E = P/(V/t) \qquad \text{Eqn. 2.6.7}$$

The average circulation time was measured using a magneto flow-follower technique. It was shown in this study that the ratio of power input to flowrate could be used for a satisfactory correlation of experimental data on mechanical damage to microorganisms.

2.6.6 Average and local shear rate considerations

The values of the average and local shear rates in a stirred tank are significantly different (Poncelet and Neufield, 1989). The average shear rate in a stirred tank has been defined as (Metzner and Otto, 1957):

$$\gamma_{ave} = A\,N \qquad \text{Eqn. 2.6.8}$$

where: γ_{ave} = average shear rate, s^{-1}
A = constant, usually expressed as 10 or 13
N = impeller speed, rps

Poncelet and Neufield (1989) investigated shear effects in stirred tanks using nylon microcapsules to simulate microorganisms. Due to the high velocity fluctuations present in a stirred tank, a great range in local shear rate is expected. Hence it is useful to try to quantify the local shear stress. It was also likely that the shear stress causing any cell damage in the reactor was of the magnitude of a local shear stress in the vicinity of the impeller. The average shear stress was expected to be a conservative estimate of the shear stress causing disruption. The system used was a flat bottomed tank with four baffles, stirred by a six-blade turbine. The shear rate was not constant in this type of reactor and thus as a simple approximation the linear average shear rate was computed by:

$$\gamma = 2\,\omega\,D_T/(D_R - D_T) \qquad \text{Eqn. 2.6.9}$$

where: γ = linear average shear rate, s^{-1}
ω = turbine angular velocity, s^{-1}
D_T = turbine diameter, m
D_R = reactor diameter, m

Van Suijdam and Metz (1981) reported that the region of highest shear in tanks agitated by a turbine impeller was situated directly behind the stirrer blades.

2.6.7 Kinetics of cell damage

Cell damage kinetics have been found to be relevant not only in bead milling but also in stirred bioreactors.

The modelling of cell damage due to shear using nylon membrane microcapsules was investigated by Poncelet and Neufeld (1989). Nylon membrane microcapsules were used to simulate the biological systems because the physical structure of the microcapsule was well defined and controllable. The membrane skin simulated the membrane around many biological cells. Damage to a microcapsule membrane resulted in release of contents which were well defined and quantifiable, while damage to mammalian, plant or microbial cells was more difficult to define given the irregular shape of cells and the complex nature of their contents. First and second order expressions were proposed for the breakage mechanism. The second order expression was rejected because its rate constant varied with initial microcapsule concentration whilst the first order rate constant remained relatively constant. The influence of temperature, capsule size, turbine diameter and angular velocity on the kinetic constant of breakage were investigated. The kinetic constant was found to be a function of shear rate, blade velocity and particle velocity. The linearity between the kinetic constant and the shear rate indicated that the shear effect was the primary process in microcapsule breakage.

Reuss (1988) reported that the disruption of *Tetrahymena pyriformis* was first order with respect to time when subjected to mechanical agitation. Abu-Reesh and Kargi (1991) investigated the kinetics of hybridoma cell damage in a stirred tank reactor by monitoring viable cell concentration. Normalized viable cell concentration versus time showed a linear correlation, indicating that cell damage was a first order process. They observed that the "death rate constant" increased with increasing agitation rate.

2.7 EFFECTS OF ORGANISM TYPE AND GROWTH CONDITIONS ON CELL DISRUPTION

In addition to the operational parameters of cell disruption, there is also an effect due to the type of organism and the culture growth conditions at the time of disruption.

Engler (1985) cited the work of Rehacek *et al.* (1969) in which it was found that *Escherichia coli* was more difficult to disrupt than *Aspergillus niger* or a *Basidiomyces* species. In further work done by Rehacek and Schaefer (1977) they reported that *Candida utilis* was more difficult to disrupt than baker's or brewer's yeast. This was confirmed by the work of Mogren *et al.* (1974). Schutte *et al.* (1983) observed that several different bacteria were more difficult to disrupt than yeast and that this could be attributed to the smaller size of the bacteria.

Growth conditions were found to affect the disruption of microorganisms by Engler and Robinson (1981). They found that the growth of yeasts (*C.utilis* particularly) at high growth rates produced weaker cells. They did not study the effect of growth rate of bacteria but expected similar results since cells with a high growth rate did not produce material for reinforcing the cell wall structure. In addition, a greater percent of cells were in the separation stage and therefore could have been more susceptible to disruption.

Cumming *et al.* (1985) investigated the effect of the growth phase of *Bacillus amyloliquefaciens* on the rate of protein release by bead milling, ultrasonication and autolysis. They found that protein release was higher for logarithmic phase cells than for stationary phase cells. This could have been due to either the change in size of cells as they grew from the logarithmic to the stationary stage or a change in the strength of the cell wall. They concluded that if log phase cells instead of stationary phase cells were used disruption times would be shorter as the disruption rate was quicker. This trend was confirmed by Harrison *et al.* (1991) on studying the disruption of the Gram-negative bacterium *Alcaligenes eutrophus* by high pressure homogenization.

2.8 ANALYSIS OF CELL DAMAGE

In this work , cell disruption is defined as the breakage of the cell envelope with concomitant release of intracellular products. Analysis of cell disruption is achieved by direct and indirect measurement (Engler, 1985). Direct measurement includes cell counting by microscopy or an electronic particle counter. Indirect measurement involves the measurement of a consequence of cell envelope breakage eg. the amount of a particular cell component released during cell disruption.

2.8.1 Direct measurement

Direct counting of whole cells can be done by light microscopy or using an electronic particle counter before and after subjection to disrupting conditions. For light microscopy, a fixed volume counting chamber is utilized. Particle size analysis can be achieved using micrographs obtained from a scanning electron microscope. These methods of cell counting may be hindered subsequent to disruption by the presence of cell fragments and intracellular material such as DNA and other polymeric constituents. The cells may be stained to assist in distinguishing damaged from whole cells eg. damaged Gram-positive bacteria frequently stain as if they were Gram-negative. Yeast cells appear purple if undamaged and light red if damaged. A disadvantage of this technique is its tedious and time-consuming nature (Engler, 1985; Harrison, 1990).

The electronic particle counter has been used successfully for determining the extent of disruption of yeast cells but is not sensitive enough to measure the disruption of bacteria (Engler, 1985).

2.8.2 Indirect measurement

The indirect measurement of the fraction of damaged cells may be based on the amount of an intracellular constituent found in the extracellular environment before and after disruption. The measurement of soluble protein released, intracellular enzymes released, nitrogen released and DNA or RNA released are examples of methods of indirect measurement. Alternatively the release of intracellular compounds may be estimated by the change in absorbance of the

cell suspension at characteristic wavelengths and changes in conductivity (Engler, 1985; Harrison, 1990).

2.8.3 Soluble protein analysis

The amount of soluble protein released from the cell suspension may be determined using the Lowry, BCA or Biorad protein assays. Choice of assay depends on the interfering substances present (Harrison, 1990; Peterson, 1979). Denaturation of a protein, occurs at temperatures exceeding 35°C. This reduces protein solubility irreversibly thus interfering with the assay. Hence the maintenance of low temperature and neutral pH is very important when monitoring cell disruption by protein release (Engler, 1985; Harrison, 1990).

The Lowry protein assay is based on the reduction of the phosphomolybdic-tungstic mixed acid, the active ingredient of the Folin phenol reagent of Folin and Ciocalteu, by a protein-copper complex. This complex is formed when the protein reacts with the cupric ion. Electrons can then be transferred between the phosphomolybdate-phosphotungstate and the protein to form one or more reduced species with a characteristic blue colour that can be determined spectrophotometrically. The principal amino acids causing the reduction of phosphomolybdate-phosphotungstate are tyrosine and tryptophan. Cysteine, cystine, histidine and peptide bonds also contribute to the reduction. Many substances cause interference in the above reactions. These are detailed by Peterson (1979).

The Biorad assay is based on the colour change caused by the reduction of the dye, Coomasie Brilliant Blue G-250, in the presence of protein. The absorbance maximum of the dye shifts from 465 to 595 nm when binding to protein occurs. The standard assay procedure allows protein determination in the range 100-1400 μg ml^{-1}. A microassay procedure allows the determination of protein concentrations less than 25 μg ml^{-1}.

The BCA assay is based on the reaction of proteins with alkaline copper II to produce copper I. The Bicinchoninic Acid reacts with copper I to give an intense purple colour at 562 nm. The BCA assay produces a stable environment for quantitative protein in the presence of buffer salts, detergents and chaotrophic agents (Harrison, 1990; Smith *et al.*, 1985).

2.8.4 Release of nucleic acids (DNA or RNA)

The quantity of nucleic acids released may be determined by the measurement of phosphate content, the amount of purine and pyrimidine bases or the amount of pentose sugars. Using a measurement method based on the determination of carbohydrates a characteristic DNA release profile is found on cell rupture. The determination of DNA concentration can be carried out using a dinitrophenyl assay. This assay is based on the reaction between deoxyribose and diphenolamine to give a blue coloured compound, which is determined spectrophotometrically. The concentration of RNA can be determined by the Orcinol assay which provides a standard assay for pentose sugars in which the sugar moieties are detected by the production of a green chromagen on reaction of aldopentoses with acidified orcinol (Harrison, 1990).

2.8.5 Absorbance at characteristic wavelengths

The concentration of nucleic acids and proteins can be determined by the measurement of absorbance at 260 and 280 nm respectively. However the readings may be affected by the presence of other biochemicals. There is a further source of inaccuracy known as the hyperchromic effect. The hyperchromic effect is caused by the difference in the absorbance of double and single stranded nucleic acids. The chains must be equally unraveled for accurate comparison. This is very difficult to achieve unless the samples have an identical history (Harrison, 1990).

2.8.6 Conductivity measurements of suspending medium

Lovitt *et al.* (1986) proposed a method of rapidly estimating the microbial content of an immobilized cell suspension using the low frequency conductivity of free living cell suspensions.

The following equation is given which defines the conductivity of a suspension of non-conducting cells:

$$\phi = x (r_0 - r) / (r + x r_0) \qquad \text{Eqn. 2.8.1}$$

where: x = shape factor

r = conductivity of suspension
r_o = conductivity of suspending medium
ϕ = volume fraction

For spherical particles, x has a value of 2. Hence the equation reduces to:

$$r/r_o = (1 - \phi) / (1 + \phi/x) \qquad \text{Eqn. 2.8.2}$$

For non-spherical particles the Bruggemann approximation is cited:

$$r/r_o = (1 - \phi)^{3/2} \qquad \text{Eqn. 2.8.3}$$

(Lovitt *et al.*, 1986).

2.8.7 Radiofrequency dielectric permittivity of microbial suspensions

Harris *et al.* (1987) recognised that the radiofrequency dielectric permittivity of microbial cell suspensions is a direct and monotonic function of the volume fraction. This resulted in the development of a probe to measure the radiofrequency dielectric permittivity of microbial suspensions to provide a rapid estimation of the volume fraction specifically enclosed within the cytoplasmic membrane of the cells. Their method utilizes the fact that radiofrequency dielectric properties of microbial cell suspensions are a direct and monotonic function of the volume fraction. The apparatus consists of four metal electrodes. The two outer electrodes produce the electric field whilst the inner electrodes measure the charge separation that the field induces.

By changing the electric field direction, the polarisation of the cell membrane is changed. The capacitance decreases as the frequency of changing polarisation increases, due to the time taken for the field transported ions to reach the cell membrane and cause polarisation. Larger cells have lower critical frequencies than smaller cells provided they are suspended in mediums with the same conductance. The slope of the capacitance versus frequency curve is dependent on cell size. Microorganism suspensions are dielectric dispersions because of their frequency dependent passive electrical properties. Radiofrequency permittivity of suspensions of yeast cells was found to be a linear and monotonic function of the biomass present and therefore the measurement of RF permittivity

is a possible means of assessing the fraction of intact cells present (Harrison, 1990).

2.8.8 Enzyme release

The measurement of the enzyme content in the extracellular environment is an indication of the degree of disruption. If there are only periplasmic enzymes present then only the outer cell membrane (of bacteria) has been ruptured. Yeast cells contain wall-associated enzymes which are released on solubilisation of the outer mannoprotein layer of the cell wall (Hunter and Asenjo, 1988). If cytoplasmic enzymes are also present then the cell wall and inner cell membrane have also been broken. The presence of mitochondrial enzymes in the extracellular environment means that the mitochondria has been ruptured indicative of extreme disruption (Harrison, 1990; Kula and Schutte, 1987).

CHAPTER 3
EXPERIMENTAL MATERIALS AND METHODS

3.1 EXPERIMENTAL APPARATUS

3.1.1 Reactors

The majority of experiments were conducted in a fully baffled stirred tank of 1 dm^3 capacity with a working volume of 0.75 dm^3. A variable speed overhead motor fitted with a torque meter and a Rushton turbine was used. The dimensions of the tank and impeller are as follows:

liquid height (H)	=	0.100 m
height of impeller above tank bottom (H/3)	=	0.030 m
diameter of tank (D)	=	0.104 m
impeller diameter ($D/2 = D_i$)	=	0.054 m
impeller disk diameter ($2D_i/3$)	=	0.036 m
blade width ($D_i/5$)	=	0.011 m
blade length ($D_i/4$)	=	0.014 m

Four fully-baffled stirred tanks of 4 dm^3 capacity were used in the testwork on thiobacilli. Two types of impeller were used, the standard Rushton turbine and the axial impeller. Variable speed overhead motors were used.

3.1.2 Torque measurement

The power consumption of the system was calculated from torque measurements. A device was designed to measure the torque exerted on the impeller by the fluid. This was quantified by measuring the axial torsion of the rotating shaft with a strain gauge-like meter. The motor was mounted to enable it to turn freely and a weight on a cord was attached via a pulley system to the motor. The weight rested on an electronic mass balance when the motor was turned off. Upon switching the motor on and as it rotated, the weight was lifted from the electronic mass balance. The difference in mass between the resting position and the position of the motor during operation was used to calculate the force exerted on the impeller by the fluid. The force was used to determine the torque and thus power consumption was calculated.

Force	=	mass * g	Eqn. 3.1.1
Torque	=	force * distance from fulcrum	Eqn. 3.1.2
Power	=	Torque * 2* π * N	Eqn. 3.1.3

where g = acceleration due to gravity, 9.81 m s^{-2}
N = speed in rps

The device was tested by measurement of the torque using Newtonian fluids of known viscosities. Plots of power number as a function of impeller Reynolds' number were compared with those found in literature. These results can be found in Appendix 6. Measurement of high viscosity fluids (60% sucrose, μ = 0.058 Pa s, and 99.5% glycerol, μ = 1.67 Pa s) produced data which fitted the literature curve well, however low viscosity fluid (distilled water, μ = 0.001 Pa s, 56% glycerol, μ = 0.0084 Pa s, 30% sucrose, μ = 0.0032 Pa s) data showed some deviation from the literature curve. Hence it is postulated that the low residual friction within the system overshadows the torque exerted by the low viscosity fluids.

3.1.3 Microorganisms

Saccharomyces cerevisiae (Bakers' yeast) was used as a model microorganism in the central phase of the research. A very preliminary set of experiments were conducted using mixed thiobacilli to assess changes in metabolic rate.

3.1.4 Solid particle type

The solid particles used in the project were the following:

i) Silica particles of density 2700 kg m^{-3} with a size range of particles of 25 μm to 1800 μm.
Crushed silica particles with a particle size range of 235 μm to 569 μm.

ii) Activated carbon of density 1600 kg m^{-3} and a particle size range of 231 μm to 541 μm.

iii) Chromite particles of density 4500 kg m^{-3} and a particle size range of 229 μm to 533 μm

iv) Pyrite ore of density 4800 kg m^{-3} and a particle size range of 11 μm to 152 μm.

The silica, activated carbon and chromite particles were acid washed, rinsed and then sieved into size fractions. The particles were dried prior to experimentation. The pyrite particles were sieved into size fractions and dried. High sulphur (48% S) containing pyrite was obtained from Prieska, Northern Cape, South Africa and low sulphur (1.5% S) containing pyrite was obtained from St. Helena mine, Orange Free State, South Africa.

3.2 EXPERIMENTAL METHOD

The yeast was obtained from Anchor Yeast, Epping, Cape Town as yeast cream harvested post vacuum filtration. The supernatant was removed by centrifugation, in a Beckman TJ-6 centrifuge, at 5700 rpm and 4470 g for 15 minutes. The cells were washed and resuspended in phosphate buffered saline (Appendix 2) to a concentration of 50-60 kg m^{-3} (dry weight biomass) before experimentation. This resuspension was necessary to ensure no interference in the analysis after the experiments by the substances in the fermentation broth.

The thiobacilli used was a mixed culture developed for the biooxidation of gold-bearing pyrite ores. It was grown in stirred tank culture on 9 K media (Silverman and Lundgren, 1959; Appendix 2) at 35°C and a pH of between 1.6 and 1.9.

The following experimental protocol was used for the experiments investigating the disruption of yeast. Experiments were carried out in the 1 liter vessel with no aeration and were 2 hours in duration. The growth of the yeast cells was inhibited by the addition of the growth inhibitor, Actidione (cycloheximide, Sigma Chemical Co. catalogue no. C6255) at a concentration of 10 μg cm^{-3}. Actidione is active for up to 72 hours and is particularly effective against yeasts and other fungi. Samples were taken before the start of agitation and at two minute intervals for the first ten minutes and thereafter after 60 minutes and 120 minutes of each yeast experiment. The samples were centrifuged in a microfuge to remove cells and particulates. The supernatants were analysed for the presence of soluble protein and where necessary enzyme activity.

Experiments were conducted in the 1 dm^3 stirred tank with thiobacilli. Samples of 50 ml were taken before the start of agitation and at the end of each two hour run. Fresh media was added to these samples (in 250 ml

Erlenmeyer shake flasks) to a total volume of 100 ml. There were no solids present in the shake flasks. The biooxidation rate of the samples was monitored over a time period of up to 120 hours.

The four large stirred tanks were used to investigate the biooxidation rate of thiobacilli under batch biooxidation conditions. The experiments were run over a period of two to three weeks. Samples were taken daily and the redox potential measured. The tanks were aerated at a rate of 1 vvm and the pH was monitored and kept between 1.6 and 1.9. The temperature of the tanks was 35°C.

3.3 ANALYTICAL TECHNIQUES

Yeast cell disruption was monitored by protein analysis and was visually observed by microscope. The amount of cell disruption was used as a measure of the stress to which the cells were subjected under the various operating conditions. Invertase (wall-associated enzyme) activity in the samples was monitored in a specific set of experiments. The concentration of the yeast was measured by dry weight analysis.

The metabolic activity, represented by the rate of biooxidation, of thiobacilli was used as a measure of the stress response of the cell cultures during certain conditions. The biooxidation rate of ferrous to ferric iron was determined by measurement of the redox-potential of the samples. The number of cells in solution was also determined by cell counting.

Reagents, solutions and assay methods are recorded in detail in the Appendices 1 and 2.

3.3.1 Dry biomass

Dry biomass was determined by centrifuging a known volume of the cell sample in dried and pre-weighed microfuge tubes. The supernatants were removed and the tube left to dry in a dessicator at 60°C for two to three days, until a constant mass was obtained. The mass of the tube and its contents were determined to four decimal places. A six-fold replication was used for each dry weight measurement

3.3.2 Protein analysis

The protein content in the sample supernatants was determined with the Lowry method (Lowry *et al.*, 1951) using bovine serum albumin (Sigma Chemical Co., St Louis, catalogue no. A4378) as the protein standard. The method is based on the reduction of Folin-Ciocalteu reagent (Sigma Chemical Co., catalogue no. F9252) by a copper-protein complex to yield an intense blue colour which is then determined spectrophotometrically. A standard curve of the spectrophotometric reading as a function of the concentration of the standard protein was prepared for each assay and the protein content of the sample calculated from the resulting standard curve (Figure A1). Details of the assay reagents, method and method reliability can be found in Appendices 1 and 2.

3.3.3 Invertase analysis

The activity of invertase in the sample supernatant is determined by the quantification of the enzymic hydrolysis of sucrose to glucose (Goldstein and Lampen, 1975). The hydrolysis occurs in an acid environment provided by sodium acetate buffer (pH 4.9) at 30°C and is stopped by the addition of potassium phosphate buffer (pH 7) and immersion in a 100°C water bath. The amount of glucose is then determined using the Glucose GOD-Perid test kit (Boehringer Mannheim GmbH Diagnostica, catalogue no. 124036). This is based on the conversion of glucose to gluconate with the production of hydrogen peroxide. The hydrogen peroxide combines with di-ammonium 2,2-azino-bis(3-ethylbenzothiazoline-6-sulfonate), which will be referred to as ABTS, to form a green coloured complex which is measured spectrophotometrically. A unit of invertase activity is defined as the amount of enzyme which hydrolyses sucrose to produce 1 μmole of glucose per minute at 30°C and pH 4.9. Specific activity is expressed as units per mg protein. A standard curve of the glucose concentration as a function of the invertase activity was prepared with standard invertase activities (Sigma Chemical Co., catalogue no. I9253). A typical standard curve is shown in Figure A2. Details of assay reagents, method and method reliabilty can be found in Appendices 1 and 2.

3.3.4 Cell counting

The disruption of yeast cells was estimated visually by counting in a Neubauer improved and a Thoma counting chamber (depending on volume required) under a light microscope. The number of whole cells was counted before and after experimentation. Cell counts were also performed on thiobacilli samples. Attachment of thiobacilli was determined by counting free cells in suspension before and after contact with solid particles.

3.3.5 Redox-potential measurement

The metabolic rate of the thiobacilli is determined by the measurement of the biooxidation rate. The ferrous iron is oxidised to the ferric iron. A simplified equation, neglecting the effects of hydrolysis and complexation, for the oxidation of pyrite is:

$$4\ FeS_2 + 15\ O_2 + 2\ H_2O + 4\ H^+ \text{ -----> } 4\ Fe^{3+} + 8\ HSO_4^- \qquad \text{Eqn. 3.3.1}$$

In bacterial oxidation the oxidants are oxygen and iron (III). The oxidising power of the oxidant is expressed by the value of its standard reduction potential, E^o. The oxidant under non-standard conditions is expressed by the appropriate Nernst equation. The reduction of oxygen is :

$$O_2(g) + 4\ H^+(aq) + 4\ e^- \text{ -----> } 2\ H_2O(l) \qquad \text{Eqn. 3.3.2}$$

The standard reduction potential for this half-reaction is 1.23 V and the Nernst equation, which expresses the variation of its potential, E, with the hydrogen ion activity is:

$$E = E^o - (RT/4F)\ \ln(1/(p_{O2}\ a_{H+}{}^4)) \qquad \text{Eqn. 3.3.3}$$

where:

a_{H+}	=	activity of the hydrogen ion
p_{O2}	=	partial pressure of oxygen
F	=	function of equilibrium constants of half-reactions

The appropriate half-reactions with their derived Nernst equations for the oxidation of pyrite are:

$$Fe^{2+} + 2\,S + 2e^{-} \text{ -----> } FeS_2 \qquad \text{Eqn. 3.3.4}$$

$$E = 0.424 \qquad \text{Eqn. 3.3.5}$$

$$Fe^{2+} + 2\,HSO_4^{-} + 14\,H^{+} + 14\,e^{-} \text{ -----> } FeS_2 + 8\,H_2O \qquad \text{Eqn. 3.3.6}$$

$$E = 0.351 - 0.0592*pH \qquad \text{Eqn. 3.3.7}$$

$$FeSO_4^{+} + HSO_4^{-} + 15\,H^{+} + 15\,e^{-} \text{ -----> } FeS_2 + 8\,H_2O \qquad \text{Eqn. 3.3.8}$$

$$E = 0.373 - 0.0592*pH \qquad \text{Eqn. 3.3.9}$$

The value of the oxidation/reduction (redox) potential (Eh) serves as an indicator of the intensity of oxidising processes. The measurement of Eh was used as a measure of the biooxidation and thus the metabolism of the cell population. Measurement was effected by the use of a set of platinum and calomel electrodes.

3.3.6 Particle size measurement

The size of the solid particles was analysed by size analysis in either a Malvern size analyser, or in a Sympatec Helos Vectra size analyser, both of which are based on diffraction of a laser beam. The Malvern analyser was only equipped to determine size fractions of less than 500 μm, whereas the Sympatec analyser analsyed size fractions up to 1750 μm. The size range (d_{10} to d_{90}), d_{50} and geometric mean diameter (d_{ave}) were determined for each solid particle sample.

3.3.7 Particle density measurement

The densities of the different solid particles were measured in a Micrometrics AccuPyc 1330 pycnometer. This model is a fully-automatic gas displacement pycnometer which determines the density (of known mass of substance) by measuring the pressure change of helium in a calibrated volume.

3.3.8 Impeller speed

The speed of the impeller was measured in revolutions per minute using a hand-held Veeder-Root tachometer. This speed was then converted to impeller tip speed as the diameter of the impeller was known.

3.4 DISRUPTION OF YEAST EXPERIMENTS

3.4.1 Effect of the concentration of silica on the disruption of yeast

Experiments were carried out in the 1 dm^3 stirred tank at a constant impeller speed of 772 rpm and volume fractions of silica (particles of mean size 1245 μm) of 0.05, 0.10, 0.20, 0.30 and 0.40. A Rushton turbine of diameter 0.054 m was used resulting in a tip speed of 2.2 m s^{-1}. The samples were assayed for soluble protein.

3.4.2 Effect of the impeller speed on the disruption of yeast

A set of experiments were carried out in the 1 dm^3 stirred tank at a constant volume fraction of 0.20 of 1245 μm silica particles and impeller speeds of 150 rpm, 200 rpm, 250 rpm, 300 rpm, 380 rpm, 540 rpm, 772 rpm and 1090 rpm. The samples were analysed for soluble protein.

3.4.3 Effect of silica particle size on the disruption of yeast

Investigations into the effect of varying particle size on the disruption of yeast at a volume fraction of silica of 0.20 and an impeller speed of 772 rpm were carried out. Particles of geometric mean size of 114 μm, 161 μm, 255 μm, 304 μm, 691 μm, 703 μm, 735 μm and 1245 μm were used. The samples were analysed for soluble protein.

3.4.4 Effect of particle density on the disruption of yeast

Experiments were carried out in the 1 dm^3 stirred tank at a volume fraction of solids of 0.20 and an impeller speed of 772 rpm. Activated carbon, silica and chromite particles were used. Their respective densities are 1600 kg m^{-3}, 2700 kg m^{-3} and 4500 kg m^{-3}. The samples were analysed for soluble protein.

3.4.5 Effect of the concentration of yeast on the disruption of yeast

The effect of the concentration of yeast on the disruption of yeast was investigated in the stirred tank using yeast suspensions of concentration 20 kg m^{-3}, 55 kg m^{-3}, 102 kg m^{-3} and 130 kg m^{-3}. The volume fraction of 1245 μm silica particles was kept constant at 0.20 and a constant impeller speed of 772 rpm was used. The release of soluble protein was monitored.

3.4.6 Determination of the maximum available soluble protein, R_m

The maximum soluble protein available for disruption was determined using three methods: the French Press; specific operating conditions in the stirred tank and enzyme lysis.

The French Press is an example of a disruption technique which utilizes liquid shear as the disruption mechanism. In the French Press, cells are disrupted on rapid decompression and extrusion through a narrow capillary. Different batches of yeast suspension were passed through the French Press 4 times. The samples were assayed for soluble protein.

Experiments were conducted in the 1 dm^3 stirred tank at a volume fraction of 0.40 of 1245 μm silica particles and an impeller speed of 1090 rpm. The release of soluble protein was monitored.

Cytophaga lysing enzymes (Sigma Chemical Co., catalogue no. L9893) were used in the enzyme lysis experiments. A yeast suspension of 20 kg m^{-3} was obtained by diluting the yeast suspended in phosphate buffered saline with 50 mM HCl-Tris buffer. The enzymes were added to the yeast to a concentration of 0.5 kg m^{-3} of the *Cytophaga* enzymes. The samples were incubated at 37°C for 95 minutes. Samples were taken at 15 minute intervals and were assayed for soluble protein.

3.4.7 Release of wall-associated protein, invertase

Experiments were conducted in the stirred tank at a constant volume fraction of 0.20 of 1245 μm silica particles and impeller speeds of 115 rpm, 150 rpm, 200 rpm, 250 rpm, 300 rpm, 350 rpm and 772 rpm. The samples were

assayed for both soluble protein release and the activity of the enzyme invertase.

A second set of experiments was carried out at a constant impeller speed of 772 rpm and volume fractions of 1245 μm silica particles of 0.05, 0.10 and 0.20. The samples were analysed for soluble protein and enzyme activity.

3.5 THIOBACILLI EXPERIMENTS

The effects of concentration of solid particles, impeller speed, particle size and particle type on the rate of biooxidation due to thiobacilli were studied. Two experimental protocols were used. The experimental rig, consisting of a 1 dm^3 laboratory stirred tank equipped with an overhead motor and Rushton turbine, was used to investigate the effects of concentration of silica, silica particle size, concentration of pyrite, pyrite particle size and impeller speed. A further set of experiments was undertaken in 4 dm^3 stirred tanks, equipped with overhead motors, in which the effects of the concentration of pyrite, impeller speed and impeller type were examined.

3.5.1 Shake flask growth and attachment of thiobacilli

A set of experiments was carried out in shake flasks using thiobacilli in 9K media. Volume fractions of 0.05 of silica particles and pyrite particles were added to separate flasks. The number of free bacteria were enumerated before and after agitation with particles for two hours. Cell counting was carried out in a Thoma counting chamber using a light microscope.

The number of free thiobacilli in solution before and after 2 hours of agitation in the stirred tank at a volume fraction of solids of 0.20 and an impeller speed of 772 rpm was also determined microscopically.

The shake flask growth of thiobacilli in the presence of a volume fraction of 0.05 pyrite particles was monitored by Eh measurement.

3.5.2 Effect of the concentration of silica

This set of experiments was carried out at an impeller speed of 772 rpm (equivalent to a tip speed of 2.2 m sec^{-1}) and volume fractions of solids (fraction of volume of solids to total volume) of 0.5, 0.10 and 0.20. Silica particles with a geometric mean diameter of 53 μm were used.

3.5.3 Effect of silica particle size

Experiments were carried out at 772 rpm and with a volume fraction of solids of 0.05 of silica particles of different sizes. The geometric mean particle diameters ranged from 53 μm to 255 μm.

3.5.4 Effect of concentration of pyrite

Pyrite particles of geometric mean diameter of 55 μm were used to investigate the effect of agitation at 772 rpm with volume fractions of solids of 0.05, 0.10 and 0.20 in the 1 dm^3 stirred tank.

3.5.5 Effect of pyrite particle size

The mean particle diameters investigated were 41 μm, 55 μm and 80 μm. The experiments were carried out at a volume fraction of solids of 0.20 and an impeller speed of 772 rpm.

3.5.6 Effect of impeller speed

The effect of impeller speed was examined using 55 μm pyrite particles at a volume fraction of solids of 0.20. The speeds investigated were 400 rpm (equivalent tip speed of 1.1 m s^{-1}), 772 rpm (equivalent tip speed of 2.2 m s^{-1}) and 1090 rpm (equivalent tip speed of 3.1 m sec^{-1}).

3.5.7 Continuous monitoring of rate of biooxidation in 4 dm^3 stirred tanks

Several experiments were carried out in 4 dm^3 stirred tanks to investigate the effects of the concentration of pyrite and impeller speed on the rate of

biooxidation due to thiobacilli. Thiobacilli was grown on 9K (Silverman and Lundgren, 1959) media, containing 44.8 kg m^{-3} iron (II), to a cell concentration of approximately $1*10^8$ to $2*10^8$ cells per milliliter. This culture was used as an inoculum for the stirred tanks. Inoculum and fresh 4K media, containing 19.8 kg m^{-3} iron (II), were mixed together in equal quantities. The concentration of pyrite was calculated on a mass per volume basis. The tanks were aerated at 1 vvm and the pH of the solution was kept between 1.6 and 1.9. The temperature of the water bath in which the tanks stood was 35°C. The activity of the cells was monitored by daily Eh measurement. The experiments ran over a period of 21 days.

3.5.8 Effect of concentration of low sulphur pyrite

Low sulphur pyrite residue ore (1.5% total S) from St. Helena mine, South Africa, was used to investigate the effect of the concentration of pyrite on the growth of thiobacilli to ensure that no oxygen limitation occurred at high solids concentrations (Hansford and Bailey, 1993). Pyrite ores with high sulphur content (48% S) have exhibited oxygen limitation at high concentrations of solids (above 10% pyrite, mass/volume). Concentrations of pyrite of 0, 10, 20 and 30% (mass/volume) were used in the four stirred tanks. Equivalent volume fractions of solids are 0, 0.02, 0.04 and 0.06. Rushton turbine impellers were employed at an agitation rate of 350 rpm (equivalent tip speed of 1.4 m s^{-1}). The dissolved oxygen concentration in each tank was measured on day 4 of the experiment to ensure that limitation did not occur.

3.5.9 Effect of impeller speed and impeller type

Pyrite of high sulphur content (48% S) from Prieska, Northern Cape, South Africa, at a concentration of 10% (mass/volume) was used in these experiments. A Rushton turbine, yielding radial flow, and an axial-flow impeller were compared at two impeller speeds 350 rpm (1.4 m s^{-1}) and 630 rpm (2.6 m s^{-1}). The Eh of the tanks was monitored daily for 20 days.

CHAPTER 4
EFFECTS OF PARTICULATES ON YEAST DURING AGITATION

4.1 INTRODUCTION

Presented in this chapter are the results of the experimental investigations into the disruption of yeast in the laboratory stirred tank as a function of concentration of solids, impeller speed, particle size, particle density, particle shape and concentration of yeast. The volume fractions of solids ranged from 0.05 to 0.40. Impeller speeds in the range 115 rpm to 1090 rpm were utilized. A Rushton impeller of diameter 0.054 m was used, resulting in impeller tip speeds ranging from 0.33 m s^{-1} to 3.08 m s^{-1}. Silica, activated carbon and chromite particles were used in the experiments. The densities of these particles were 1600 kg m^{-3}, 2700 kg m^{-3} and 4500 kg m^{-3}, respectively. The mean size of the particles varied from 114 μm to 1245 μm. The concentration of yeast (dry biomass) varied from 20 kg m^{-3} to 130 kg m^{-3}.

First order kinetics of the form $\ln[R_m/(R_m - R)] = kt$ were used to describe the process of cell disruption. The amount of soluble protein released per unit mass of yeast was termed R. The maximum available soluble protein for release from the cell population, R_m, was determined. The maximum disrupted soluble protein, R_i, was defined as the amount of soluble protein released at specific operating conditions after infinite time. The extent of disruption was determined from the ratio of soluble protein released and the maximum available soluble protein, R/R_m. In addition, the maximum extent of disruption was determined from the ratio of the maximum disrupted soluble protein and the maximum available soluble protein, R_i/R_m. The rate constant of disruption, k, was determined using the first order rate equation.

The disruption rate constant in this study was determined from first order kinetics. The disruption of cells has been proposed to be first order with respect to concentration of whole cells (Currie *et al.*, 1972; Schutte *et al.*, 1986; Kula and Schutte, 1987). This is expressed as follows:

$$-dN/dt = kN \qquad \text{Eqn. 4.1.1}$$

where N = number of cells at time, t
k = first order rate constant

t = time

Integrating

$$\ln N_o/N = k\,t \qquad \text{Eqn. 4.1.2}$$

where N_o = initial number of cells

It is convenient to quantify cell disruption in terms of soluble protein release. An expression for the soluble protein content is substituted for the number of intact cells as follows:

$$R_m = C_P\,N_o$$
$$R = C_P\,N_o - C_P\,N = C_P\,(N_o - N)$$

where R_m = total soluble protein content of cell population
R = soluble protein released
C_P = protein content of one cell

Upon rearrangement:

$$N = N_o - R/C_P$$
$$= R_m/C_P - R/C_P \qquad \text{Eqn. 4.1.3}$$

Substituting Eqn. 4.1.3 into Eqn. 4.1.2 and rearranging:

$$\ln R_m / [R_m - R] = k\,t \qquad \text{Eqn. 4.1.4}$$

The release of the wall-associated enzyme, invertase, was used to investigate the disruption of the cell wall.

The literature covering bead mills and mammalian microcarrier cultures was used as a basis for comparison of the experimental results obtained. It must be noted, however, that direct comparisons to bead mills and microcarrier cultures are not advisable due to the extensive difference in the systems. In microcarrier cultures the mammalian cells are attached to the particles. Furthermore mammalian cells do not have a cell wall and are larger than bacterial or fungal cells. Therefore

mammalian cells are more fragile. In bead mills the cells remain unattached to the particles. The beads are not suspended in the fluid as in a stirred tank. The grinding motion of the beads in a bead mill is similar to rods or balls in the mills utilized in mineral processes.

4.2 RESULTS AND DISCUSSION

4.2.1 The standard disruption test and protein release data fitted to the first order rate equation

A standard experiment at a volume fraction of silica particles of geometric mean size 1245 μm of 0.20, an impeller speed of 772 rpm and a concentration of yeast of 50-60 kg m^{-3} was repeated over a nine month period to investigate the variability in experiments. The results of the standard disruption tests were presented in terms of the soluble protein released per unit mass of yeast. Reproducibility of the results and experimental error were tested under these conditions.

The results of the standard tests are shown in Figures 4.2.1, 4.2.2 and 4.2.3. The data has been fitted to the first order kinetic model and the model fits are shown. Figure 4.2.1 shows the variation between standard tests conducted 6 months apart. The results shown in Figure 4.2.2 are from standard tests conducted with the same batch of yeast 3 days apart. The variation between values of protein released in the standard experiments conducted on different occasions over a period of 9 months was 9.98%.

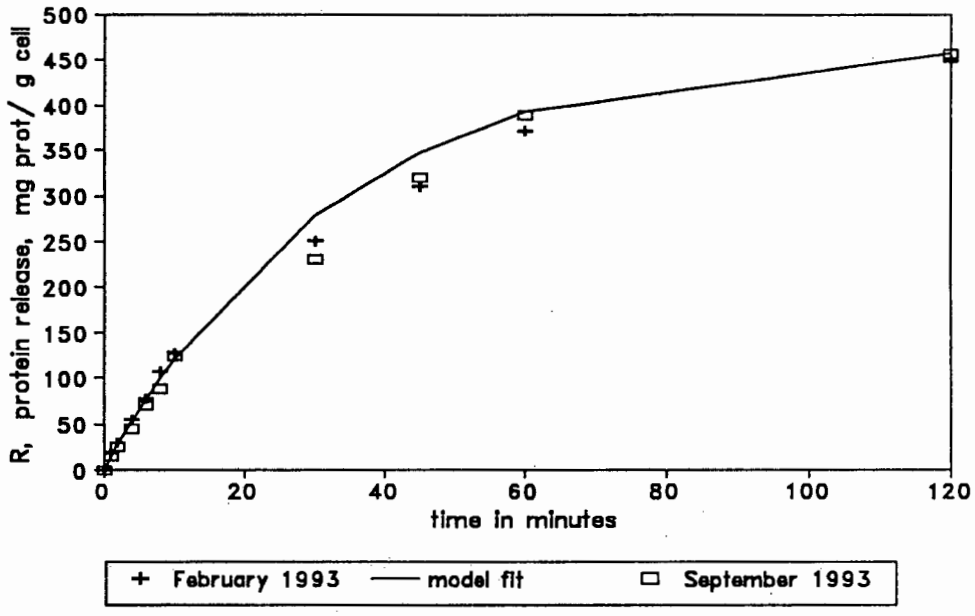

Figure 4.2.1 The effect of different yeast batches on the soluble protein released from yeast suspensions (50-60 kg m^{-3}) at a volume fraction of 0.20 of 1245 μm silica particles and an impeller speed of 772 rpm.

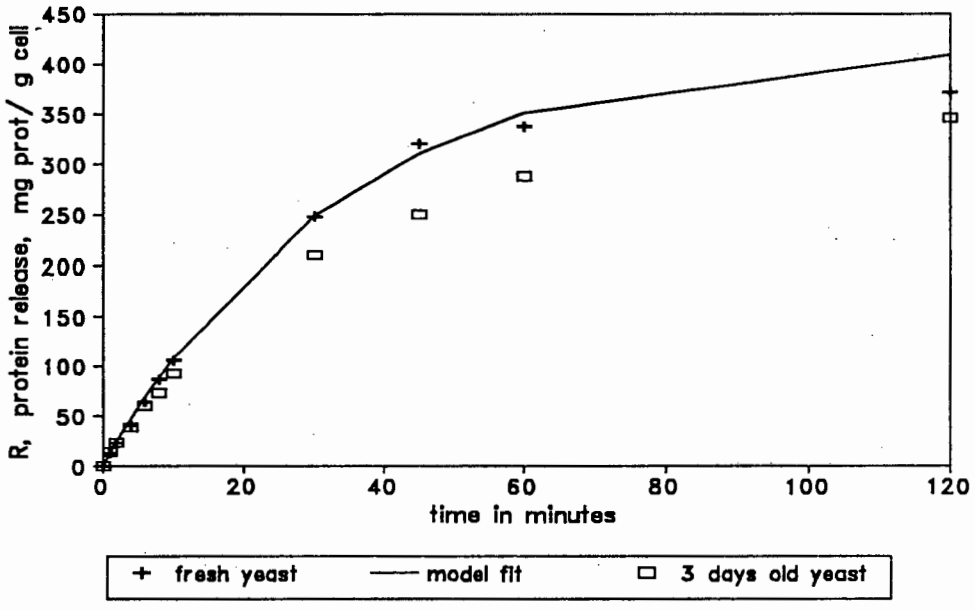

Figure 4.2.2 The effect of age of yeast batch on the soluble protein released from yeast suspensions (50-60 kg m^{-3}) at a volume fraction of 0.20 of 1245 μm silica particles and an impeller speed of 772 rpm.

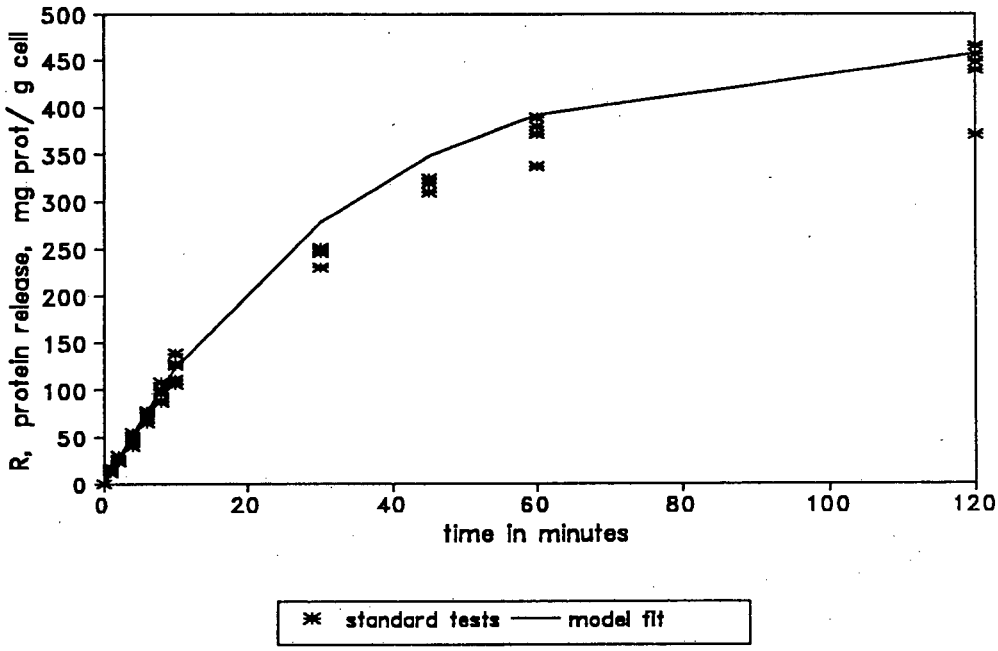

Figure 4.2.3 Soluble protein released from yeast suspensions in the standard tests conducted at operating conditions of a volume fraction of 0.20 of 1245 μm silica particles, an impeller speed of 772 rpm and concentration of yeast of 50 kg m^{-3}

The application of the first order equation, shown in Section 4.1, to the soluble protein released in a typical standard test is shown in Figure 4.2.4.

In Figure 4.2.4, $\ln R_m/(R_m-R)$ is plotted as a function of time (t) for a standard test. The correlation coefficient of the straight line was 0.9978 for the first 10 minutes of the experiment and 0.9955 for the overall duration of the experiment. This is shown by the two linear fits in Figure 4.2.4, which have different gradients. The value of the disruption rate constant used in the subsequent sections is determined from the slope of the overall model fit. The results obtained indicate an initial rapid rate of disruption denoted by the steep gradient of the initial line, and a lower overall disruption rate constant.

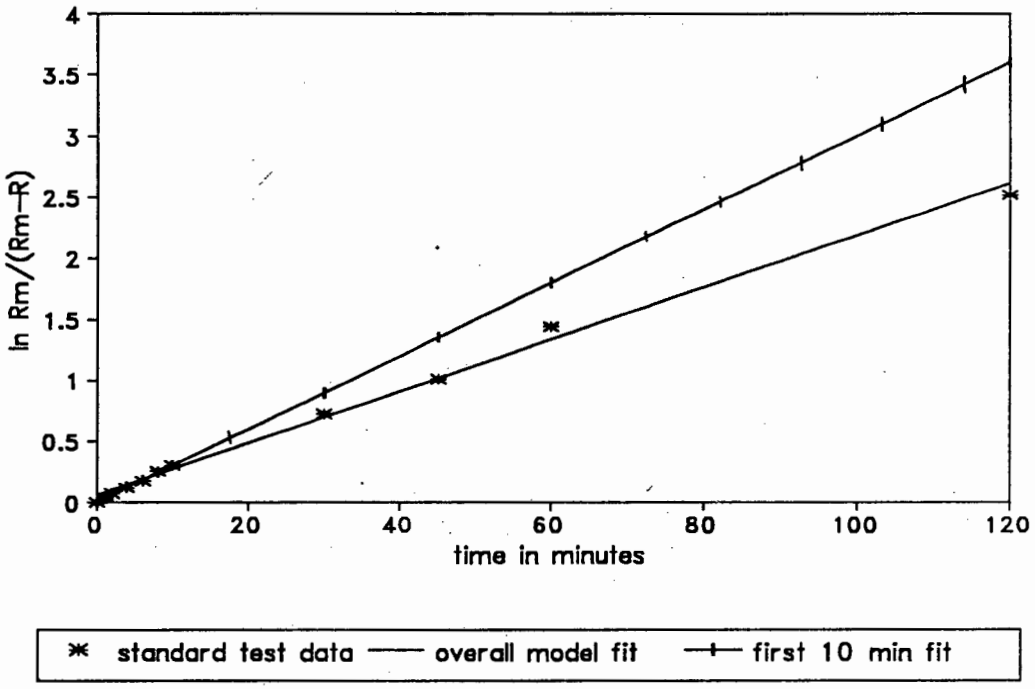

Figure 4.2.4 Soluble protein release data from a typical standard test fitted to the first order rate equation, $\ln[R_m/(R_m - R)] = kt$ to obtain first order disruption rate constant, k

The disruption rate constant, maximum disrupted soluble protein and maximum extent of disruption for all the standard tests are shown in Table 4.2.1.

Table 4.2.1 The disruption rate constant, maximum disrupted soluble protein and maximum extent of disruption for the standard tests conducted at a volume fraction of 0.20 of 1245 μm silica, an impeller speed of 772 rpm and a concentration of yeast of 50-60 kg m^{-3}.

date	disruption rate constant, s^{-1}	maximum disrupted soluble protein, R_i, mg protein	maximum extent of disruption R_i/R_m, in %	r^2 for fit to model
25/2/93	0.00050	470	96	0.9955
15/3/93	0.00047	440	90	0.9926
16/3/93	0.00045	430	88	0.9924
17/3/93	0.00042	440	90	0.9973
19/3/93	0.00048	460	94	0.9937
22/3/92	0.00033	380	78	0.9925
22/3/93	0.00050	440	90	0.9968
07/4/93	0.00042	370	76	0.9952
04/5/93	0.00045	430	88	0.9960
01/9/93	0.00048	470	96	0.9971

4.2.2 Determination of maximum available soluble protein, R_m

In the first order equation used to correlate disruption data the maximum available soluble protein, R_m, is used. This is a measure of the total available soluble protein. The maximum available soluble protein, R_m, was determined by the three methods detailed in Section 3.4.6 using the French Press, specific operating conditions in the stirred tank and enzyme lysis.

The French Press is an example of a disruption technique which utilizes liquid shear as the disruption mechanism. Different batches of yeast cells were passed through the French Press in nine different experiments over a 9 month period. The samples were assayed for soluble protein content. The variation in protein release in these experiments was 12% of the mean value.

The values of R_m obtained in the French Press over a series of tests is shown in Table 4.2.2.

Table 4.2.2 The maximum available soluble protein released on disruption of yeast after 4 passes through the French Press.

date	maximum available soluble protein R_m, mg protein/ g cell
16/3/93	479
18/3/93	506
19/3/93	482
22/3/93	480
25/3/93	505
25/3/93	503
25/3/93	476
01/4/93	477
07/4/93	487
average	487

The soluble protein released by disruption of yeast in the stirred tank at operating conditions of a volume fraction of 0.40 of 1245 μm silica and an impeller speed of 1090 rpm was determined. The experiment was repeated several times resulting in an average value of R_m. The variation between the experiments was 9.5% of the average value. The values of R_m obtained in the stirred tank are shown in Table 4.2.3.

Table 4.2.3 The soluble protein released from yeast (concentration of 50-60 kg m^{-3}) at an impeller speed of 1090 rpm and a volume fraction of 1245 μm silica of 0.40

date	maximum available soluble protein R_m, mg protein per g yeast
11/3/93	460
13/7/93	464
14/7/93	474
15/7/93	470

Yeast cell disruption using enzyme lysis was carried out using lysing enzymes from the *Cytophaga* species. The enzymes included yeast glucanase and protease. The experiment was conducted in triplicate and the average soluble protein released was significantly lower than the values obtained by the other two methods. Hunter and Asenjo (1987) investigated the lysis of yeast cells by *Cytophaga* lysing enzymes. *Cytophaga* lysing enzymes include, among other, a protease, hence degradation of protein molecules is expected. The complete hydrolysis of a protein reduces the colour produced in the Lowry assay (Bailey, 1967; Peterson, 1979). The hydrolysed protein and the native long chain proteins were not separated in the enzyme lysis performed for determination of R_m and this could explain the low value obtained in the assay.

The average values of the maximum available soluble protein determined by the three methods are shown in Table 4.2.4.

Table 4.2.4 The maximum available soluble protein, R_m, obtained from disrupting yeast of concentration 50-60 kg m^{-3}, as determined using the French Press, a volume fraction of solids of 0.40 and an impeller speed of 1090 rpm in the stirred tank and enzyme lysis by *Cytophaga* enzymes.

method of disruption	maximum available soluble protein, R_m, mg protein per g yeast cell (average value)
French Press	487
stirred tank	469
enzyme lysis	302

The value of R_m was taken to be the average obtained from the French Press. R_m is used as a measure of the maximum amount of soluble protein in the yeast population and is therefore a constant value, independent of the operating conditions in the stirred tank.

4.2.3 Determination of maximum disrupted soluble protein, R_i

In the disruption tests the soluble protein released tended asymptotically to a maximum value which is called the maximum disrupted soluble protein, R_i. This is obtained from a regression of R as a function of t according to the equation $\ln R_i/(R_i - R) = kt$. The maximum disrupted soluble protein is dependent on the operating conditions in the stirred tank as it is determined using the protein release data from the experiments.

The extent of disruption is defined as the ratio of soluble protein released to the maximum available soluble protein, R/R_m. The maximum extent of disruption is

therefore defined by the ratio of the maximum disrupted soluble protein to the maximum available soluble protein, R_i/R_m.

The maximum available soluble protein as well as the maximum disrupted soluble protein for a typical standard test are shown in Figure 4.2.5.

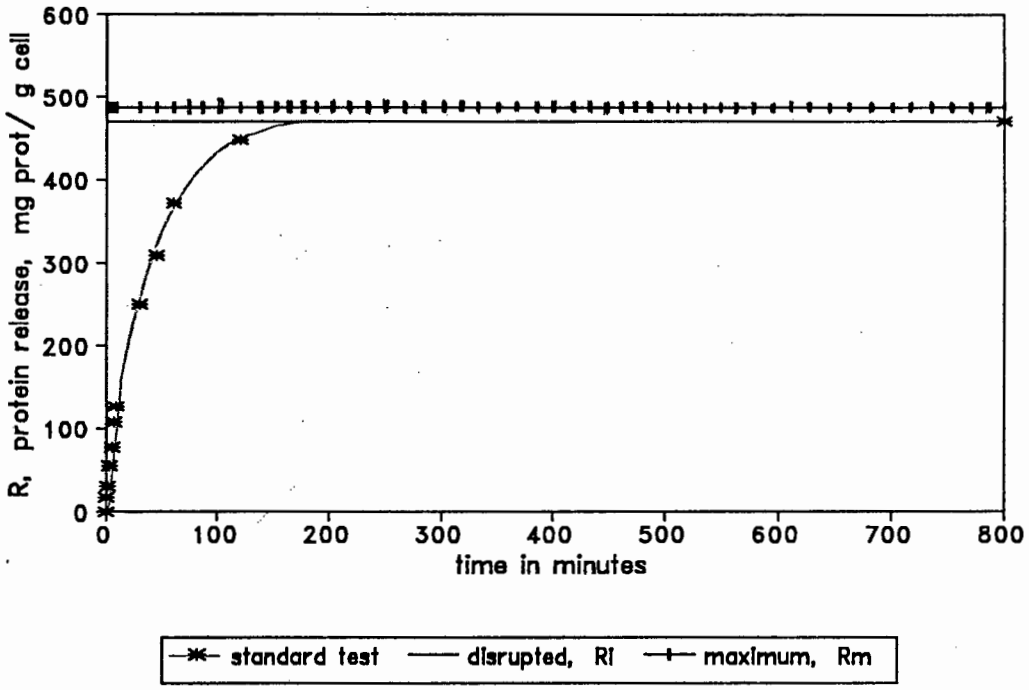

Figure 4.2.5 The maximum available soluble protein, R_m, obtained from the French Press and the maximum disrupted soluble protein, R_i, for a typical standard test at operating conditions of an impeller speed of 772 rpm and a volume fraction of solids (silica, 1245 μm) of 0.20.

4.2.4 The effect of the concentration of solids

Disruption tests were carried out at constant yeast concentration of 50-60 kg m^{-3} and agitation speed of 772 rpm with varying concentrations of 1245 μm silica particles. The volume fractions of solids investigated were 0.05, 0.10, 0.20, 0.30 and 0.40. The results are shown in Figures 4.2.6 and 4.2.7.

The extent of disruption, R/R_m, as a function of time is shown in Figure 4.2.6. The extent of disruption obtained when no solids are present is insignificant over the period of the experiment (less than 3%). There is minimal disruption at volume fractions of solids less than 0.10 and significant disruption at volume fractions of solids greater than 0.20.

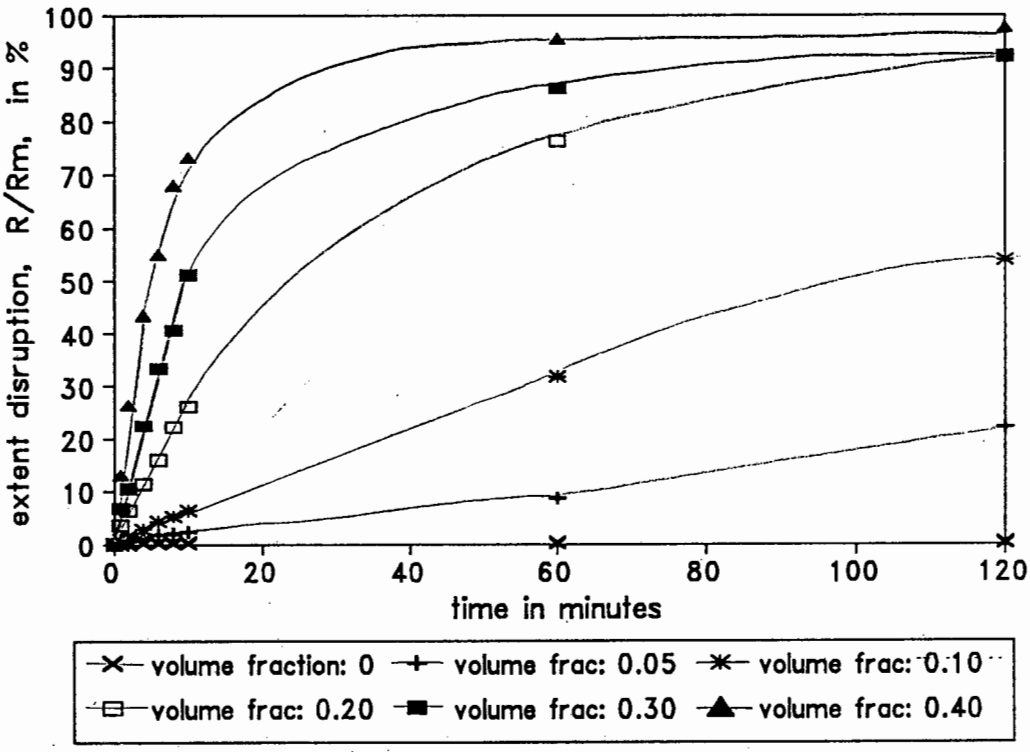

Figure 4.2.6 The effect of the concentration of the particulates (concentration of 1245 μm silica particles given in terms of volume fraction) on the extent of disruption, R/R_m, of yeast cells of concentration 50-60 kg m^{-3} at an impeller speed of 772 rpm

The protein release data was then fitted to the first order rate equation to obtain k. The maximum extent of disruption, R_i/R_m, was determined using R_i, which had been calculated by regression. These results are shown in Figure 4.2.7.

From Figure 4.2.7, it can be seen that the maximum extent of disruption is independent of the concentration of solids as it remains at a constant value over

the range of concentrations of solids investigated. The disruption rate constant increases slowly initially and then more rapidly.

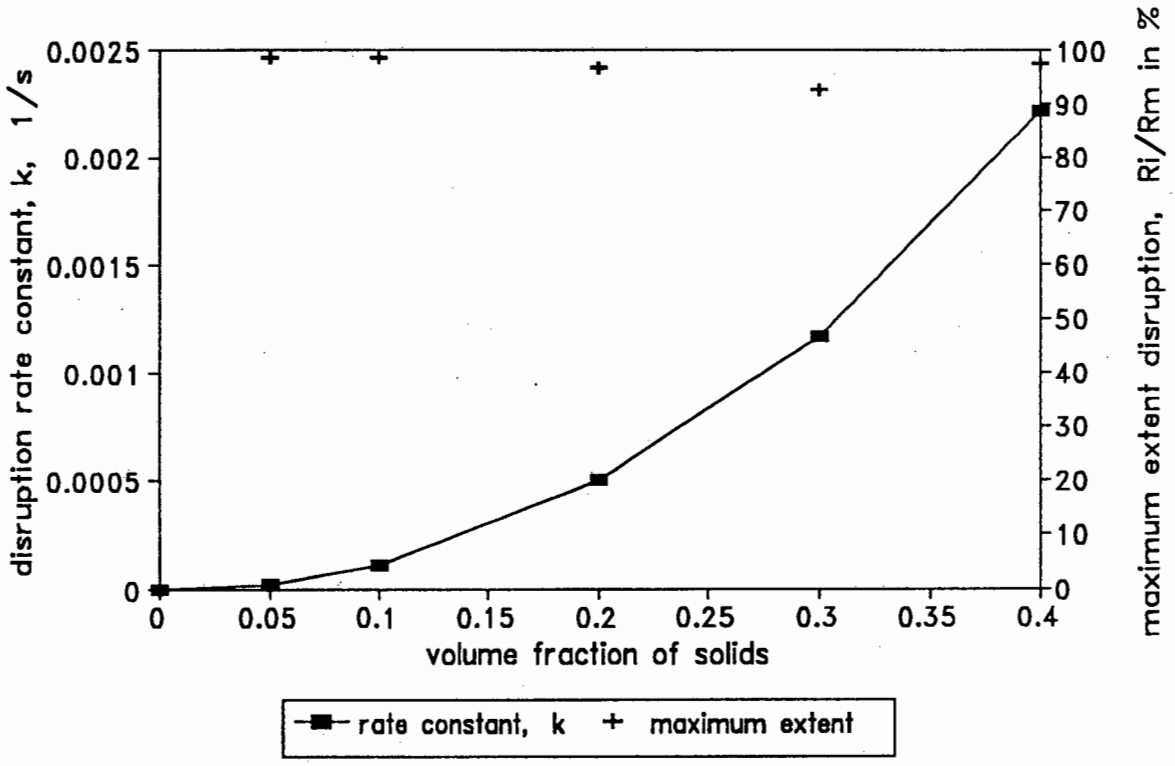

Figure 4.2.7 The effect of the volume fraction of solids on the disruption rate constant and the maximum extent of disruption of yeast at a constant impeller speed of 772 rpm (silica particle size, d_{ave}, of 1245 μm and concentration of yeast 50 - 60 kg m^{-3})

The increase in the disruption rate constant can be compared with the disruption rate constants obtained in a bead mill by Currie *et al.* (1972). The rate constants obtained in the bead mill are not directly analogous due to their dependence on the flowrate and total volume of the continuous bead mill system. The rate constants determined in this study originate from batch studies and therefore do not have to take flowrate into account. Currie *et al.* (1972) used a bead mill with a 4.2 dm^3 capacity grinding chamber and flowrate of 1.4 dm^3 min^{-1} of 60 kg m^{-3} yeast suspension. Beads of 800 μm were used. The disruption rate constants obtained in the bead mill have been divided by the volume of the bead

mill to enable comparison with the rate constants obtained in this study. The results of this study and of Currie *et al.* (1972) are shown in Table 4.2.5.

Table 4.2.5 Disruption rate constants determined in this study and by Currie *et al.* (1972) in a bead mill.

type of apparatus	volume fraction of solids	disruption rate constant, $dm^3\ s^{-1}$	disruption rate constant, s^{-1}
experimental stirred tank	0.05		0.000017
	0.10		0.000100
	0.20		0.000500
	0.30		0.001170
	0.40		0.002220
bead mill Currie *et al.* (1972)	0.35	0.004	0.000950
	0.50	0.010	0.002380
	0.70	0.017	0.004050
	0.90	0.027	0.006430

The disruption rate constants obtained in this study are of the same order of magnitude as those obtained in the bead mill. The dependency of the disruption rate constant on the concentration of solids is discussed further in Section 5.2.1.

4.2.5 The effect of impeller speed

Disruption tests were conducted at a yeast concentration of 50-60 kg m^{-3} and a volume fraction of silica (1245 μm) of 0.20 over a range of impeller speeds from 150 rpm to 1090 rpm. A 0.054 m diameter Rushton impeller was used giving tip speeds of 0.42 m s^{-1} to 3.08 m s^{-1} respectively. The results are shown in Figure 4.2.8. Below 540 rpm (equivalent tip speed of 1.52 m s^{-1}) both the

disruption rate constant and maximum extent of disruption are low. For speeds between 380 rpm and 540 rpm the disruption rate constant increases steadily to 0.0005 s^{-1}. The maximum extent of disruption increased rapidly until reaching a maximum value of 96% above an impeller speed of 772 rpm. There is a sharp rise in the maximum extent of disruption between impeller speeds of 150 rpm and 300 rpm even though the disruption rate constant remains low. The increase in disruption rate constant takes place between the higher impeller speeds of 380 rpm and 540 rpm.

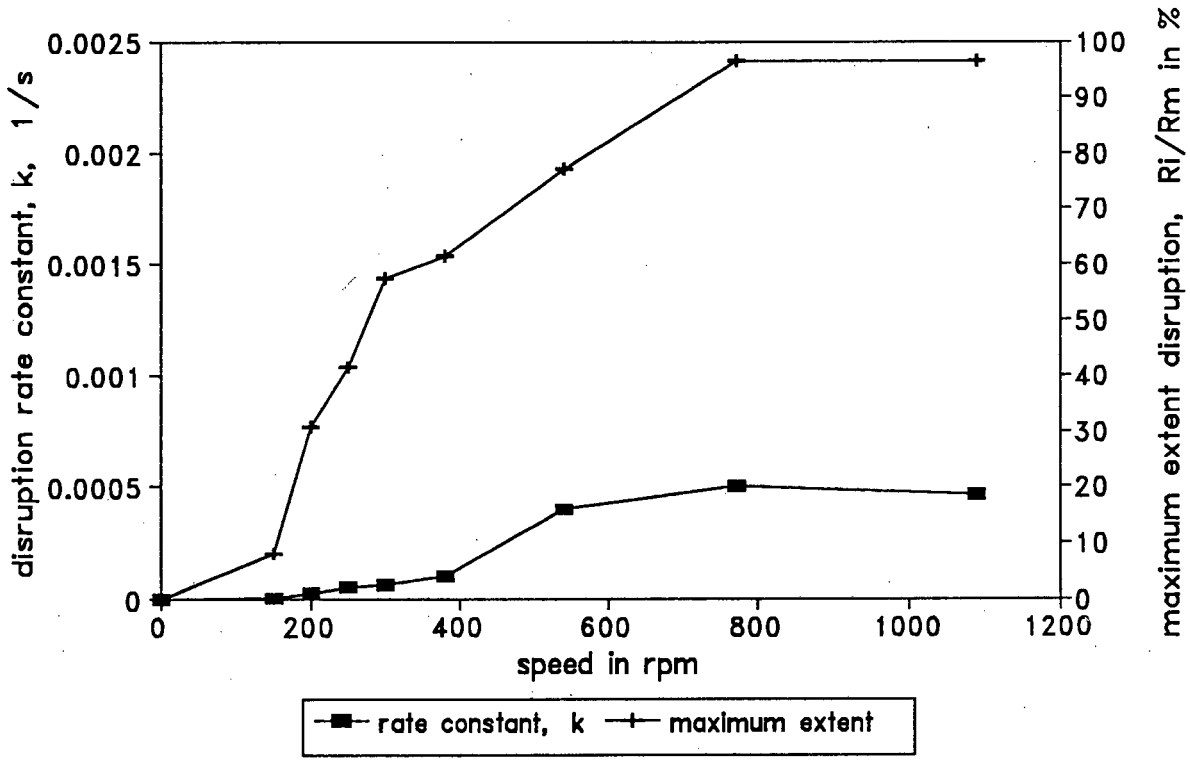

Figure 4.2.8 The effect of impeller speed on the disruption rate constant and the maximum extent of disruption for yeast at a constant volume fraction of solids of 0.20 (silica particles of geometric mean size 1245 μm and a concentration of yeast of 50-60 kg m^{-3})

These results have been compared to rate constants obtained in bead mills. Table 4.2.6 shows the disruption rate constant obtained by Currie *et al.* (1972) as well as the disruption rate constants obtained in this study. The bead mill has been described in Section 4.2.4. The operating conditions were the same as

Table 4.2.7 The soluble protein release data, from yeast as a function of impeller speed, as reported by Schutte *et al.* (1983) and as shown in this study

type of apparatus	impeller speed in rpm	soluble protein released mg protein per g yeast
experimental stirred tank	150	40
	200	150
	250	202
	300	280
	380	300
	540	376
	772	470
	1090	470
bead mill Schutte *et al.* (1983)	700	175
	913	400
	1100	450
	1340	525
	1450	550

As can be seen from Table 4.2.7 the amounts of soluble protein released in the stirred tank used in this bead mill compare favourably with the amounts obtained by disruption of yeast in a bead mill, irrespective of the difference in the two systems.

4.2.6 The effect of particle size

The effect of particle size on the disruption rate constant and extent of disruption was determined at a speed of 772 rpm and a yeast concentration of 50-60 kg m^{-3}. The concentration of solids was kept constant at a volume fraction of 0.20 of silica particles of varying size. The geometric mean size of the

particles used ranged from 114 μm to 1245 μm. The results are shown in Figure 4.2.9.

The disruption rate constant was low initially but increased rapidly between particle sizes of 256 μm and 304 μm. The disruption rate constant levels off at a particle size of 703 μm. The maximum extent of disruption increases rapidly up to a particle size of 304 μm and then reaches the maximum value of 96% at a particle size of 1245 μm.

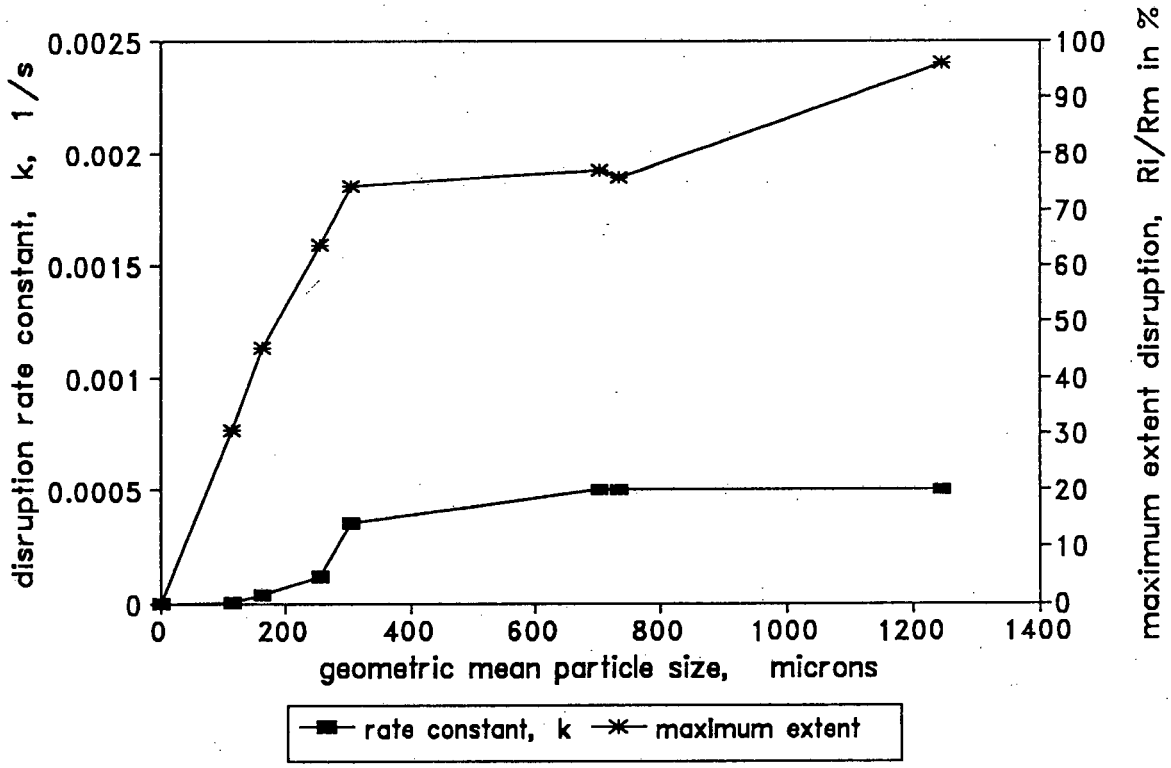

Figure 4.2.9 The effect of particle size on the disruption rate constant and the maximum extent of disruption for yeast at a constant impeller speed of 772 rpm, constant volume fraction of solids of 0.20 (concentration of yeast 50 - 60 kg m^{-3}).

The optimal size of beads used in bead mills is dependent on the size of the microorganism. The disruption of yeast was found to be favoured by utilization of beads of diameter larger than 0.5 mm (Kula and Schutte, 1987), whilst beads of less than 0.5 mm diameter were reported for disruption of bacteria. The

results obtained in this study confirm the ineffectual use of particles less than 300 μm for the disruption of yeast.

The trends illustrated in Figure 4.2.9 imply that the particle size may be responsible for a change in disruption mechanism. It is suggested that the off-bottom suspension of small particles (diameters less than 304 μm) results in the formation of slurries of particles of low kinetic energy, whilst the larger particles are not suspended and cause greater disruption due to their grinding action on the tank floor.

The extent of disruption did not approach total disruption when small particles were used. Large particles carry greater kinetic energy in comparison to smaller particles due to their larger mass. This large kinetic energy leads to large differences in the velocity profile of the particles and to increased shear forces. It would thus seem plausible that the small particles were unable to disrupt the cells completely and only damaged the cells, thereby releasing some, but not all, the soluble protein. However, for the same concentration of solids, the number of particles increased considerably with decreasing particle diameter. This increased the frequency of collision between particles. The results imply that a critical kinetic energy content of single particles must be exceeded before the number of collisions can take effect.

The results shown in Figure 4.2.9 imply that there may be a critical ratio of particle to cell size. There is a critical size of particle which can be crushed in ball mills in minerals processes. Crushing of mineral particles is achieved in the minerals processing industry by use of crushing rollers and ball mills. The rollers crush by nipping the mineral particles between the roller faces (Pryor, 1978). It is essential that the mineral material being crushed is seized by the rollers and drawn between them and thus the size of the particles relative to the angle between the rollers is critical. The calculation of the maximum size of mineral which may be crushed by rollers of a certain size may be applicable to determining the size of cell which may be damaged by round particles of a certain size. The ratio of the size of roll to the maximum size of particle which will be gripped and crushed is 25:1 when a coefficient of friction of 0.3 is used (Pryor, 1978). Yeast cells range from 4 to 10 μm in size. The geometric mean size (d_{yave}) of yeast cells is 6 μm. A solid particle to cell size ratio of 25:1 occurs when particles of 150 μm are used. This illustrates, according to the nip angle

theory, that yeast cells are too large to be gripped by particles of less than 150 μm.

The breadth of the size fractions is not obvious from the values of mean particle sizes. The breadth of the fractions may have an effect on the disruption rate constant and maximum extent of disruption. Three size fractions are shown in Figure 4.2.10. As can be seen the distributions of the particles are totally different. The fraction with mean particle size of 256 μm has a broad distribution of particles in comparison with the fraction of mean particle size of 304 μm. It is interesting to note that the large increase in disruption rate constant occurs between these two size fractions.

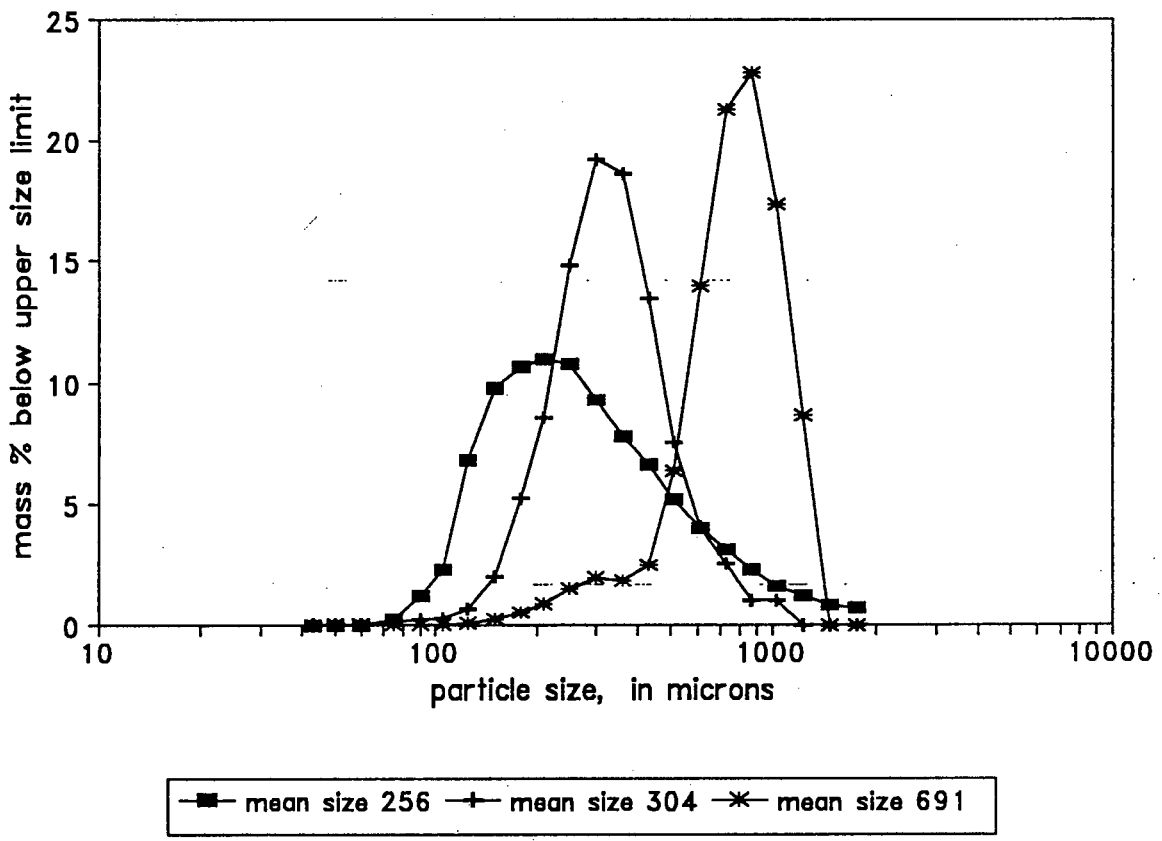

Figure 4.2.10 The distributions of three size fractions of silica particles showing the difference in breadth of the fractions

The size fractions, breadths, disruption rate constants and maximum extents of disruption found in this set of experiments are shown in Table 4.2.8.

Table 4.2.8 Range of particle size fractions, median sizes (d_{50}) of the fractions, geometric mean particle sizes (d_{ave}) and the disruption rate constants and extents of disruption for agitation of yeast (concentration of 50-60 kg m^{-3}) in slurries containing a volume fraction of solids (silica) of 0.20 at an impeller speed of 772 rpm

80% particles within size fraction μm	breadth of size fraction μm	median size, d_{50}, μm	geometric mean, d_{ave} μm	disruption rate constant min^{-1}	extent R_i/R_m in %
+59-222	160	125	114	0.0003	30.80
+106-247	140	176	162	0.002	45.20
+180-363	180	238	256	0.007	63.60
+185-501	315	297	304	0.021	74.30
+508-973	460	710	703	0.030	77.00
+526-1027	500	752	735	0.030	75.80
+881-1761	880	1338	1245	0.030	96.00

4.2.7 The effect of particle density

The rate and extent of disruption were determined as functions of the density of the particles, in the range 1600 kg m^{-3} to 4500 kg m^{-3}, at an impeller speed of 772 rpm and a volume fraction of solids of 0.20. Activated carbon, silica and chromite particles of mean diameter 364 μm were used in these experiments. The results are shown in Figure 4.2.11. Minimal increases in the rate and extent of disruption with increased density of the particles were observed.

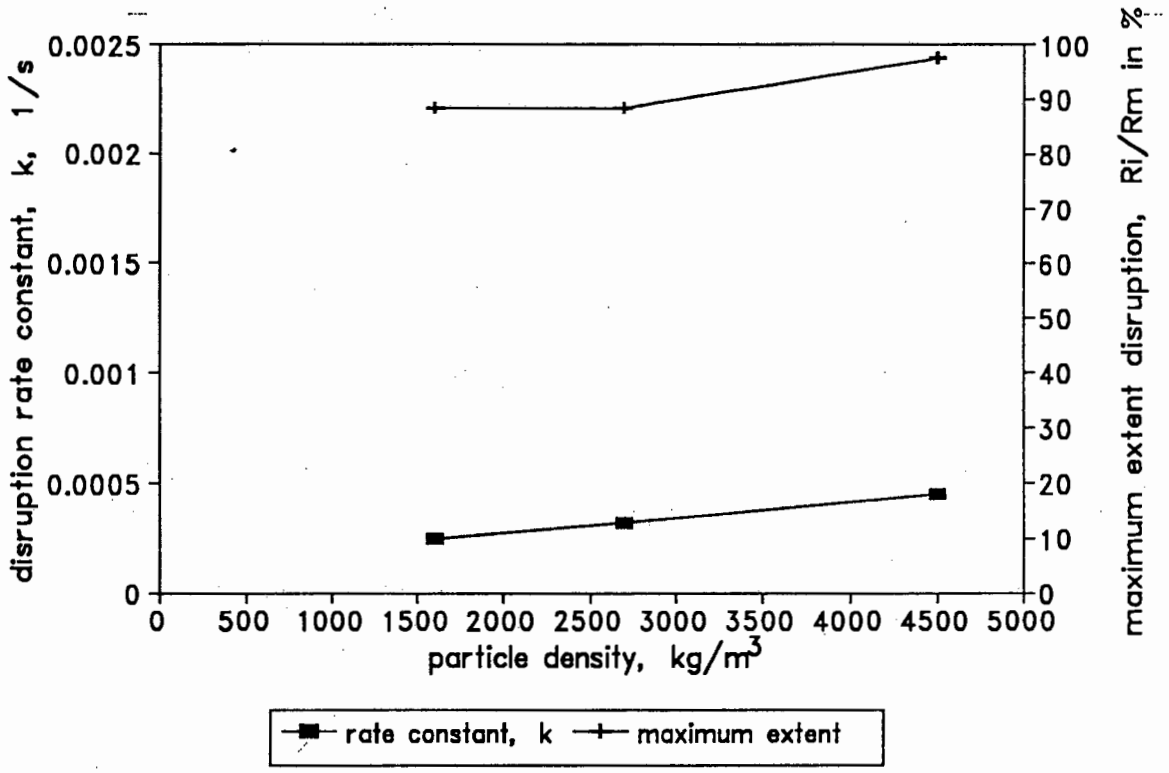

Figure 4.2.11 The effect of particle density on the disruption rate constant and the maximum extent of disruption for yeast at a constant impeller speed of 772 rpm, constant volume fraction of solids of 0.20 (concentration of yeast 50 - 60 kg m^{-3})

The disruption obtained in a bead mill operating with glass beads of densities in the range of 2500 to 2900 kg m^{-3}, ceramic beads of density of 3800 kg m^{-3} and zirconium oxide beads of density of 5400 kg m^{-3} was reported by Kula and Schutte (1987). A 40% (w/v) cell suspension and agitation speed of 3000 rpm were utilized. They observed that the extent of disruption, as monitored by the release of enzymes, did not increase with increased density of grinding agent. However they did report that beads of high density improved cell disruption in viscous suspensions.

The kinetic energy of the particles will increase with increasing density and thus larger differences in velocity profile and larger shear forces will be produced. These effects may have caused the marginal increase in the cell disruption rate and extent of disruption.

4.2.8 The effect of particle shape

The effect of the shape of particles on cell damage is important due to the shape of mineral ore particles found in biooxidation processes. Pyrite and other ores consist of particles which have sharp, irregular edges. In bead mills glass beads are used as the crushing agents. These beads are smooth and rounded. It is therefore relevant to observe the effect of different shaped particles on cell damage.

The silica particles used in the particle density experiments (Section 4.2.7) were jagged. It is interesting to compare the results obtained with these jagged particles with results obtained with smooth particles of a similar size fraction (Section 4.2.6).

The results are shown in Table 4.2.9 and Figure 4.2.12.

Table 4.2.9 The effect of particle shape on the disruption constant and the maximum extent of disruption of yeast (concentration of 50-60 kg m^{-3}) at a volume fraction of solids of 0.20 of particles of geometric mean sizes 304 μm and 364 μm and an impeller speed of 772 rpm

particle shape and geometric mean size (μm)	disruption rate constant, k (min^{-1})	maximum extent of disruption R_i/R_m, in %
smooth (304 μm)	0.00035	74
jagged (364 μm)	0.00028	88

The results shown in Table 4.2.9 indicate a marginal difference in that the disruption rate constant is lower using jagged particles. In contrast the maximum extent of disruption is higher when using jagged particles.

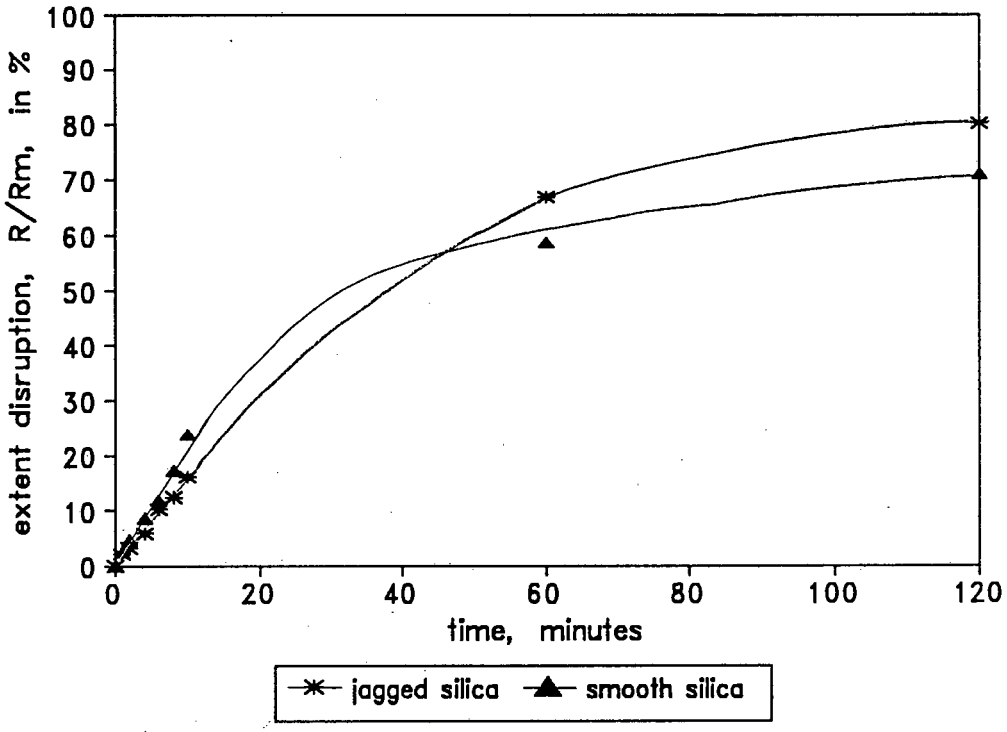

Figure 4.2.12 The effect of particle shape on the extent of disruption of yeast at an impeller speed of 772 rpm and a volume fraction of silica of 0.20 (jagged silica of 364 μm, smooth silica of 304 μm)

As can be seen from Figure 4.2.12 the initial rate of disruption is more rapid with smooth particles, however the extent of disruption reaches a lower maximum than that obtained using jagged particles. The difference in texture of smooth and jagged silica particles is shown in Figure 4.2.13.

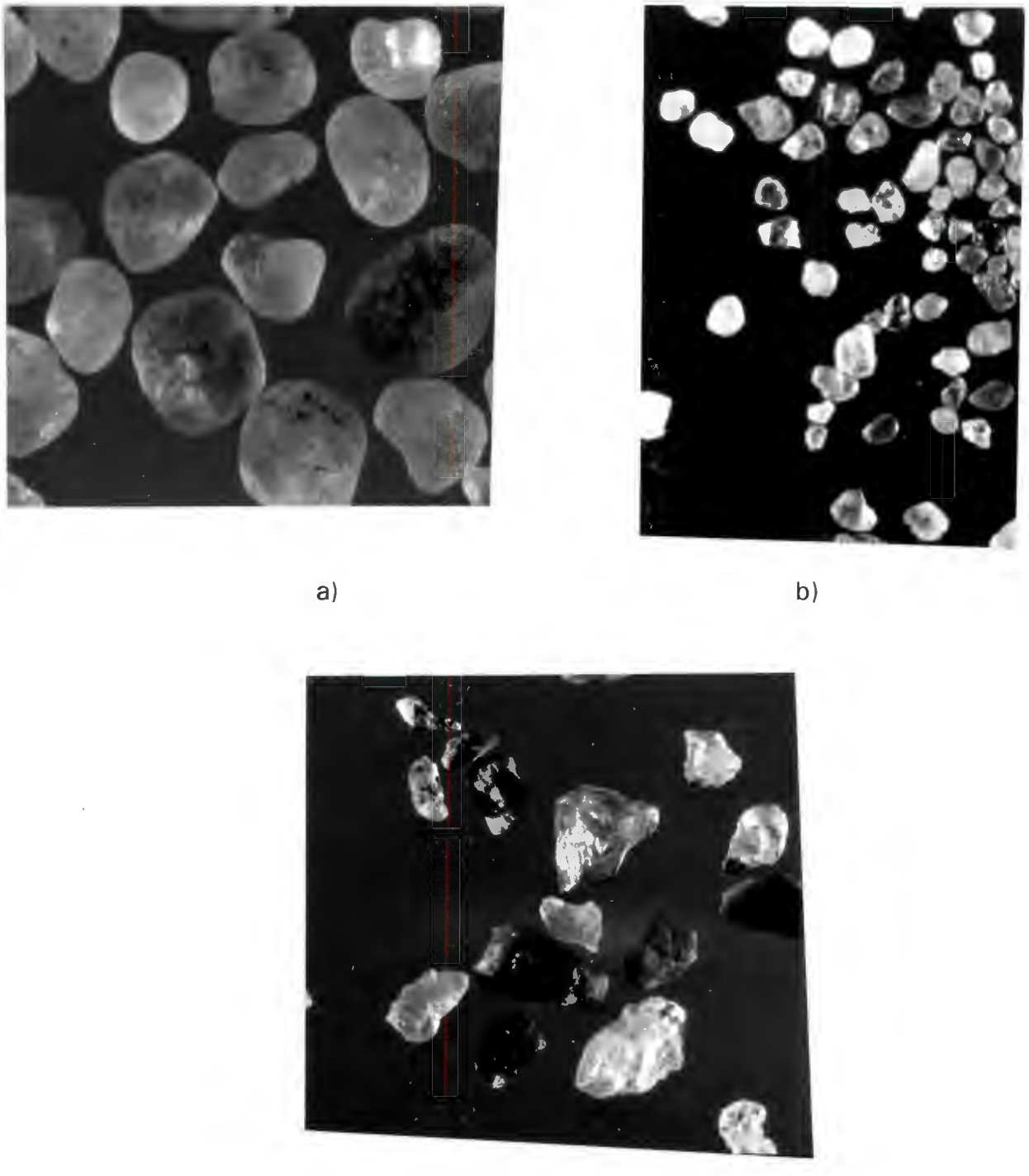

a) b)

c)

Figure 4.2.13 Photomicrograph of smooth and jagged silica particles. a) smooth silica of mean size 1245 μm, b) smooth silica of mean size 304 μm, c) jagged silica of mean size 364 μm. Magnification: 1 mm

4.2.9 The effect of the concentration of yeast

The effect of concentration of the yeast in the range 20 kg m^{-3} to 130 kg m^{-3} on the rate and extent of disruption was investigated at an impeller speed of 772 rpm and a volume fraction of solids (silica particles of 1245 μm diameter) of 0.20.

The results of the experiments are shown in Figure 4.2.14. A marginal decrease in the disruption rate constant of approximately 0.00016 s^{-1} with increasing concentration of yeast was observed. After an initial increase in the extent of disruption, on increasing the concentration of yeast from 20 to 55 kg m^{-3}, the extent remained constant for the higher concentrations of yeast.

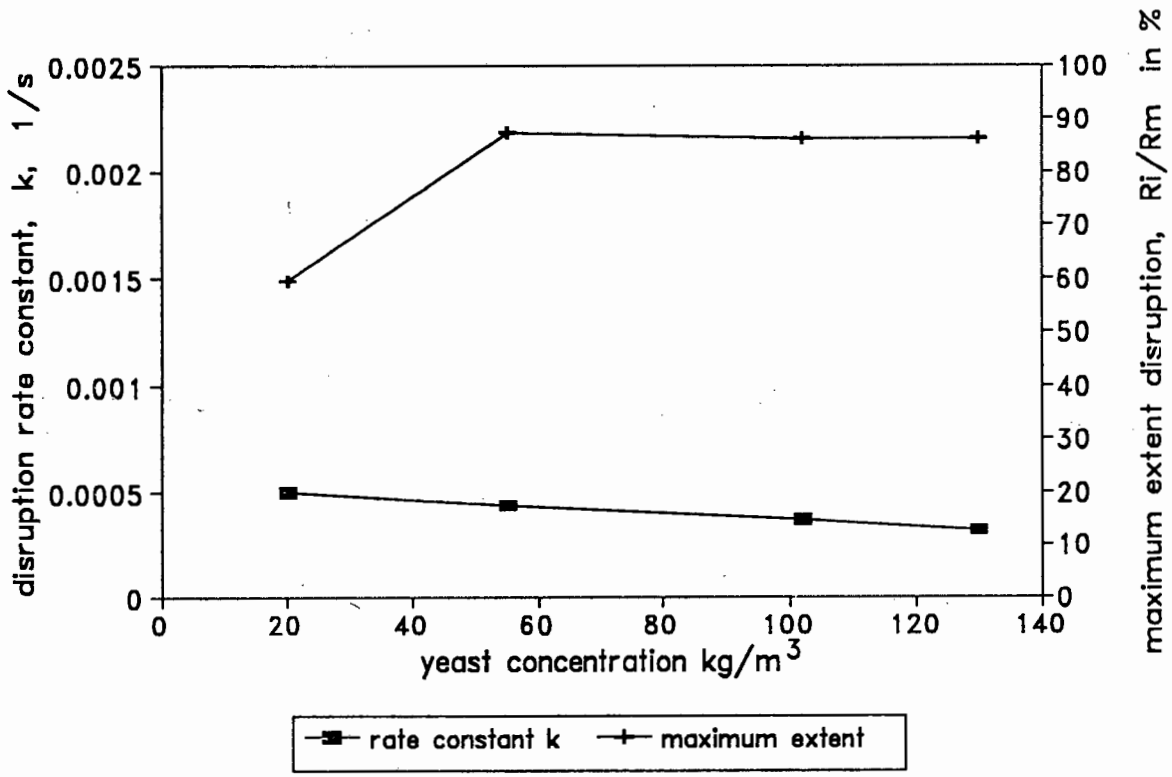

Figure 4.2.14 The effect of the concentration of yeast on the disruption rate constant and the maximum extent of disruption of yeast at a volume fraction of solids of 0.20 (silica particles of mean size 1245 μm) and an impeller speed of 772 rpm

The results obtained by Limon-Lason *et al.* (1979) displayed a similar trend of decreasing disruption rate constant with increasing yeast concentration in a bead mill. The protective effect of viscosity in mammalian microcarrier cultures was reported by Croughan *et al.* (1989) and Lakhotia and Papoutsakis (1992).

4.3 THE RELEASE OF A WALL-ASSOCIATED PROTEIN, THE ENZYME INVERTASE

4.3.1 Introduction

In all of the disruption tests presented in Section 4.2 the value of the maximum extent of disruption was never found to exceed 98%. The experiments carried out at a constant impeller speed of 772 rpm and volume fractions of solids 0.05, 0.10, 0.20, 0.30 and 0.40, the resulting maximum extents of disruption were 98%, 98%, 96%, 93% and 97% (Section 4.2.4). Similarly in the experiments carried out at a constant volume fraction of 0.20 of silica and impeller speeds ranging from 150 rpm to 1090 rpm, the maximum extents of disruption ranged from 8% to 96%, respectively (Section 4.2.5). Therefore the question arises as to why the maximum disrupted soluble protein, R_i, released in the stirred tank is consistently lower than the maximum available soluble protein, R_m.

In order to examine the type of breakage in the stirred tank, the release of a wall-associated protein, namely the enzyme invertase, was investigated. The enzyme invertase is found in the outer mannan layer of the yeast cell wall (Hunter and Asenjo, 1987). The release of invertase may indicate the degree of damage inflicted on the yeast wall. The relationship between the amount of wall-associated protein and total soluble protein released may indicate whether the cell wall is bruised, releasing wall-associated protein, or ruptured, releasing the cytoplasmic soluble protein.

As enzymes are proteins, specific in function, the first order rate equation may be used to describe the kinetics of their release. Marffy and Kula (1974) investigated enzyme yields from brewers' yeast cells and utilized first order kinetics for enzyme release. The following form of Equation 4.1.1 was used:

$$\ln R_{Wmax}/(R_{Wmax} - R_W) = k_{Rw}\, t \qquad \text{Eqn. 4.3.1}$$

where R_{Wmax} = maximum available wall-associated protein (enzyme) units/ g yeast

R_W = wall-associated protein (enzyme) released, units/ g yeast

k_{Rw} = first order rate constant for release of enzyme, s^{-1}

The concentration of enzymes is expressed in terms of the activity of the enzyme. A unit of invertase activity is defined as the amount of enzyme which hydrolyses 1 μmole of sucrose to produce 1 μmole of glucose per minute at 30°C and pH 4.9.

The results of the release of invertase experiments described in Section 3.4.7 were analysed to determine the first order rate constant for the release of invertase using Equation 4.3.1, in the same manner as shown for the release of the total soluble protein (Section 4.2.1).

4.3.2 Determination of R_{Wm} and R_{Wmax}

An analogous quantity to the maximum available soluble protein, R_m, was defined for the release of the wall-associated protein, the enzyme invertase. R_{Wm} was defined as the maximum wall-associated protein released by disruption in a French Press. The maximum disrupted wall-associated protein released by disruption in the stirred tank was termed R_{Wmax}. An extent of release of wall-associated protein was defined as the ratio of the wall-associated protein release, R_W and the wall-associated protein released by disruption in the French Press, R_{Wm}.

Disruption tests were carried out with yeast of concentration 50-60 kg m^{-3} in the French Press and in the stirred tank at an impeller speed of 772 rpm and a volume fraction of 0.20 of 1245 μm silica. The release of the wall-associated protein and the total soluble protein (wall-associated and cytoplasmic protein) was monitored. The results of these experiments are shown in Table 4.3.1.

Table 4.3.1 The release of the wall-associated protein, invertase, and the total soluble protein by disruption of yeast (concentration of 50-60 kg m^{-3}) in the French Press and in the stirred tank at an impeller speed of 772 rpm and a volume fraction of 0.20 of 1245 μm silica

apparatus	wall-associated protein release, units invertase per g yeast	total soluble protein release, mg protein per g yeast
French Press	1568	490
stirred tank	2070	448

The results show that the maximum release of the wall-associated protein, invertase, is obtained by disruption of yeast in the stirred tank. The amount of wall-associated protein released by disruption in the stirred tank was thus defined as the maximum disrupted wall-associated protein, R_{Wmax}. A larger amount of total soluble protein was released by disruption in the French Press.

The extent of release of wall-associated protein, R_W/R_{Wm}, and the extent of total soluble protein release, R/R_m, for the disruption of yeast in the stirred tank at an impeller speed of 772 rpm and a volume fraction of silica of 0.20 is shown in Figure 4.3.1.

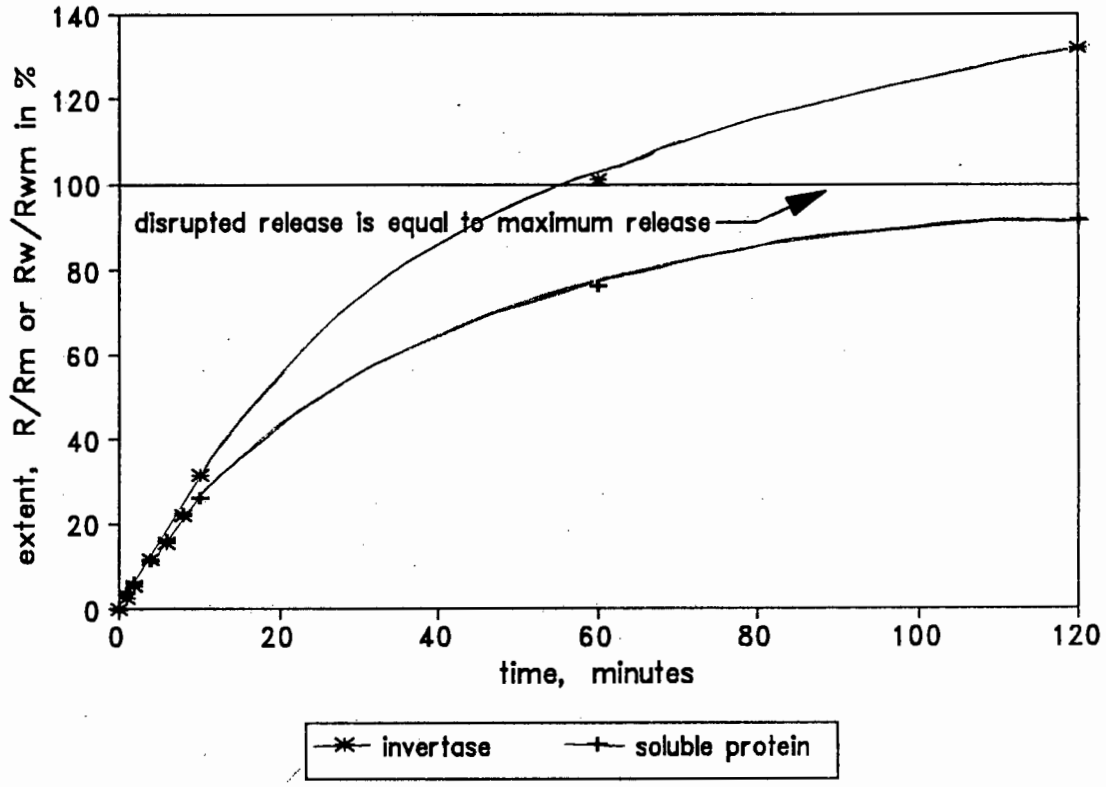

Figure 4.3.1 The extent of release of wall-associated protein, R_W/R_{Wm}, and the extent of the release of total soluble protein, R/R_m, from yeast (concentration 50-60 kg m^{-3}) at an impeller speed of 772 rpm and a volume fraction of solids of 0.20 of 1245 μm silica.

The results show that the release of wall-associated protein from yeast is greater in the stirred tank than in the French Press. In contrast, the release of the total soluble protein (wall-associated and cytoplasmic proteins) from yeast is greater by disruption in the French Press.

These results indicate that the walls of the yeast cells are being bruised and damaged more efficiently in the stirred tank than in the French Press, however the total disruption of the cells is more complete in the French Press.

In the French Press the cells are burst open upon rapid decompression and extrusion through the valve. This method of disruption may not cause equivalent damage to the cell wall and thus the release of the wall associated proteins will not be complete. The collisions between particles in the experimental rig may

cause more damage to the cell wall, in addition to rupturing the cells, therefore resulting in more complete release of the wall associated proteins.

4.3.3 The effect of the impeller speed on the release of wall-associated and total soluble protein

Disruption tests were carried out in the 1 dm^3 stirred tank with 50-60 kg m^{-3} yeast suspensions at a constant volume fraction of solids of 0.20 of 1245 μm silica and impeller speeds ranging from 115 rpm (equivalent tip speed of 0.32 m s^{-1}) to 772 rpm (equivalent tip speed of 2.2 m s^{-1}). The release of both the wall-associated protein and the total soluble protein was monitored. The disruption rate constants were calculated as shown in Section 4.2.1 for the release of total soluble protein. The rate constant for the release of invertase was calculated similarly using Equation 4.3.1.

The results of these experiments are shown in Figure 4.3.2. The ratio of the first order rate constants of the release of invertase, k_{Rw}, and the release of total soluble protein, k, is shown as a function of the impeller speed.

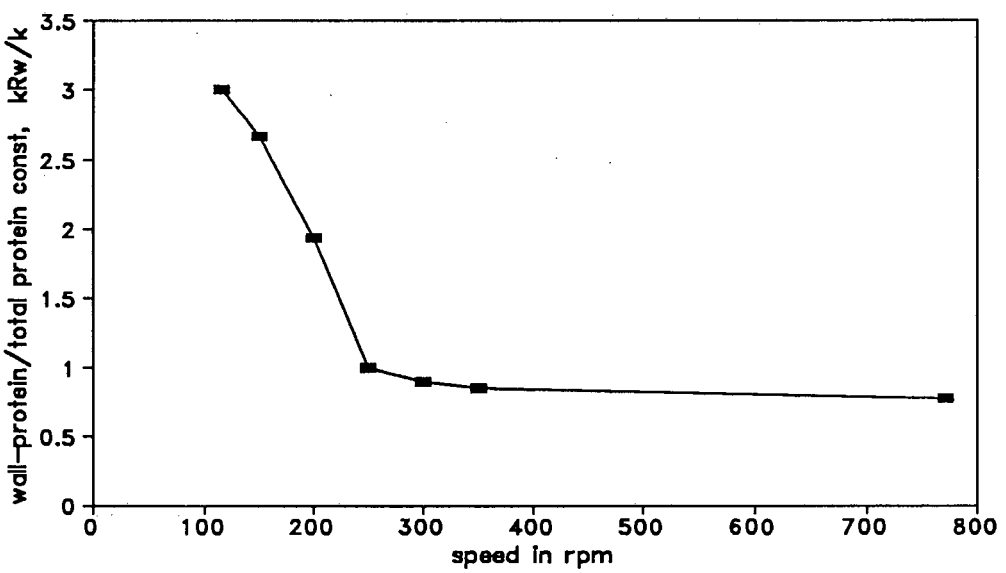

Figure 4.3.2 The ratio of the rate constant of the release of invertase (wall-associated protein), k_{Rw}, and the rate constant of the release of total soluble protein, k, as a function of impeller speed at a constant volume fraction of solids of 0.20 of 1245 μm silica

The results show that the rate constant of the release of the wall-associated protein, the enzyme invertase, is much greater than the rate constant of total soluble protein release at impeller speeds of less than 250 rpm. At impeller speeds of 350 rpm and greater the two rate constants are effectively equal in value. This indicates that at low impeller speeds the damage caused to the yeast cells is limited to the outer mannan layer of the yeast wall where invertase is located. At higher impeller speeds the cell wall is damaged more severely, releasing cytoplasmic proteins as well as wall-associated proteins.

4.3.4 The effect of the concentration of solids on the release of the wall-associated protein, invertase, and the release of the total soluble protein

Disruption tests were carried out with yeast (concentration of 50-60 kg m^{-3}) at a constant impeller speed of 772 rpm and varying volume fractions of solids from 0.05 to 0.20 of 1245 μm silica. The release of the wall-associated protein, invertase and of the total soluble protein was monitored. The ratio of the rate constants of wall-associated protein release and total soluble protein release as a function of the volume fraction of solids is shown in Figure 4.3.3.

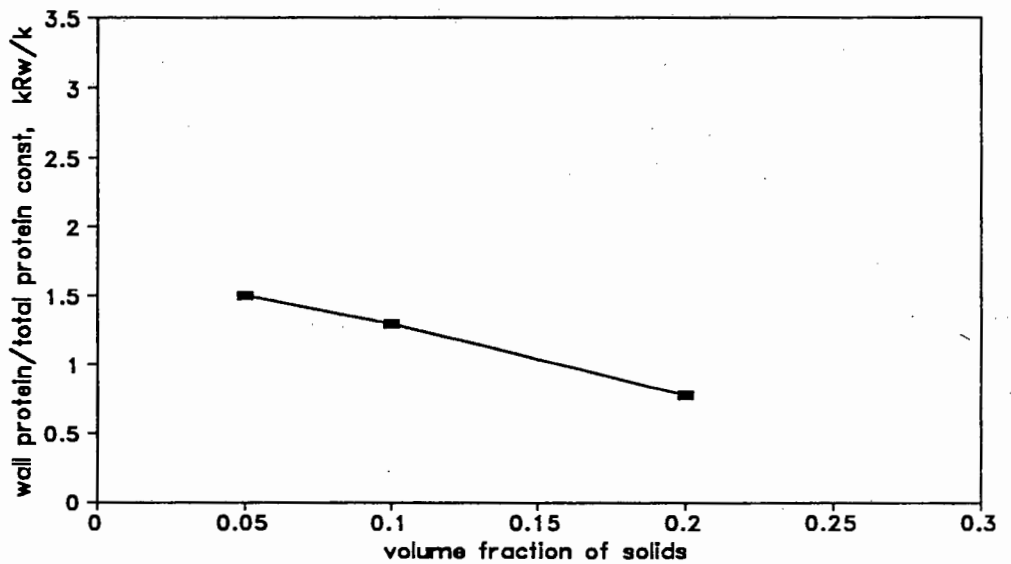

Figure 4.3.3 The ratio of the rate constant of the release of the wall-associated protein, k_{Rw}, and the rate constant of the release of the total soluble protein, k, as a function of the volume fraction of solids (silica, 1245 μm) at an impeller speed of 772 rpm

The results show that the rate constant of the release of invertase is greater than the rate constant of total soluble protein release at a volume fraction of solids of 0.05. However, the difference in the two rate constants does not appear to be as great as that observed at impeller speeds of less than 200 rpm (Section 4.3.2.2).

4.4 CONCLUSIONS

This chapter presented the results of the investigation into the effects of agitation in a stirred tank with solid particles on the disruption of yeast.

It was established that first order kinetics were applicable to describe the disruption of yeast in terms of the soluble protein released in the stirred tank.

The release of soluble protein from yeast by disruption in French Press was found to be greater than by disruption of yeast in the stirred tank at an impeller speed of 1090 rpm and a volume fraction of solids of 0.40.

The presence of particulates was found to cause cell disruption. Furthermore, the properties of the particulates have exhibited an effect on the disruption rate constant and the maximum extent of disruption of yeast. The maximum extent of disruption was not affected by increasing the volume fraction of solids from 0.05 to 0.40 at a constant impeller speed of 772 rpm. In addition, an increase in impeller speed from 772 rpm to 1090 rpm did not increase the maximum extent of disruption. The effects of the particle density in the range 1600 kg m^{-3} to 4500 kg m^{-3} on the maximum extent of disruption were insignificant. The maximum extent of disruption of yeast was not affected considerably by an increase in the concentration of the yeast from 20 kg m^{-3} to 130 kg m^{-3}. In contrast to these findings, it was observed that the maximum extent of disruption increased dramatically over an increase of impeller speed from 150 rpm to 772 rpm. Similarly, a large increase in the maximum extent of disruption was observed with an increase in particle size from 114 μm to 304 μm.

The disruption rate constant increased significantly with an increase in the concentration of solids. In addition an increase in the impeller speed up to 772

rpm resulted in an increase in the disruption rate constant. The disruption rate constant increased with increasing particle size up to 703 μm. A marginal increase in disruption rate with increased particle density was observed. An increase in the concentration of yeast caused a minimal decrease in the disruption rate constant.

Partial and complete cell damage was investigated by monitoring the release of a wall-associated enzyme, invertase. The maximum release of the wall-associated protein, invertase, by disruption of yeast was lower in the French Press than in the stirred tank at an impeller speed of 772 rpm and a volume fraction of solids of 0.20. This indicates that damage to the cell wall is more prevalent in the stirred tank. The release of total soluble protein was more complete by disruption in the French Press than in the stirred tank. These findings imply that the disruption mechanisms in the French Press cause complete rupture of the cells, whilst the mechanisms in the stirred tank cause bruising to the cell walls in addition to total disruption.

The rate constant of the release of the wall-associated protein (invertase) was greater than the rate constant of the release of the total soluble protein at impeller speeds of less than 200 rpm. Similarly, the rate of release of invertase was more rapid than the release of total soluble protein at a volume fraction of solids of 0.05. These results imply that at low impeller speeds and low volume fractions of solids the outer layer of the yeast cell wall is partially damaged, releasing wall-associated proteins, but retaining cytoplasmic proteins.

CHAPTER 5
ANALYSIS OF EFFECTS OF SOLID PARTICLES ON DISRUPTION OF YEAST

5.1 INTRODUCTION

In this chapter the analysis of the results presented and discussed in Chapter 4 are extended. Firstly, the variation of the disruption rate constant with the concentration of solids, the impeller speed and the particle size are modelled using mathematical equations such as the power law model and the exponential model.

Secondly, the correlation of the disruption rate constant against any of the well known measures of agitation intensity, such as the impeller Reynolds' number and the power number, are examined. Furthermore the impeller power input per unit mass of slurry are investigated as a measure against which to correlate the disruption rate constant.

Having studied various methods of correlating the disruption rate constant, the extent of disruption are investigated in terms of the energy required to release soluble protein from the yeast.

Finally, the suspension of the particles in the stirred tank and the effect of complete or incomplete suspension on disruption results presented in Chapter 4 are discussed.

5.2 GENERAL APPLICABILITY OF FIRST ORDER KINETICS TO MICROBIAL CELL DISRUPTION

It is necessary to consider whether first order kinetics are indeed applicable to microbial cell disruption. First order kinetics have been used to describe the process of microbial cell disruption in high pressure homogenizers and mechanical bead mills (Chisti and Moo-Young, 1986; Kula and Schutte, 1987; Harrison, 1991). Damage to cells in stirred tank bioreactors has also been reported to follow first order kinetics (Reuss, 1988; Abu-Reesh and Kargi, 1991). As was shown in Chapter 4 the first order rate equation fitted the cell disruption data with high correlation coefficients. It therefore seems reasonable to conclude that

first order kinetics may be used to describe the process of microbial cell disruption.

5.3 MODELLING OF PARAMETER EFFECTS ON THE FIRST ORDER RATE CONSTANT

In this section the dependence of the disruption rate constant against the concentration of solids, the impeller speed and the particle size will be modelled.

5.3.1 Concentration of solids

The rate constant data shown in Figure 4.2.7 showed the effect of the concentration of solids. As shown in Table 4.2.5 the rate constant data of Currie *et al.* (1972) obtained in a bead mill was of the same order of magnitude as that obtained in this study. Although, rate constant data obtained in a bead mill is not entirely comparable to the data obtained in this study, it may prove useful as a basis.

The rate constant data from this study together with the data from Currie *et al.* (1972) were fitted independently and collectively to the power law model and the exponential model. The choice of models was based on the shape of the rate constant data shown in Figure 4.2.7.

An exponential model of the following form fitted the experimental data of this study with a correlation of 0.954:

$$k = 0.00001863\ (507850)^{\phi} \qquad \text{Eqn. 5.3.1}$$

where k = first order disruption constant
ϕ = solids volume fraction

The power law model found to fit the experimental data of this study with a correlation of 0.999, was of the following form:

$$k = 0.00198\ (\phi)^{2.33} \qquad \text{Eqn. 5.3.2}$$

Analysis of the combined data of this study and of Currie *et al.* (1972) resulted in an exponential model of the following form:

$$k = 7.85*10^{-5}\,(386.3)^{\phi} \qquad \text{Eqn. 5.3.3}$$

The correlation coefficient was 0.875.
In addition the power law model which fitted the combined data with a correlation coefficient of 0.991 was:

$$k = 0.01003\,(\phi)^{2.03} \qquad \text{Eqn. 5.3.4}$$

The results of the analysis are shown in Figure 5.3.1.

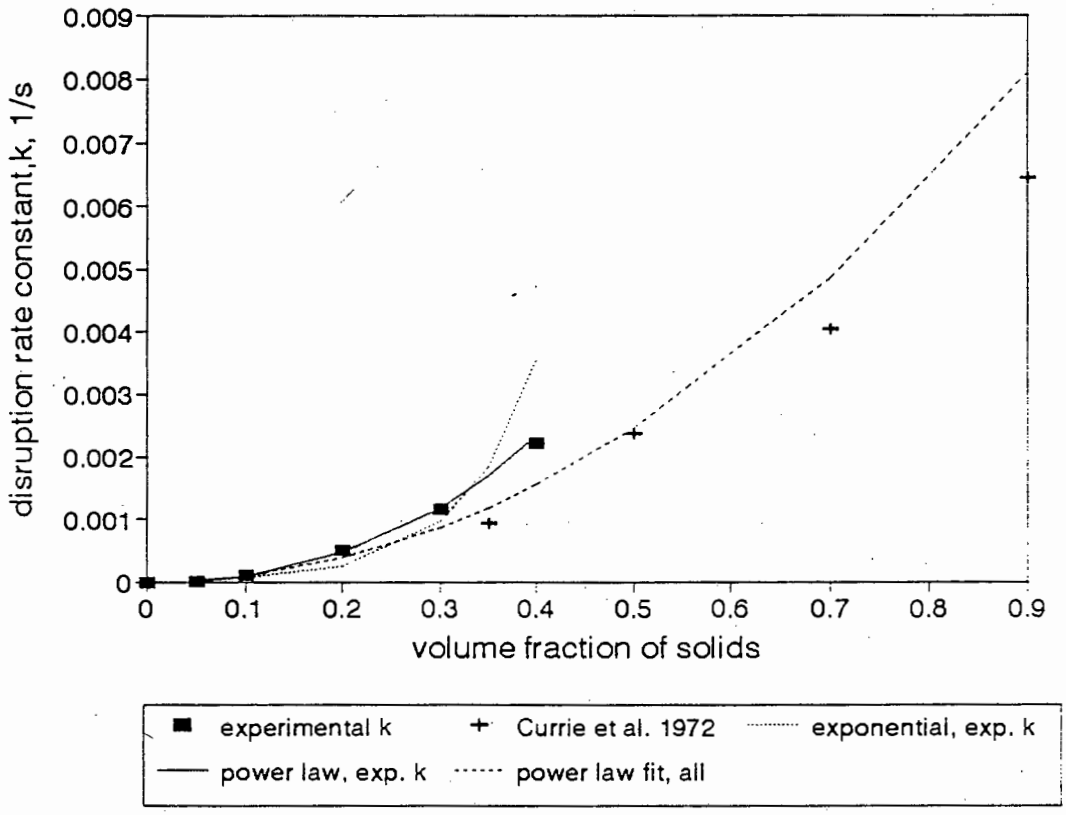

Figure 5.3.1 Mathematical model fits of the disruption rate constant of yeast suspensions (concentration of 50-60 kg m^{-3}) as a function of volume fraction of solids where silica particles of mean size of 1245 μm were suspended at an impeller speed of 772 rpm

It can be seen in Figure 5.3.1 that appropriate fits to the experimental data were obtained with the power law, however a close fit to the exponential model was not obtained.

The analysis indicates that a power law function can be used to describe the effect of solids loading on the disruption rate constant of yeast cells in agitated stirred tanks and bead mills.

5.3.2 Impeller speed

The effect of speed on the disruption rate constant is shown in Figure 4.2.8. Models investigated to describe this data include the power law function, the logarithmic function and the logistic function. The logistic curve is sigmoidal in shape and describes microbial growth by including an inhibiting factor to the population growth (Bailey and Ollis, 1977). The inhibition was assumed to be proportional to the square of the cell concentration x.

$$dx/dt = k_m x (1 - x/x_m) \qquad \text{Eqn. 5.3.5}$$

where x = cell concentration
k_m = logistic rate constant
x_m = maximum cell concentration

The integrated equation:

$$x = x_o \exp(k_m t)/ [1 - x_o/x_m (1 - \exp(k_m t))] \qquad \text{Eqn. 5.3.6}$$

is expressed more conveniently in the logarithmic form:

$$\ln[x/(x_m-x)] = k_m t + \ln[x_o/(x_m-x_o)] \qquad \text{Eqn. 5.3.7}$$

where x_o = initial cell concentration

In this study a similar form of logistic equation was investigated in which the cell concentration, x, was replaced by disruption constant k and the logistic rate constant, k_m, was replaced with the impeller speed:

$$\ln [k/(k_{max}-k)] = c^* N + \ln[k_{min}/(k_{max}-k_{min})] \quad \text{Eqn. 5.3.8}$$

where
- k = disruption rate constant
- k_{max} = maximum value of k
- k_{min} = minimum value of k
- c = slope of line
- N = impeller speed in rpm

The power law and logarithmic models were also used to fit the effect of the impeller speed on the rate constant.

The rate constant data, obtained in a bead mill, of Currie *et al.* (1972) shown in Table 4.2.6 were used in addition to the data from this study.

The experimental data from this study fitted a logistic model of the following form with a correlation of 0.923.

$$\ln [k/(k_{max} - k)] = 0.0061 N - 3.6135 \quad \text{Eqn. 5.3.9}$$

The combined data of this study and of Currie *et al.* (1972) fitted a logistic model of the following form with a correlation coefficient of 0.886:

$$\ln [k/(k_{max} - k)] = 0.0040 N - 4.109 \quad \text{Eqn. 5.3.10}$$

The power law expression obtained using the experimental data from this study was:

$$k = 1.278^*10^{-9} (N)^{1.906} \quad \text{Eqn. 5.3.11}$$

The correlation of this model was 0.953.

The results of the model fitting to the disruption rate constant as a function of impeller speed are shown in Figure 5.3.2.

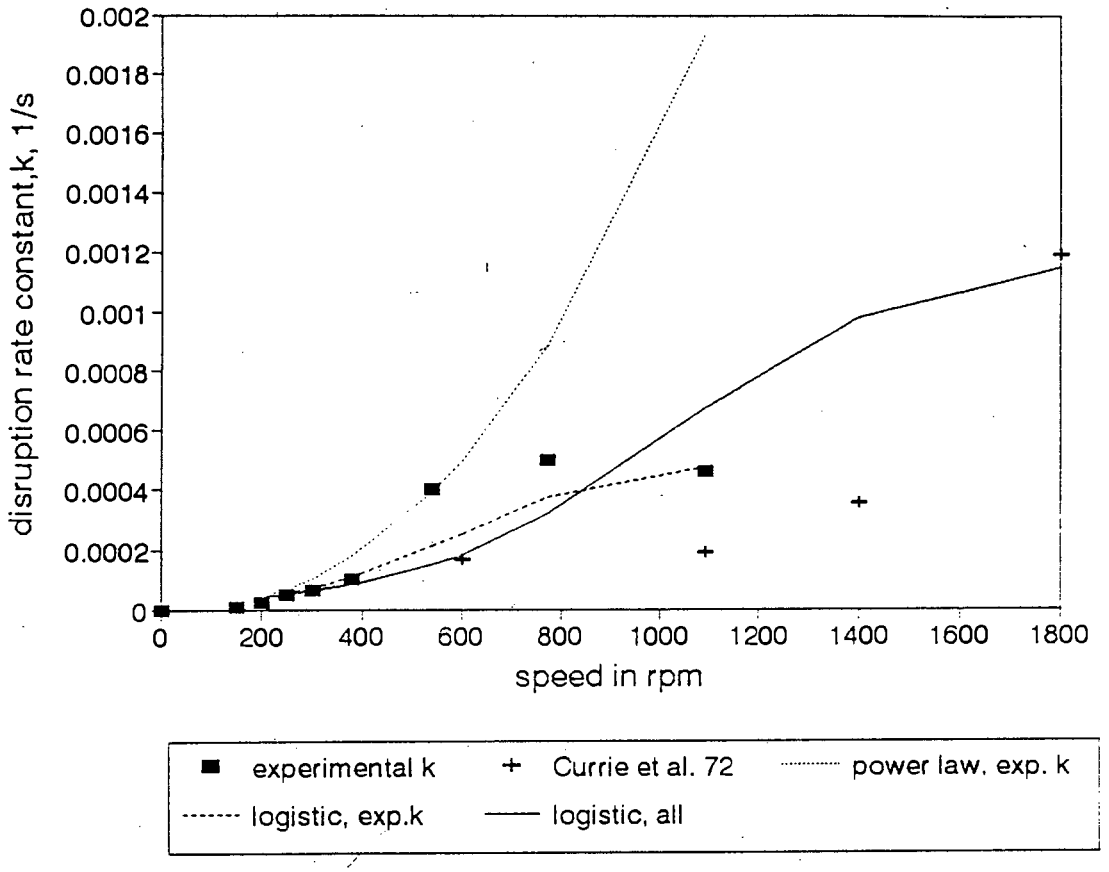

Figure 5.3.2 Model fits of disruption rate constant of yeast (concentration of yeast 50-60 kg m^{-3}) as a function of impeller speed at a volume fraction of solids of 0.20 (silica particles of mean size 1245 μm)

The disruption rate constant data shown in Figure 5.3.2 follows a power law curve initially, however the power law model separates from the data after a speed of 600 rpm. This analysis has shown that none of the models may be used to predict the disruption rates at different speeds with any degree of certainty. This implies that the use of mathematical models to describe the cell disruption process is not rigorous and that mechanistic models should be investigated.

5.3.3 Particle size

The disruption rate constant data shown in Figure 4.2.9 against the particle size was fitted to the logarithmic model. The logistic curve was also examined. The

resultant logarithmic model of the following form has a correlation coefficient of 0.945:

$$k = -0.00117 + 2.46*10^{-4} \ln d_p \qquad \text{Eqn. 5.3.12}$$

where d_p = particle mean diameter, μm

A logistic curve of the following form was used to model the effect of particle size on the disruption rate constant:

$$\ln [k/(k_{max} - k)] = c\, d_p + \ln [k_{min}/(k_{max} - k_{min})] \qquad \text{Eqn. 5.3.13}$$

where c = slope of line

The model obtained from this procedure was:

$$\ln [k/(k_{max} - k)] = 0.0061\, d_p - 2.011 \qquad \text{Eqn. 5.3.14}$$

The correlation coefficient of this curve was 0.852. The results of this analysis are shown in Figure 5.3.3.

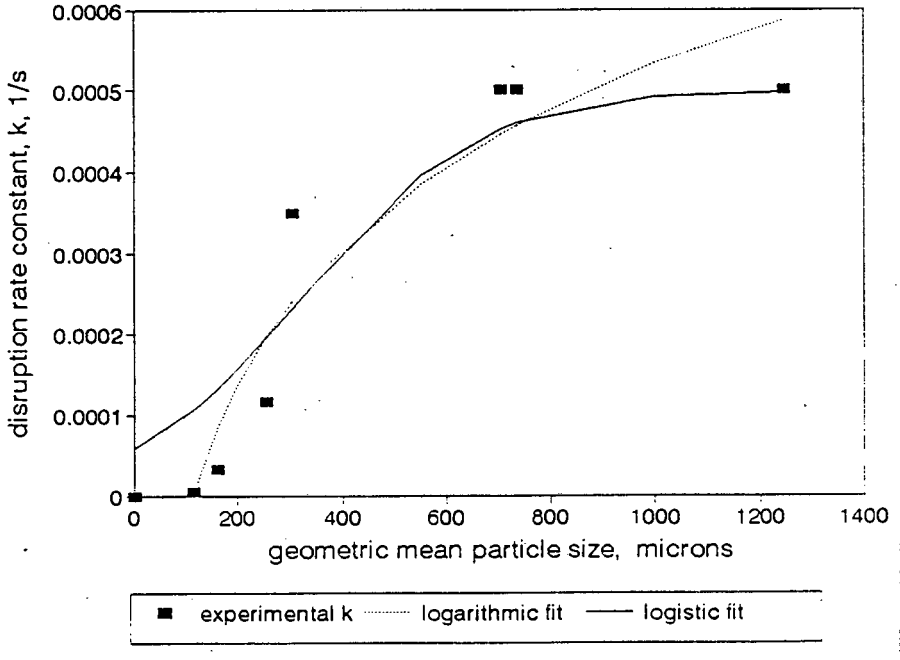

Figure 5.3.3 Mathematical modelling of the disruption rate constant of yeast (concentration of yeast of 50 - 60 kg m^{-3}) obtained upon agitation with different sizes of silica particles at a volume fraction of solids of 0.20 and an impeller speed of 772 rpm

As is shown in Figure 5.3.3 the logarithmic and logistic models follow a similar path the experimental data, however the correlation coefficients do not indicate satisfactory degrees of fit. The disruption rate on agitation with particles of a particular size may be approximated by either the logarithmic fit or the logistic curve, however the degrees of fit imply that a model based on the mechanism of disruption may be more appropriate.

5.3.4 Conclusions

This analysis has shown that mathematical forms such as the exponential model and power law model can be used in a predictive way to fit the disruption data, obtained from varying the concentration of solids, of this study. This may be useful for interpolation and predictive purposes within the range studied but in fact, the analysis adds nothing to an understanding of the mechanisms involved in cell disruption.

5.4 DEPENDENCE OF THE DISRUPTION RATE CONSTANT ON THE IMPELLER REYNOLDS' NUMBER, THE PARTICLE REYNOLDS' NUMBER AND THE POWER NUMBER

5.4.1 Introduction

An investigation into the dependence of the disruption rate constant on well known measures used to characterise agitation intensity is undertaken in this section. In Section 5.3 the dependence of the disruption rate constant on the primary independent variables has been investigated. The same data can be used to discern whether combinations of quantities such as agitator speed, slurry density and power consumption can be incorporated into the impeller Reynolds' number, the particle Reynolds' number and the power number.

In this section the impeller Reynolds' number, the particle Reynolds' number and the power number were examined as more appropriate quantities against which to correlate the dependence of the disruption rate constant.

5.4.2 Dependence of the disruption rate constant on the impeller Reynolds' number

The impeller Reynolds' number was examined as a measure against which to correlate the disruption rate constant. The following form of the Reynolds' number was used:

$$N_{Rei} = \rho_{sl} * N * D_i^2 / \mu_{sl} \qquad \text{Eqn. 5.4.1}$$

where
ρ_{sl} = density of slurry, kg m^{-3}
N = impeller speed, rps
D_i = impeller diameter, m
μ_{sl} = viscosity of slurry, Pa sec

The viscosity of the slurry was estimated from the equation of Vand (1948):

$$\mu_{sl} = \mu \exp[2.5 * \phi/(1 - 0.609\ \phi)] \qquad \text{Eqn. 5.4.2}$$

where
μ = viscosity of liquid, Pa s
ϕ = volume fraction of particles

The particles are estimated as spheres. The viscosity of the yeast was estimated using the data of Reuss *et al.* (1979).

The disruption rate constant is shown in Figure 5.4.1 as a function of the impeller Reynolds' number. The effects of the impeller speed, the particle density and the concentration of yeast at a constant volume fraction of solids of 0.20 on the disruption rate constant are presented.

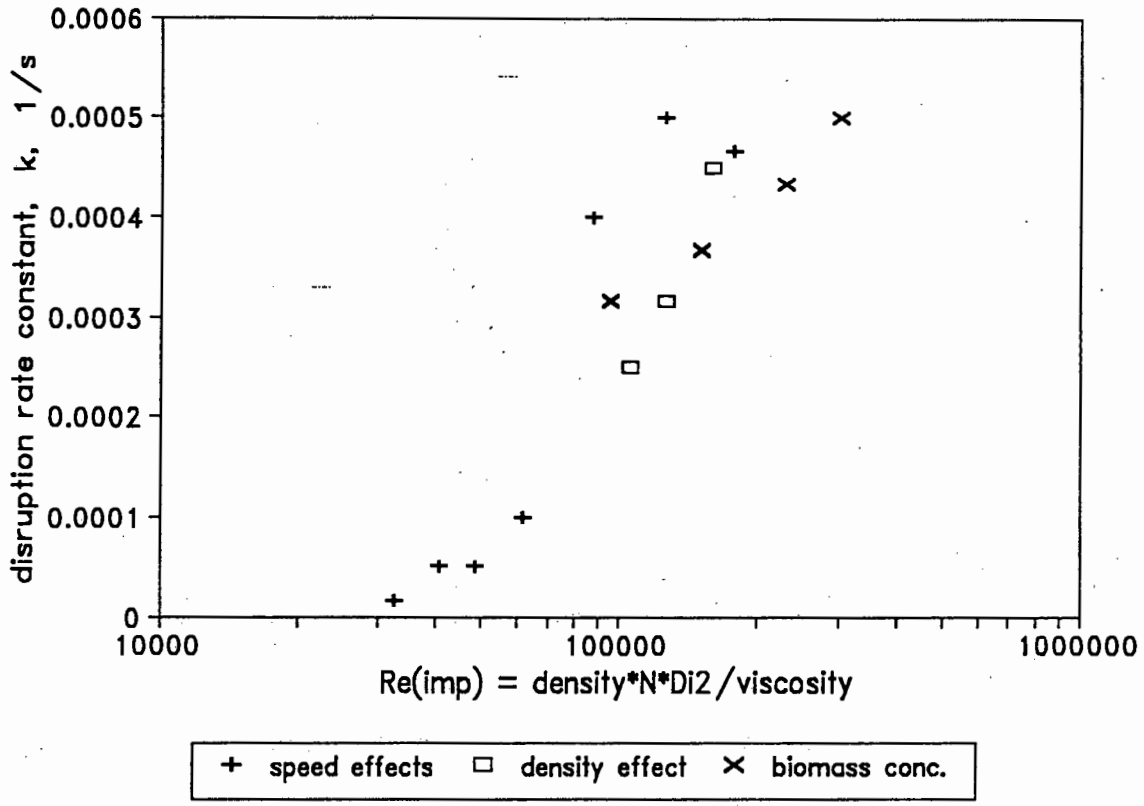

Figure 5.4.1 The disruption rate constant on variation of impeller speed, the particle density and the concentration of yeast at a volume fraction of solids of 0.20 as a function of the impeller Reynolds' number

The results showed that the disruption rate constant increased with increased impeller Reynolds' number. The data obtained from varying the impeller speed, particle density and the concentration of the yeast appeared to follow a linear trend.

5.4.3 Dependence of the disruption rate constant on the particle Reynolds' number

The disruption rate constant data obtained from the disruption tests conducted at varying particle size, particle density and the concentration of biomass at a constant impeller speed of 772 rpm and a volume fraction of solids of 0.20 were correlated against the particle Reynolds' number.

The particle Reynolds' number takes the following form:

$$N_{Rep} = \rho_{sl} * u_t * d_p / \mu_{sl} \qquad \text{Eqn. 5.4.3}$$

where u_t = settling velocity of particle, m sec^{-1}
d_p = diameter of particle, μm

The settling velocity of the particle was estimated by Stokes' law:

$$u_t = g\, d_p^2\, (\rho_p - \rho)/(18\, \mu) \qquad \text{Eqn. 5.4.4}$$

where ρ_p = particle density, kg m^{-3}
d_p = particle size, m
g = 9.81 m s^{-2}

The results are shown in Figure 5.4.2.

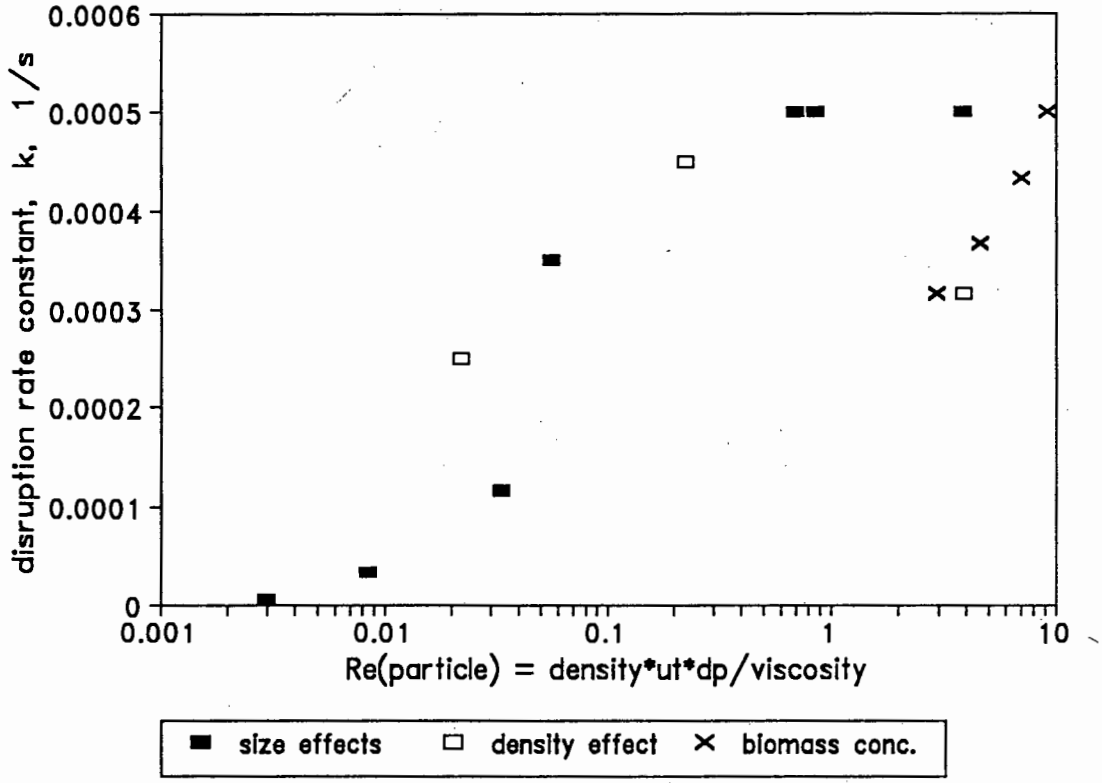

Figure 5.4.2 The disruption rate constant on variation of the particle density, concentration of the yeast and the particle size at a constant volume fraction of solids of 0.20 as a function of the particle Reynolds' number

The disruption rate constant appears to be dependent on the particle reynolds' number. The trend of the data resembles a linear function. The low disruption rate constant obtained at low particle Reynolds' numbers and the high rate constant obtained at high particle Reynolds' numbers suggests that the degree of solid suspension may play an important part in the disruption of the cells. The suspension of solids will be discussed in Section 5.6.

5.4.4 Dependence of the disruption rate constant on the power number

The power number was determined from power measurements. Power measurement was effected using a torque measurement device (Section 3.1.2). The validation of the torque measurement device is included in Appendix 6. In addition the measurements of power obtained were used to calculate power numbers which were then compared to the curves of Rushton *et al.* (1950) and Metzner *et al.* (1961). This comparison is shown in Figure 5.4.3.

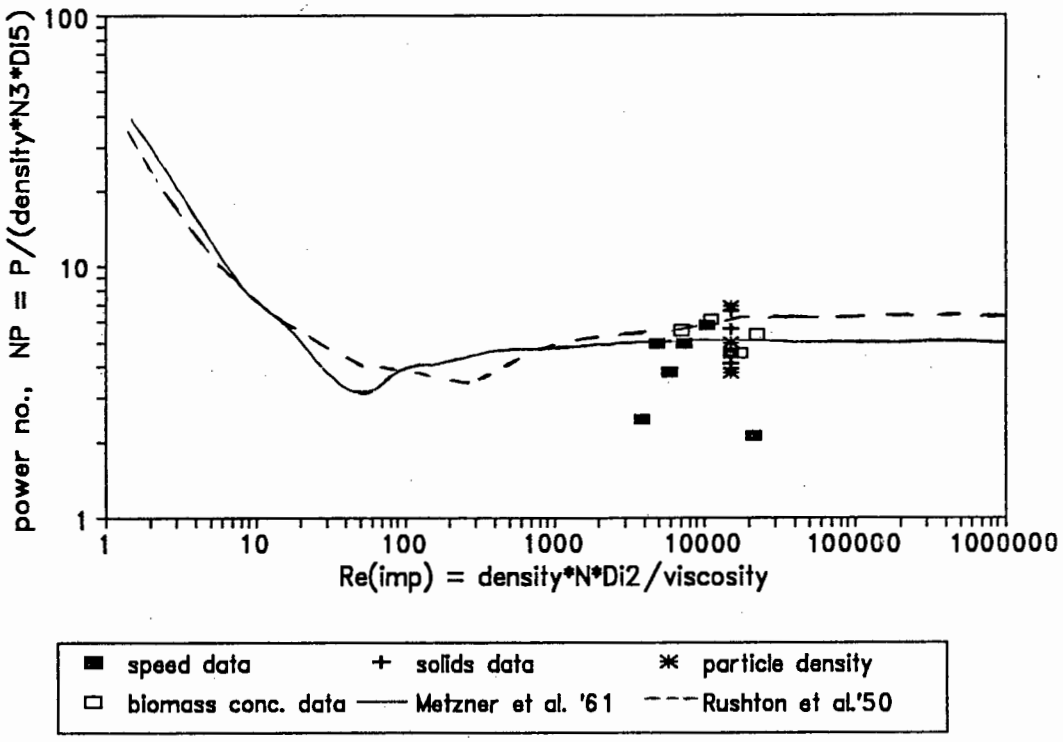

Figure 5.4.3 Impeller Reynolds' number as a function of the power number for the power measurement data of the variation of impeller speed, volume fraction of solids, particle density and the concentration of yeast experiments

The results presented in Figure 5.4.3 show that the measured power data agrees adequately with the standard power number as a function of Reynolds' number curves of Rushton *et al.* (1950) and Metzner *et al.* (1961).

The power number is represented by:

$$N_P = P/(N^3 * D_i^5 * \rho_{sl}) \qquad \text{Eqn. 5.4.5}$$

where P = power, W

The dependence of the disruption rate constant against the power number is shown in Figure 5.4.4.

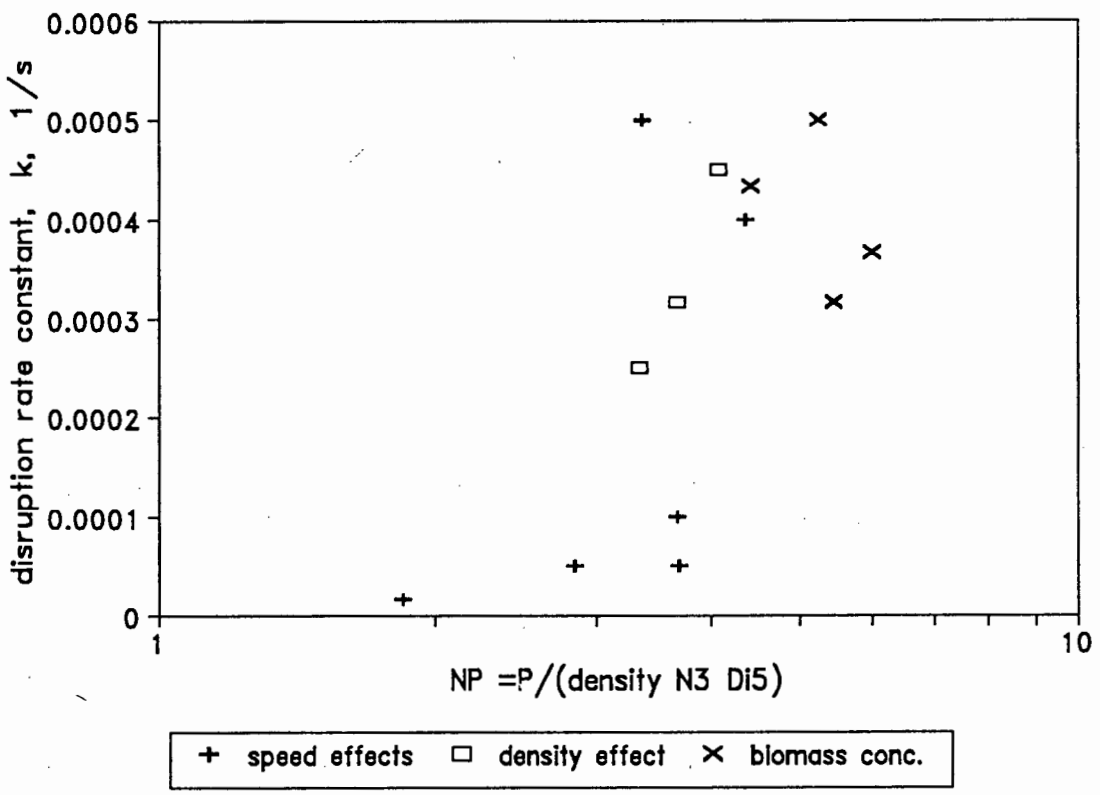

Figure 5.4.4 The disruption rate constant on variation of the impeller speed, particle density and the concentration of yeast at a constant volume fraction of solids of 0.20 as a function of the power number

It is difficult to establish a definite trend of the dependence of the disruption rate constant on the power number from Figure 5.4.4.

5.4.5 Summary of the evaluation of the dependence of the disruption rate constant on the N_{Rei}, N_{Rep} and N_P

The results shown in Figures 5.4.1, 5.4.2 and 5.4.4 indicate that although there are no definite trends, the disruption rate constant increases with increasing impeller Reynolds' number, particle Reynolds' number and power number.

The combination of the impeller Reynolds' number, the particle Reynolds' number and the power number was then investigated in order to establish whether it was possible to characterise the disruption process by an equation made up of these well known quantities. The dimensionless groups were combined in the following form:

$$k = A * N_{Rei}^{a} * N_{Rep}^{b} * N_P^{c} \qquad \text{Eqn. 5.4.6}$$

where A, a, b and c are unknown and were solved by simultaneous solution. However, the solutions led to values of A, a, b and c which when substituted in Equation 5.4.6, resulted in incorrect values of the disruption constant. The combination of parameter effects on the disruption rate constant is complex and may require analysis of the mechanisms of cell disruption.

5.5 IMPELLER POWER INPUT PER UNIT MASS SLURRY AND ENERGY REQUIREMENTS FOR DISRUPTION

5.5.1 Introduction

The dependence of the disruption rate constant on the primary variables, such as the concentration of solids, and on the impeller Reynolds' number, the particle Reynolds' number and the power number have been investigated in Sections 4.2, 5.3 and 5.4. In this section the dependence of the disruption rate constant on the impeller power input per unit mass of slurry is studied.

The preceding sections in this chapter have dealt only with the disruption rate constant data, however in this section the extent of disruption is considered in terms of the energy required for soluble protein release from the yeast cells.

5.5.2 Impeller power input per unit mass of slurry

The measured power data obtained during the disruption tests were used to calculate the impeller power input per unit mass of slurry. The method of Whitton and Nienow (1993) was used. They determined the power draw of the impeller by the measurement of the torque of the impeller shaft. This was used to calculate the impeller power input per unit mass of liquid in the following way:

$$\epsilon_M = P/(\rho V_L) \qquad \text{Eqn. 5.5.1}$$

where ϵ_M = impeller power input in W/kg
ρ = liquid density kg/m^3
V_L = volume of liquid m^3

This expression has been adapted to allow for the determination of the impeller power input per unit mass of slurry:

$$\epsilon_{sl} = P/(\rho_{sl} V_m) \qquad \text{Eqn. 5.5.2}$$

where ϵ_{sl} = impeller power input, W/kg slurry
ρ_{sl} = slurry density, kg m^{-3}
V_m = volume of slurry, m^3

The volume of the slurry was calculated by the method of Weisman and Efferding (1960) which will be discussed in detail in Section 5.6. The disruption rate constant data obtained from disruption tests at varying impeller speeds, concentrations of solids, particle densities and concentrations of yeast (Section 4.2), were correlated against the impeller power input and the results are shown in Figure 5.5.1.

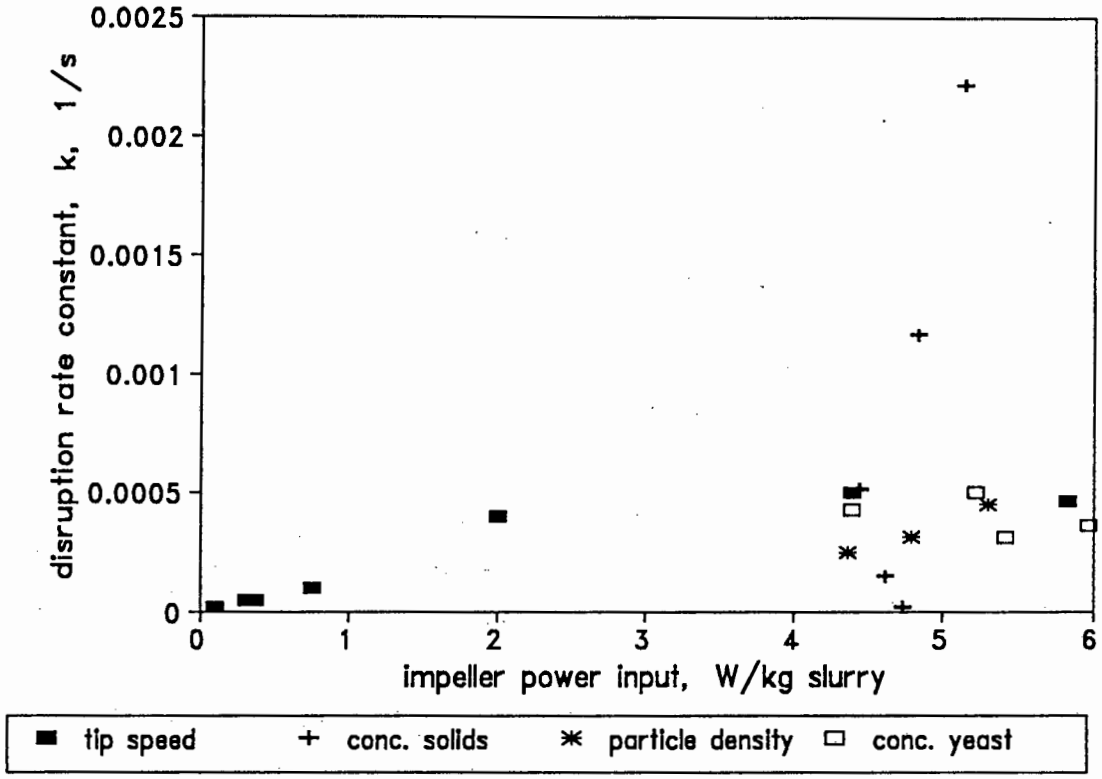

Figure 5.5.1 The effect of impeller power input per unit mass of slurry on the disruption rate constant for the impeller speed, concentration of solids, particle density and the concentration of yeast data of Section 4.2

These results show that the disruption rate constant increases with an increase in the impeller power input. The dependence of the disruption rate constant on the impeller power input is independent of the origin of the increase in power input. An increase in the tip speed causes an increase in the impeller power input and a resultant increase in the disruption rate constant. Similarly, an increase in particle density results in the same chain of events.

5.5.3 Energy requirement for the release of soluble protein from yeast cells

The following analysis was carried out to obtain information that would be useful if the stirred tank were to be used as a cell disruption apparatus. The incremental

energy requirement was calculated from the power measurement data. The extent of disruption, R/R_m, obtained from the disruption tests presented in Section 4.2 was correlated against the calculated energy.

The results are shown in Figures 5.5.2, 5.5.3, 5.5.4, 5.5.5 and 5.5.6. The results shown in Figures 5.5.2 to 5.5.5 show the extent of disruption as a function of the energy for varying concentrations of solids, impeller speeds, particle densities and concentrations of yeast. The extent of disruption for all the experiments conducted at volume fractions of solids of 0.20 and above, impeller speeds of 772 rpm and above and concentrations of yeast of 55 kg m^{-3} and above are correlated against the energy required in Figure 5.5.6.

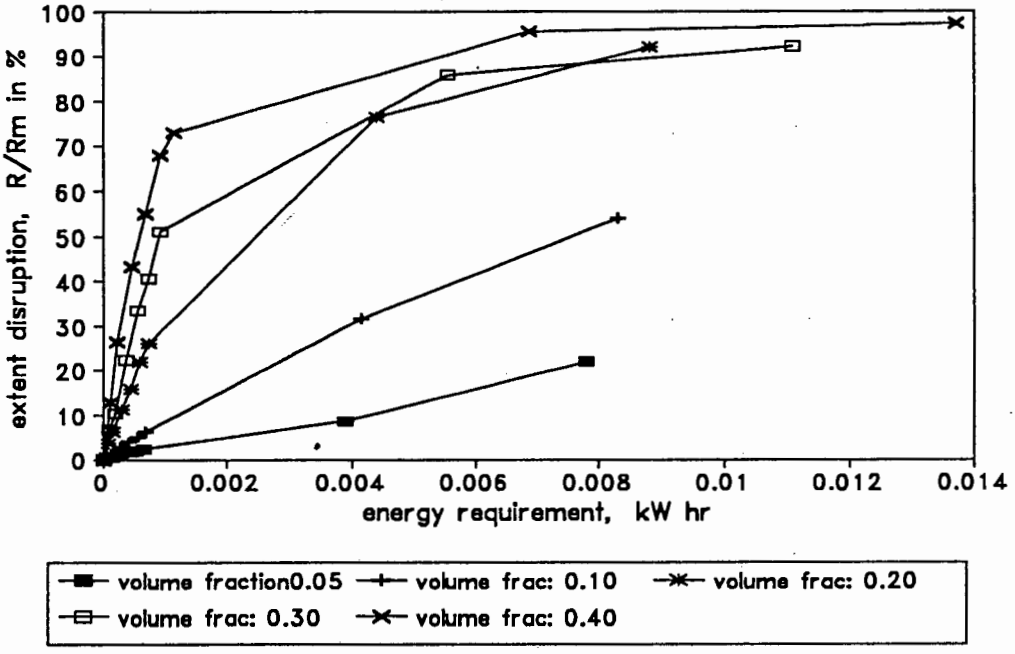

Figure 5.5.2 The effect of increasing concentration of solids (silica, particles off mean size 1245 μm) on energy requirement for yeast (50-60 kg m^{-3}) disruption at an impeller speed of 772 rpm

It can be seen from Figure 5.5.2 that to obtain a disruption extent of 50% at a volume fraction of solids of 0.10, approximately 0.008 kW hrs of energy were required, whereas to obtain the same extent of disruption using a volume fraction of 0.40 less than 0.001 kW hrs of energy were required. The results shown in Figure 5.5.2 indicate that an energy input of about 0.008 kW hrs at volume

fractions of solids of 0.20 and higher is sufficient to achieve a high extent of disruption.

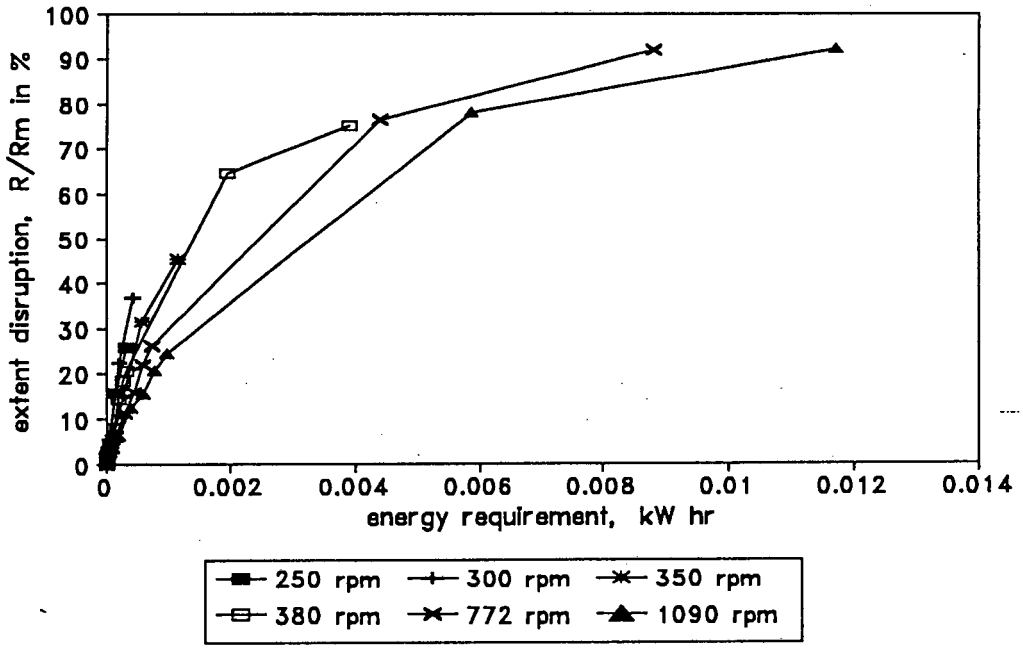

Figure 5.5.3 The effect of increased impeller speed on energy requirement for yeast disruption at a volume fraction of solids of 0.20 (silica particles of mean size 1245 μm, concentration of yeast 50-60 kg m^{-3})

The results in Figure 5.5.3 show that at a solids volume fraction of 0.20 and an impeller speed of 1090 rpm approximately 92 percent of the protein had been released on consumption of 0.012 kW hours. The same degree of protein release was obtained at an operating speed of 772 rpm on consumption of 0.090 kW hours. Hence, to maximise disruption efficiency, the system should be operated at the lowest speed giving a satisfactory level of disruption.

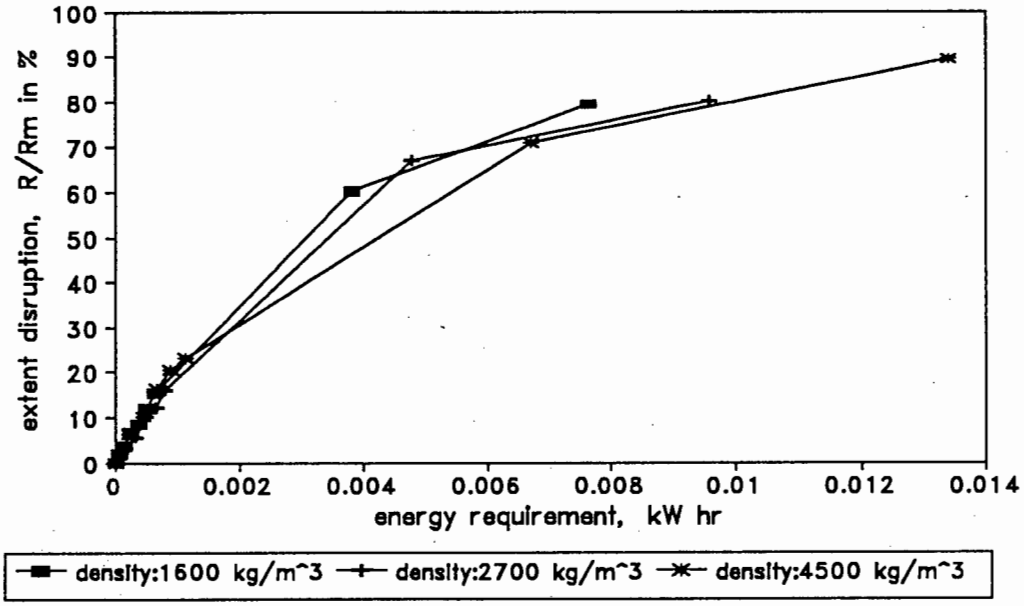

Figure 5.5.4 The effect of particle density on the energy requirement for yeast disruption at an impeller speed of 772 rpm and a volume fraction of solids of 0.20 (concentration of yeast 50-60 kg m^{-3})

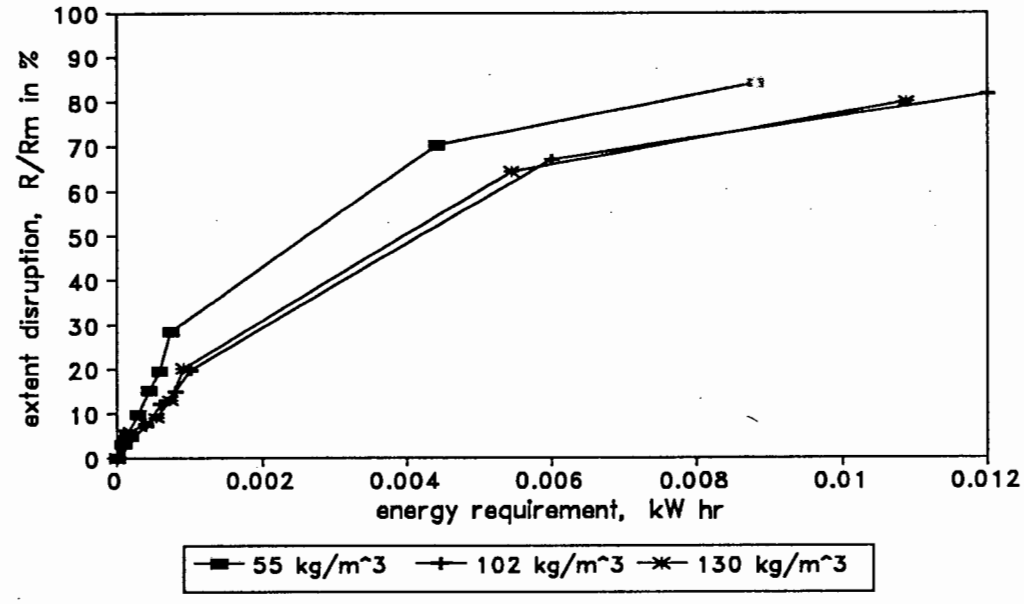

Figure 5.5.5 The effect of the concentration of yeast on energy requirement for disruption at an impeller speed of 772 rpm and a volume fraction of solids of 0.20 (silica particles of mean size 1245 μm)

The effect of particle density on the energy requirement of disruption is shown in Figure 5.4.5. The energy requirements were similar across the density range, however an increase in maximum extent of disruption is seen with increasing density, which is accompanied by an increase in energy consumption.

The effect of concentration of yeast on the energy requirement for disruption did not show any particular trend. However the energy consumption increased with increased disruption.

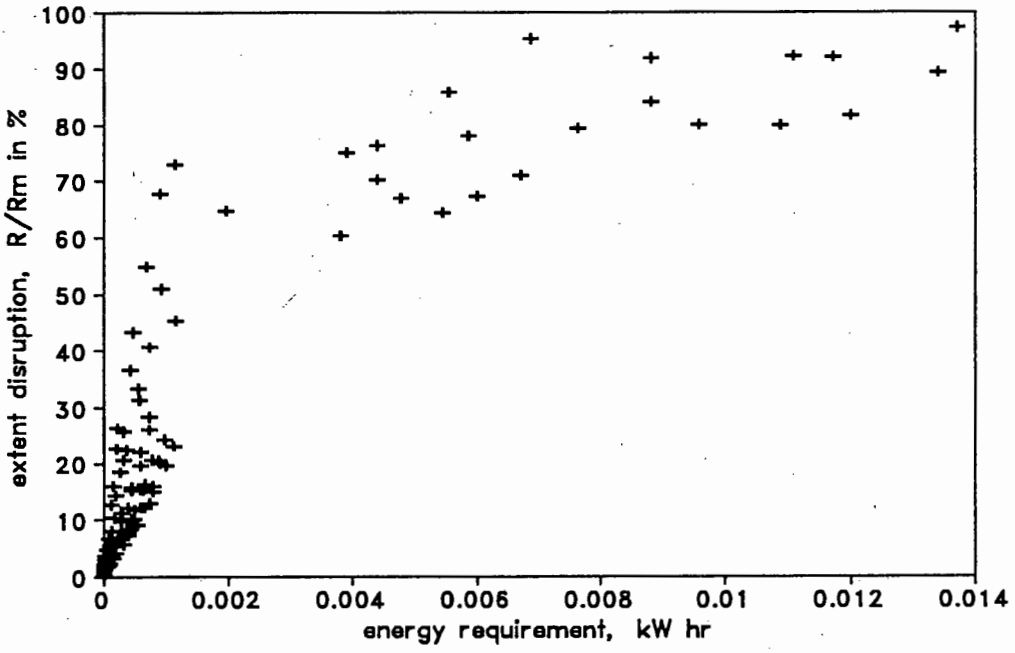

Figure 5.5.6 The extent of disruption obtained from disruption tests at volume fractions of solids ranging from 0.20 to 0.40, impeller speeds of 772 rpm and 1090 rpm, particle densities ranging from 1600 kg m^{-3} to 4500 kg m^{-3} and concentrations of yeast ranging from 55 kg m^{-3} to 130 kg m^{-3}, as a function of the energy requirement for disruption

A general trend is obvious from the data shown in Figure 5.5.6. The extent of disruption is dependent on the energy input. Furthermore it appears that providing the volume fraction of solids is 0.20 or higher and the speed is 772 rpm or higher, an energy input of approximately 0.008 kW hrs is sufficient for significant soluble protein release.

5.6 MIXING INTENSITY AND SOLIDS SUSPENSION AT DIFFERENT SPEEDS

5.6.1 Introduction

From the results presented in Section 5.5, there appears to be a minimum concentration of solids and minimum impeller speed, below which the extent of disruption is dependent on the parameters. This phenomena may be linked to the complete or partial suspension of the solid particles.

The degree of suspension of the solids is defined by several terms. Complete uniformity occurs when all the particles are suspended off the bottom of the tank, and are uniformly distributed in the tank with the exception of the top layer. The depth of the top layer is a function of the settling velocity of the particles. Complete off-bottom suspension occurs when all the solid particles are moving above the bottom of the tank with a vertical velocity component. Complete on-bottom motion of the particles occurs when all the particles are moving around on the bottom of the tank with some velocity. Any stationary fillets in the tank must be defined. The fillet is a stationary or stagnant deposit of the solids commonly around the edge of the tank but may exist in other parts of the tank depending on the flow patterns produced by the impeller. The liquid height in the tank to which solids are suspended can be used to describe the appearance of suspension.

This section includes the calculation of the critical impeller speed for off-bottom suspension of solids for varying volume fractions of solids and for varying particle sizes. The heights of the suspension of the solids and subsequent volumes of slurry are calculated at a volume fraction of solids of 1245 μm at impeller speeds ranging from 250 rpm to 1090 rpm. Visual observation of the degree of mixing occurring in the stirred tank at different impeller speeds is also included.

5.6.2 Critical impeller speed for off bottom suspension of solids

Several design equations used to determine the critical speed for off-bottom suspension were reported by Oldshue (1983). The term critical speed refers to the minimum impeller speed at which solids will be suspended off the bottom of the vessel. The equation of Zwietering (1958) was quoted as:

$$n_c = 6D^{-0.85} * (\mu/\rho)^{0.1} * d_p^{0.2} * (g(\rho_p \times \rho)/\rho)^{0.45} * (100 * \rho_p * c_v/(\rho(1-c_v)))^{0.13}$$

Eqn. 5.6.1

where n_c = critical impeller speed for off bottom solids suspension, rpm

D = impeller diameter, cm

μ/ρ = kinematic viscosity, $cm^2\ sec^{-1}$

d_p = particle diameter, cm

g = 98100 $cm^2\ sec^{-1}$

ρ_p = density of particles, g cm^{-3}

ρ = fluid density, g cm^{-3}

c_v = volume concentration of solids, cm^3

Using this correlation the critical speed, n_c, was calculated for volume fractions of solids ranging from 0.05 to 0.40 (1245 μm silica particles). The critical speeds for a volume fraction of solids of 0.20 of particles of varying size (114 μm to 1245 μm) were calculated. The results are shown in Table 5.6.1.

The table includes the maximum extents of disruption at an impeller speed of 772 rpm and the corresponding volume fraction of solids and particle size. Visual observation of the degree of particle suspension, at an impeller speed of 772 rpm and the volume fraction and particle size shown in the table, is also included. The visual observation of solid suspension will be discussed in more detail in Section 5.6.4.

The results presented in Table 5.6.1 show that the calculated values of the critical impeller speed for off-bottom suspension of solids are lower than expected. For example, at a volume fraction of 0.30 of 1245 μm silica particles, the predicted critical impeller speed for suspension of solids is 247 rpm and yet at 772 rpm, the suspension of solids is incomplete. The complete suspension of small particles (114 μm) results in a lower maximum extent of disruption (31%) than the incomplete suspension of larger particles (1245 μm). This implies that a grinding motion of large particles not completely suspended causes more cell disruption than the collisions of small particles in suspension.

Table 5.6.1 The critical speed required for off-bottom suspension of particles calculated using the equation of Zwietering (1958) for volume fractions of 1245 μm silica particles ranging from 0.05 to 0.40 and for a volume fraction of solids of 0.20 of silica particles of mean size ranging from 114 μm to 1245 μm, as well as the extent of disruption and the visual suspension at an impeller speed of 772 rpm

volume fraction of solids	geometric mean particle size, μm	critical speed for off-bottom suspension of solids, rpm	maximum extent of disruption R_i/R_m, at speed 772 rpm	visual degree of suspension at 772 rpm
0.05	1245	188	98	complete
0.10	1245	207	98	complete
0.20	1245	230	96	incomplete
0.30	1245	247	93	incomplete
0.40	1245	262	97	incomplete
0.20	114	143	31	complete
0.20	256	168	64	complete
0.20	304	174	74	complete
0.20	735	207	76	incomplete
0.20	1245	230	96	incomplete

5.6.3 Calculation of height of solids suspension above impeller

The heights of solids suspension above the impeller at different operating conditions were calculated by the method of Weismann and Efferding (1960) using the following equation:

$$Pg_c/(g*n*\rho_{sl}*V_m*v_{ts}) = \phi^{0.667}*(T/D)^{0.5}*\exp(4.35*(Z'/T-0.1) \qquad \text{Eqn. 5.6.3}$$

where P = power input by impeller, W
g_c = gravitational constant (=1 for SI units)
g = 9.81 $m^2\ sec^{-1}$
n = number of impellers = 1
ρ_{sl} = density of slurry, kg m^{-3}
V_m = pulp volume to height Z'+C, m^3
Z' = interface height above impeller to which particles are suspended, m
C = clearance of impeller above tank base, m
v_{ts} = particle terminal velocity, m sec^{-1}
ϕ = volume fraction solids
T = tank diameter, m
D = impeller diameter, m

The volume fraction of solids relative to the pulp volume was estimated as follows:

$$\phi = S/(\rho_p * V_m) \qquad \text{Eqn. 5.6.4}$$

where S = mass of solids, kg
ρ_p = particle density, kg m^{-3}

The terminal settling velocity was estimated from Stokes' law:

$$v_{ts} = g * d_p^2 * (\rho_p - \rho)/(18 * \mu_l) \qquad \text{Eqn. 5.6.5}$$

where μ_l = liquid viscosity, kg m sec^{-1}

The pulp volume was determined from:

$$V_m = f(Z') = (\pi * T^2/4) * (Z' + C) \qquad \text{Eqn. 5.6.6}$$

The slurry density was calculated from:

$$\rho_{sl} = \phi * \rho_p + (1-\phi) * \rho_l \qquad \text{Eqn. 5.6.7}$$

The interface between the slurry and liquid was assumed to be on the verge of merging. Hence the settling and suspension forces were taken as being in

equilibrium at Z'. The method has been successfully applied for flat bladed turbine impellers with impeller Reynolds' numbers greater than 1000.

The calculation is based on substituting Equation 5.6.6 into Equation 5.6.3. The resultant equation is rearranged to result in the following form:

$$V_m = f(Z') = (Z'/T - 0.1) - 0.23 \ln\{ [P/(g*n*v_{ts}*V_m*\rho_{sl})] * \phi^{-0.66} * (T/D)^{-0.5} \quad \text{Eqn. 5.6.8}$$

The equation was solved for f(Z') equal to zero, resulting in a value for Z', the height of suspension above the impeller. This procedure was followed for each speed and the results are shown in Figure 5.6.1. From this figure the interface height above the impeller to which particles were suspended were calculated for impeller speeds of 250 rpm, 300 rpm, 380 rpm, 540 rpm, 772 rpm and 1090 rpm. The values are tabulated in Table 5.6.2. Details of the calculations of slurry densities, particle terminal velocities *etc.* can be found in Appendix 8.

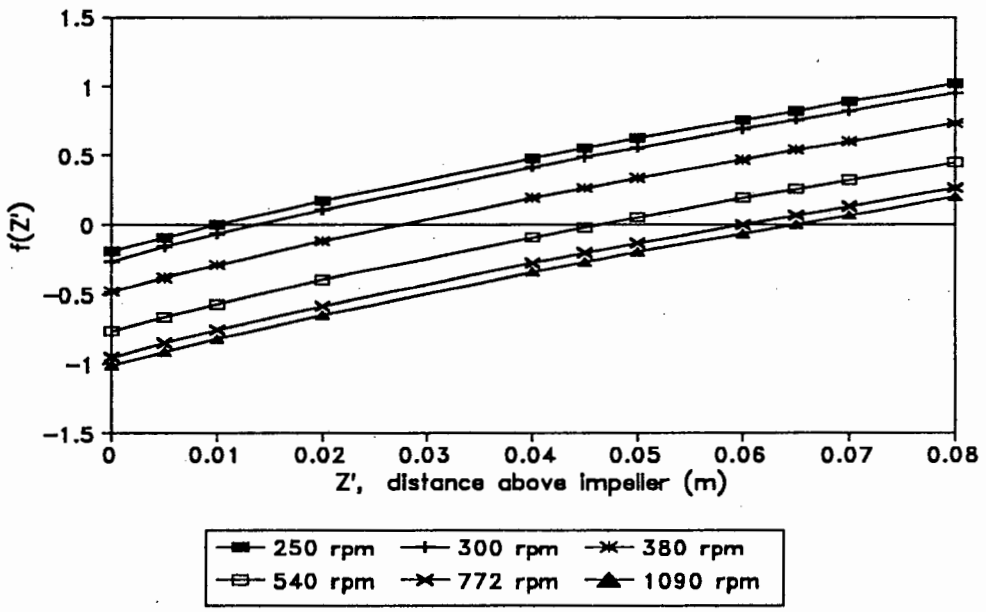

Figure 5.6.1 Correlation of f(Z') using the method of Weisman and Efferding (1960) to calculate Z', the height above the impeller to which silica particles, of mean diameter 1245 μm, were suspended at different impeller speeds when agitated at a volume fraction of solids of 0.20

The height of the liquid in the tank was 0.100 m and the height of liquid above the impeller (Z) was 0.066 m. The clearance of the impeller above the tank base was 0.033 m.

Table 5.6.2 The height of suspension of solids above impeller, Z', the fraction of the height of suspension, Z'/Z, and the pulp volume, V_m at various speeds and a volume fraction of solids of 0.20 (silica particles of mean size 1245 μm)

impeller speed,(rpm)	height to which particles are suspended above impeller Z', m	fraction of height of suspension Z'/Z, where Z = liquid height above impeller	total height of pulp, Z'+C, m, where C is the impeller clearance off the base of the tank	pulp volume to height Z'+C , V_m, m^3
250	0.010	0.15	0.043	0.00039
300	0.014	0.21	0.047	0.00043
380	0.028	0.42	0.061	0.00056
540	0.046	0.70	0.079	0.00072
772	0.060	0.91	0.093	0.00085
1090	0.065	0.98	0.098	0.00089

The calculated heights of suspension of solid particles and resultant pulp volumes presented in Table 5.6.2 show that below an impeller speed of 772 rpm the solid particles are not completely suspended. Furthermore the correlation predicted no suspension at a speed of 150 rpm and suspension to less than 0.5 cm for a speed of 200 rpm. The suspension of the solids will be discussed further in the following section.

5.6.4 Observation of suspension of solids and mixing patterns

The critical impeller speed required for off-bottom suspension of solids and the height of suspension above the impeller were calculated for various operating conditions in Sections 5.6.3 and 5.6.4. In this section the visual observations of the suspension of solids at impeller speeds varying from 115 rpm to 1090 rpm are reported.

The mixing patterns which occurred in the stirred tank at different impeller speeds and a volume fraction of 0.20 of 1245 μm silica were observed. The mixing patterns are shown in Figures 5.6.2 to 5.6.8.

At an impeller speed of 115 rpm (Figure 5.6.2) the particle bed was stationary with only a few particles from the surface of the bed thrown up into the liquid. An increase in the speed to 200 rpm caused small vortices containing particles to form around the impeller. The main bed of particles (bed height of about 2.5-3 cm) remained stationary, with some particles thrown up into fluid body (Figure 5.6.3).

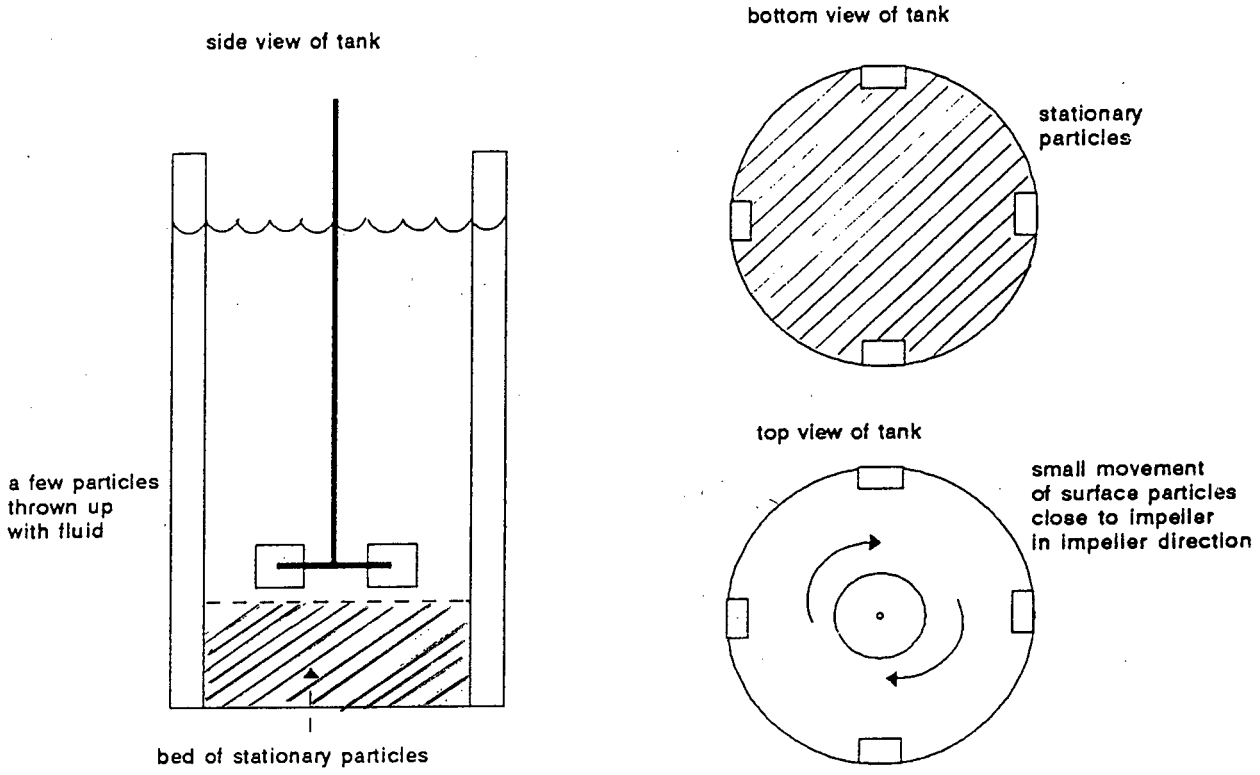

Figure 5.6.2 Flow patterns at an impeller speed of 115 rpm and at a volume fraction of solids of 0.20 of 1245 μm (d_{ave}) silica particles.

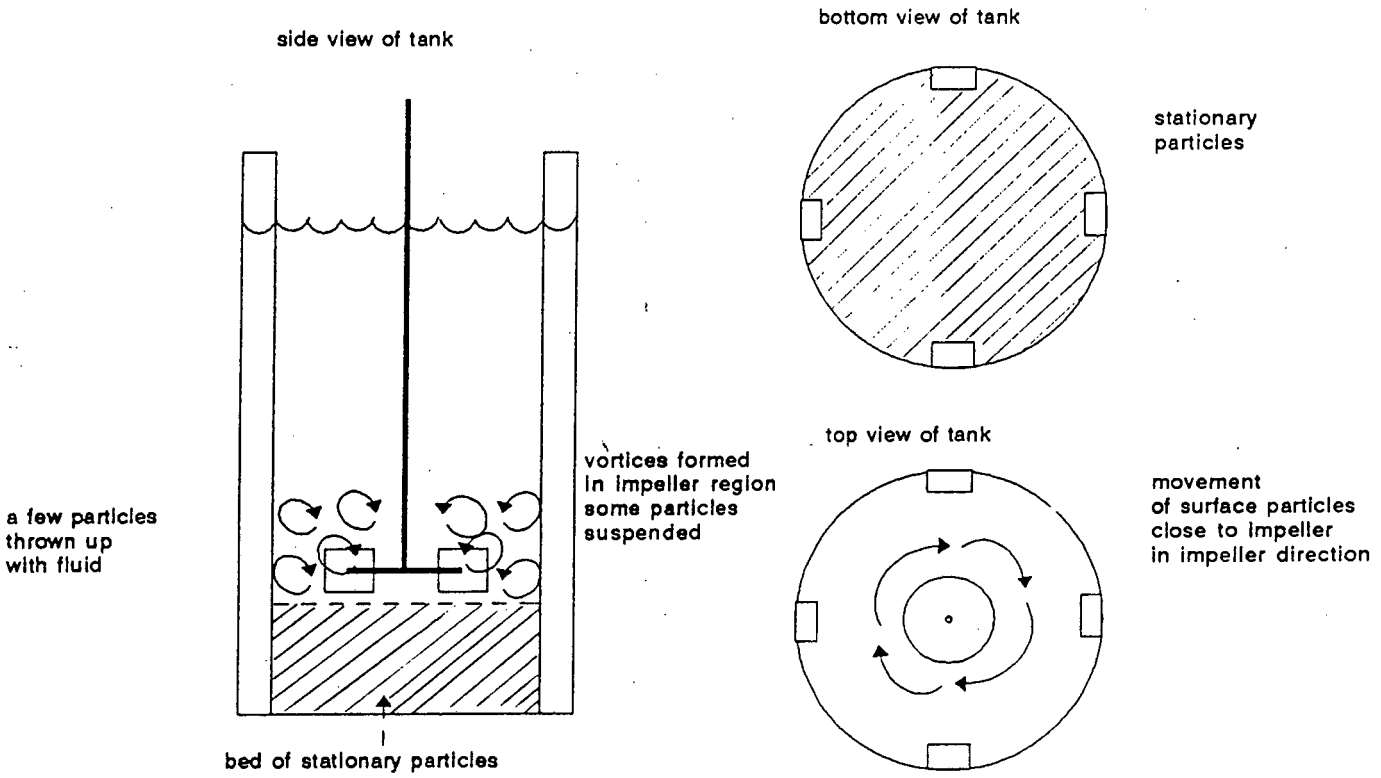

Figure 5.6.3 Flow patterns at an impeller speed of 200 rpm and a volume fraction of solids of 0.20 of 1245 μm (d_{ave}) silica particles

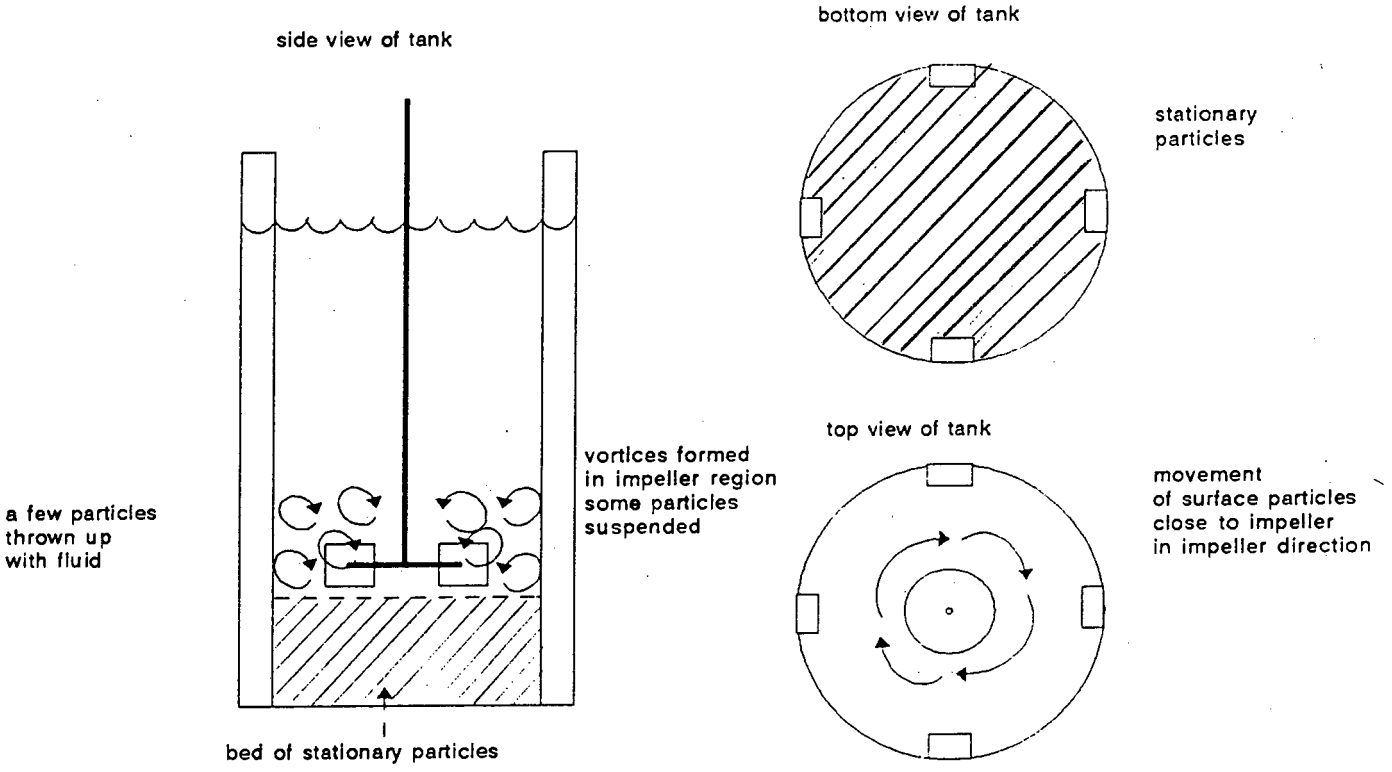

Figure 5.6.4 Flow patterns at an impeller speed of 300 rpm and a volume fraction of solids of 0.20 of 1245 μm (d_{ave}) silica particles.

The typical radial flow patterns which are caused by radial flow impellers began to form at an impeller speed of 380 rpm (Figure 5.6.5). The fluid with some entrained particles flowed radially towards the tank walls from the impeller tips and then flowed up the walls towards the surface of the tank. Despite the presence of baffles, vortices formed in the impeller vicinity. The size of the stationary bed decreased and the surface of the bed was in continual motion.

The stationary bed appeared, from the side view of the tank, to have almost completely disintegrated at an impeller speed of 540 rpm. The particles, although not suspended, were in motion. However, the bottom view of the tank showed that there was still a stationary layer of particles on the tank floor (Figure 5.6.6). At an impeller speed of 772 rpm, the whole tank appeared to be in motion from the side view (Figure 5.6.7). Viewed from below, there remained a zone (about 4 cm in diameter) directly beneath the impeller which contained a layer of stationary particles, although the particles on the outside of this zone were moving in the direction of the impeller. Complete off-bottom suspension was observed at an impeller speed of 1090 rpm (Figure 5.6.8).

These observations agreed well with the predicted solid suspension discussed in Section 5.6.3.

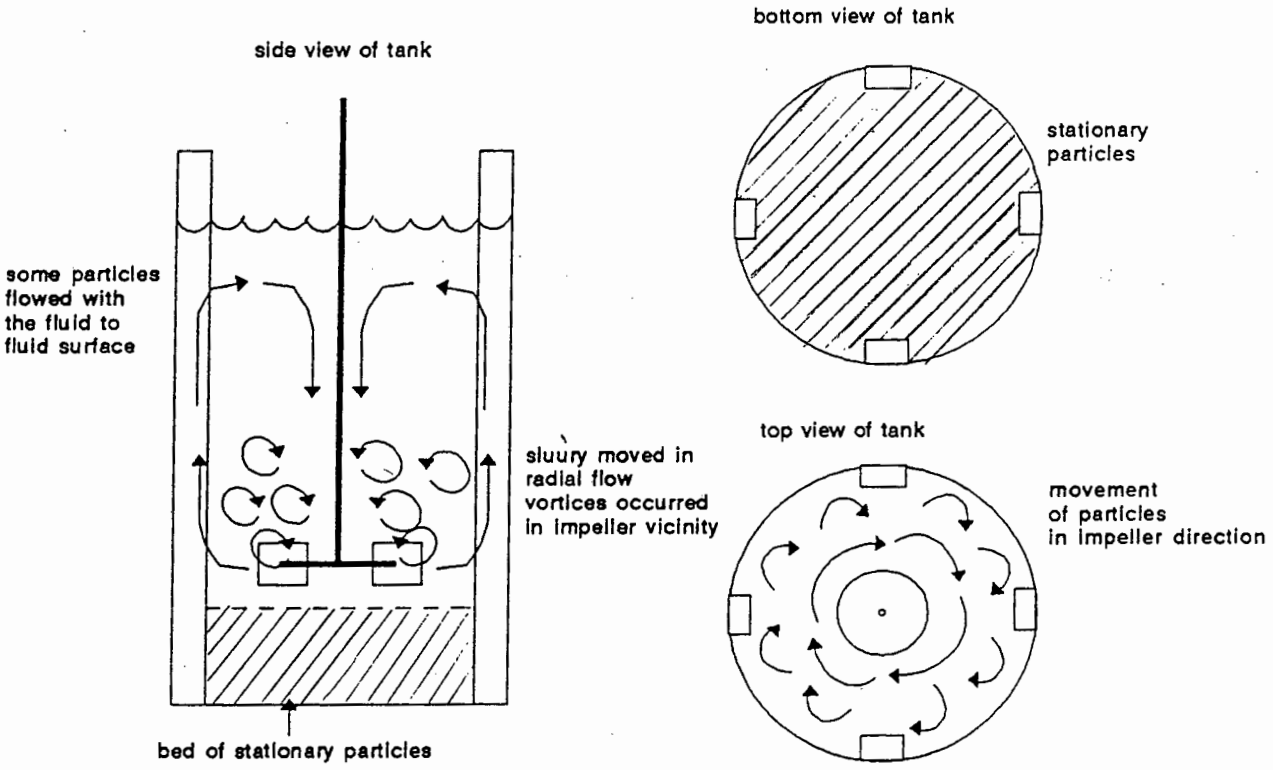

Figure 5.6.5 Flow patterns at an impeller speed of 380 rpm and a volume fraction of solids of 0.20 of 1245 μm (d_{ave}) silica particles

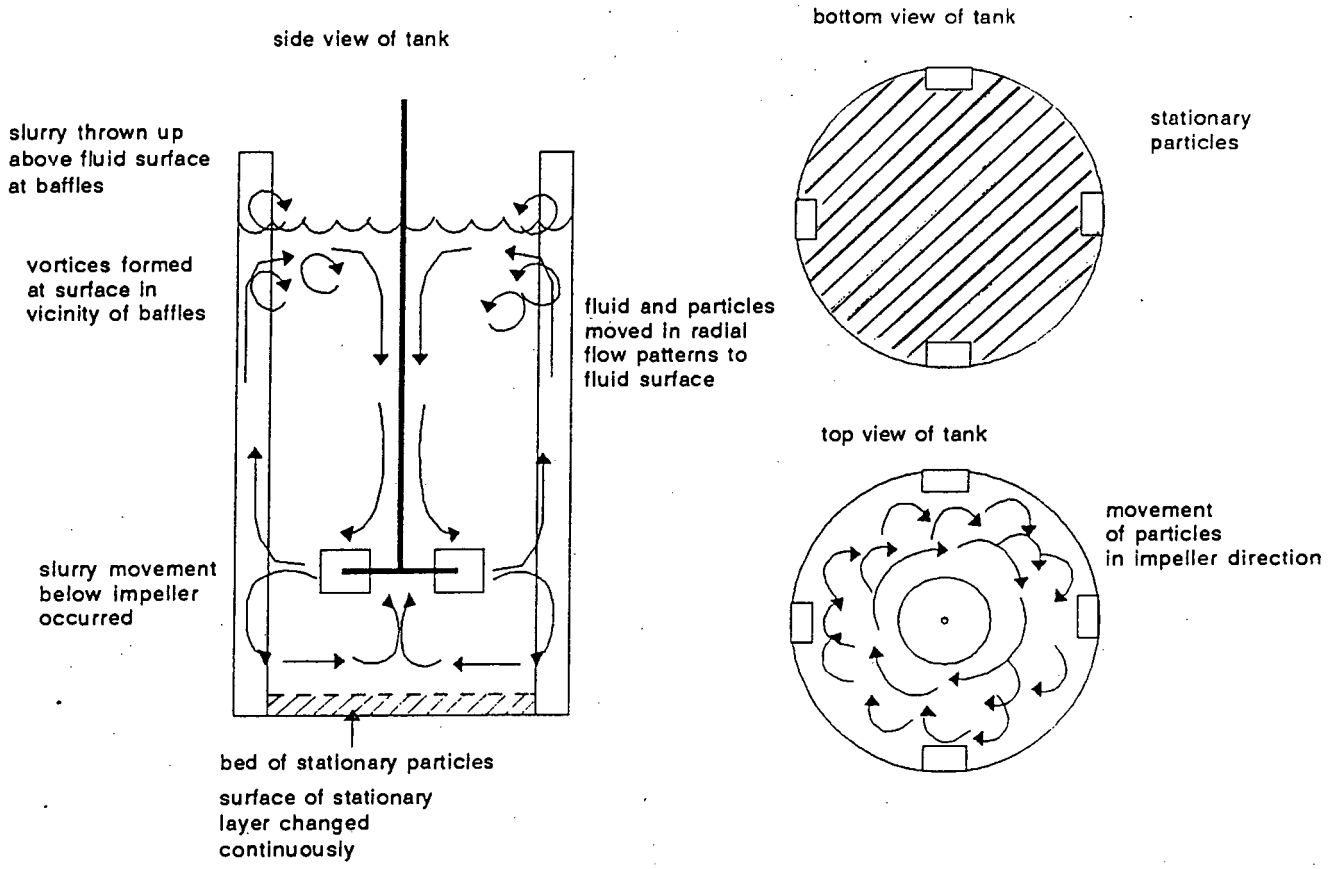

Figure 5.6.6 Flow patterns at an impeller speed of 540 rpm and volume fraction of solids of 0.20 of 1245 μm (d_{ave}) silica particles

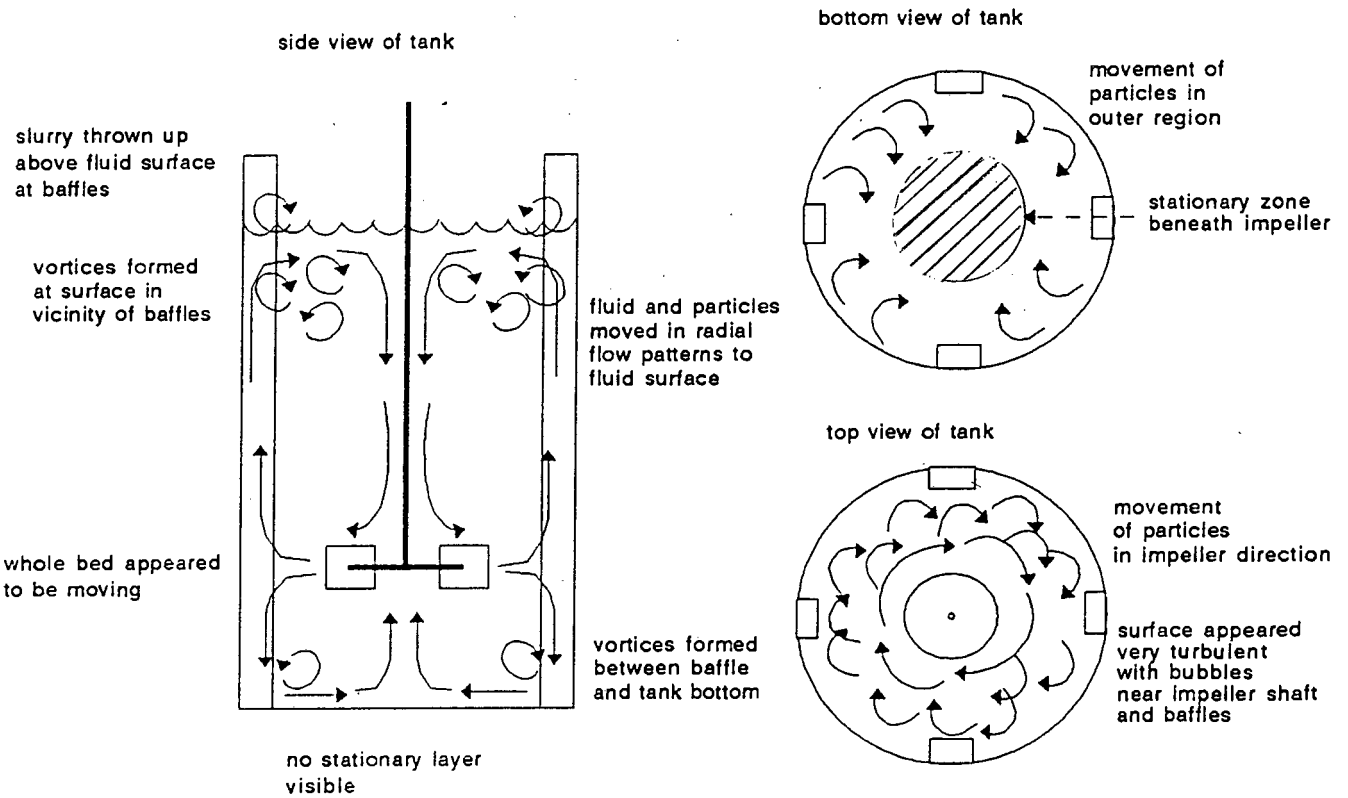

Figure 5.6.7 Flow patterns at an impeller speed of 772 rpm and volume fraction of solids of 0.20 of 1245 μm (d_{ave}) silica particles

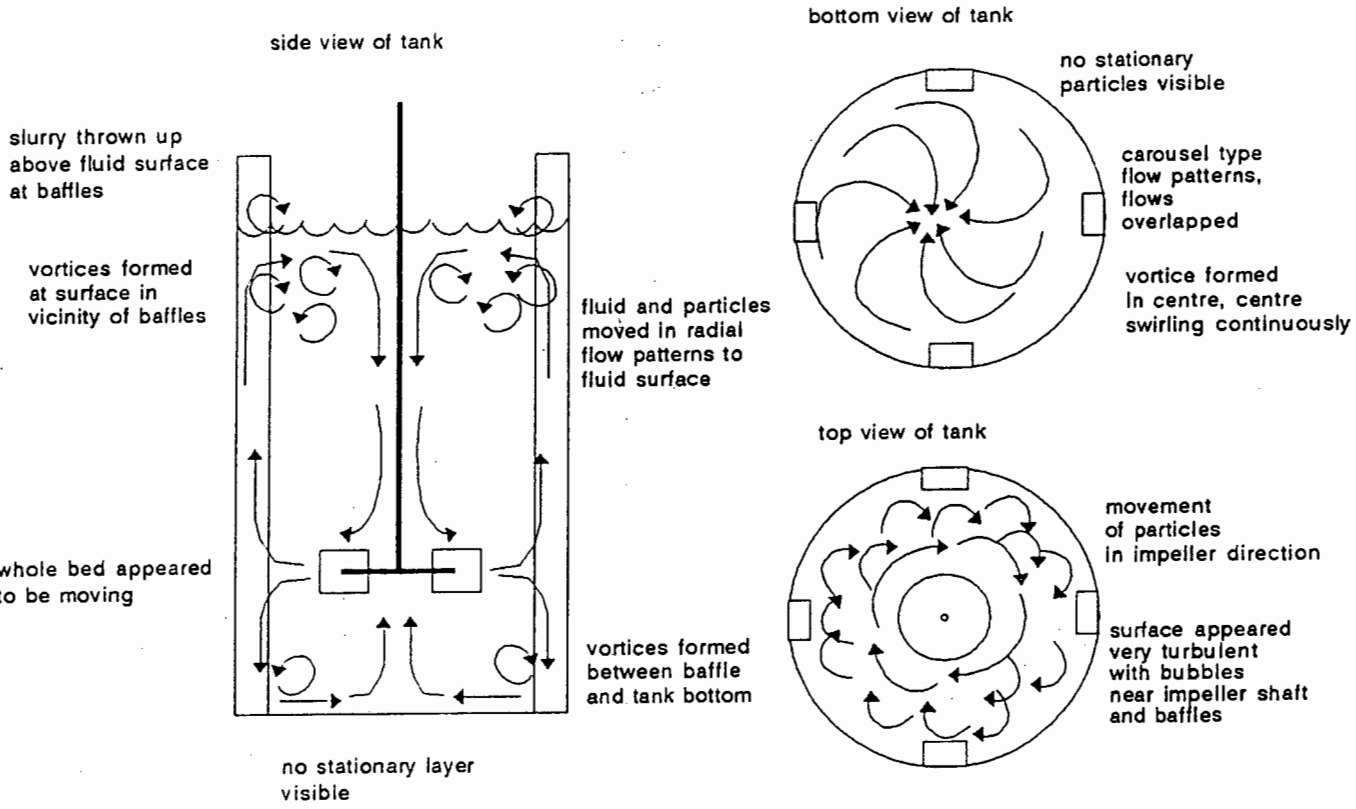

Figure 5.6.8 Flow patterns at an impeller speed of 1090 rpm and volume fraction of solids of 0.20 of 1245 (d_{ave}) silica particles

The maximum extent of disruption, R_i/R_m, obtained at impeller speeds in the range 150 rpm to 1090 rpm at a volume fraction of 0.20 of 1245 μm silica was examined in terms of the observations of suspension presented in this section. The maximum extent of disruption is shown as a function of the impeller speed in Figure 5.6.9. The mixing patterns observed at the impeller speeds are included in the figure.

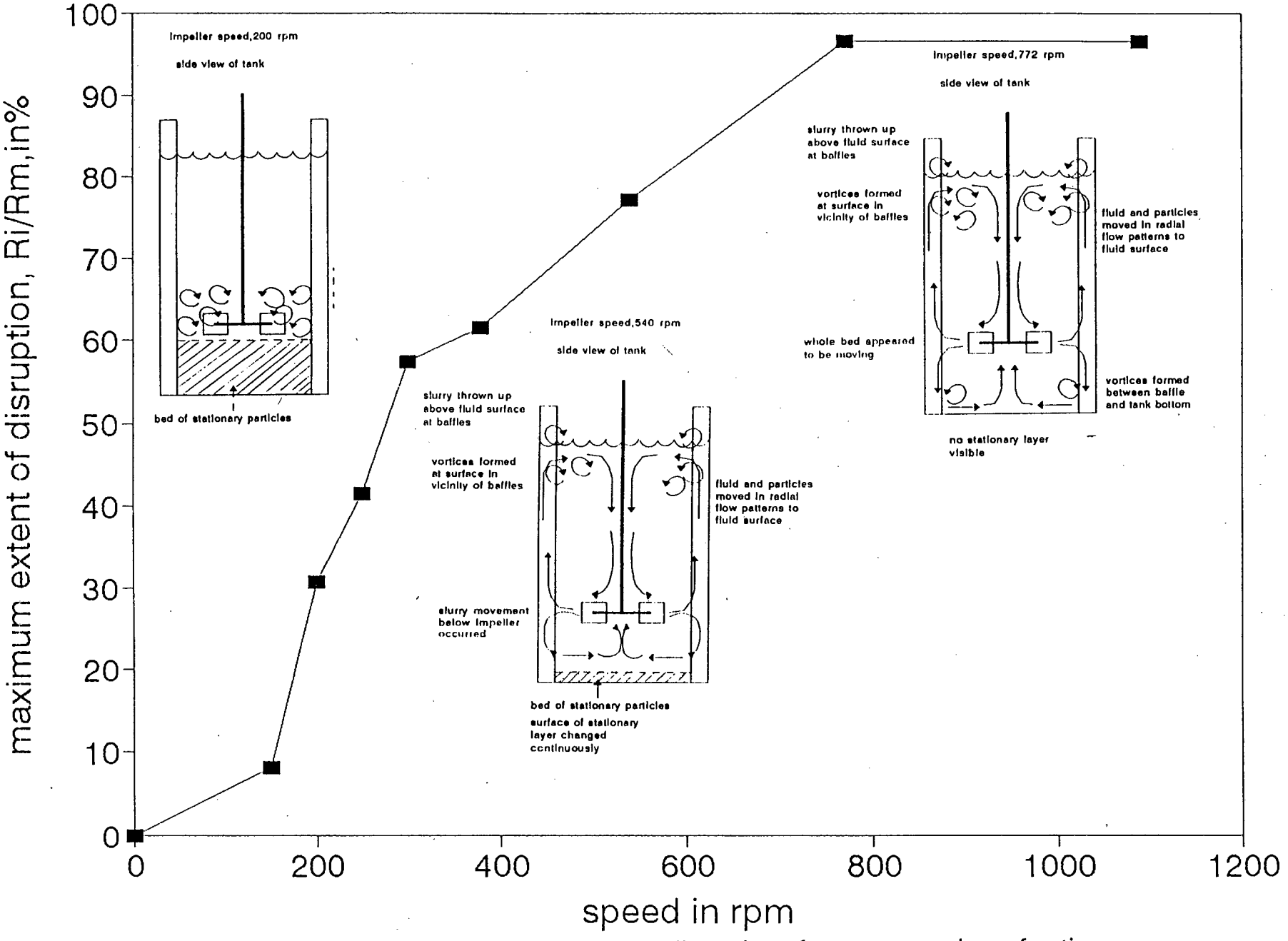

Figure 5.6.9 The maximum extent of disruption of yeast at a volume fraction of 0.20 of 1245 μm silica particles, as a function of the impeller speed, showing the regimes of suspension of solids

In Figure 5.6.9 there appears to be several regimes of mixing and therefore corresponding levels of disruption. The maximum extent of disruption obtained at impeller speeds of less than 200 rpm is marginal and this is reflected by the inadequate solid and liquid mixing at these speeds. Between impeller speeds of 200 rpm and 772 rpm the increase in the maximum extent of disruption is considerable. This increase in disruption is accompanied by an intensified degree of mixing and suspension of solids. The suspension of solids is complete at an impeller speed of 1090 rpm. This is reflected by the high value of the extent of disruption.

From this analysis, it appears that where a significant amount of solids are not suspended, cell disruption is not complete.

5.6.5 Damage of the cell wall

The release of a wall-associated protein, the enzyme invertase, was reported in Section 4.3. In this section the damage to the cell wall will be discussed, qualitatively, in terms of the degree of mixing in the tank at specific operating conditions.

The degree of the suspension of solids has been discussed in detail in Sections 5.6.2, 5.6.3, and 5.6.4. Using these results, the degree of damage to the yeast cell wall has been analysed. The ensuing discussion is speculative.

The release of invertase (wall-associated enzyme) at low impeller speeds was found to be more rapid than the release of total soluble protein. This suggests that the inner glucan layer of the cell wall remained intact and thus the overall release of protein was low (Section 4.3.2.2). Only wall associated enzymes were released. At intermediate speeds, the glucan layer of the cell wall was damaged but not completely broken and thus some of the cytoplasmic proteins were released. The disruption at high speeds was complete as the glucan layer of the cell walls was totally disintegrated, resulting in complete protein release.

This theory was strengthened by the observations of mixing within the tank. Some of the mechanisms postulated to cause cell damage include collisions between particles which crush the cells, collisions between particles and reactor parts entrapping and crushing the cells and interactions with turbulent eddies.

Increased fluid mixing and particle suspension with higher speeds will lead to more cell damage by increasing the frequency of collision, the level of turbulence and the kinetic energy of collision.

5.7 CONCLUSIONS

From the preceding sections of this chapter, the following conclusions have been drawn. First order rate kinetics have been shown to be applicable to cell disruption.

Empirical modelling of the disruption rate constant as functions of the volume fraction of solids, the impeller speed and the particles size were investigated as a method of prediction of disruption constants. The prediction of the disruption rate constant as a function of the volume fraction of solids using a power law model was found to be adequate. However the prediction of the rate constant as a function of impeller speed and particle size using empirical models was not satisfactory. The mathematical modelling of the disruption rate constant did not provide information on the mechanisms of cell disruption.

The use of the impeller Reynolds' number, the particle Reynolds' number and the power number as measures against which to correlate the disruption rate constant resulted in trends which may or may not present the accurate situation.

The disruption rate constant was shown to be dependent on the impeller power input. Increasing the impeller power input by increasing the concentration of solids, the impeller speed, the particle density and biomass concentration each caused an increased disruption rate constant.

A dependency of the disruption of yeast on the energy input was observed.

The mixing intensity in the stirred tank varied considerably at different impeller speeds (Sections 5.6.2, 5.6.3 and 5.6.4). Low speeds, in the range 200 rpm to 380 rpm, resulted in a low degree of mixing. The low extents of disruption obtained at speeds less than 772 rpm, are partially attributed to the decreased frequency of collisions between particles, particles and reactor parts and particles and turbulent eddies at conditions of marginal mixing and particle suspension. It

was observed that where a significant amount of solids were not suspended, the cell disruption was incomplete.

CHAPTER 6
EFFECTS OF AGITATION IN THE PRESENCE OF PARTICULATES ON THIOBACILLI

6.1 INTRODUCTION

Thiobacilli are being used industrially for the biooxidation of sulphide minerals in the process of treating gold-containing ores. Having completed a study of the model microorganism, yeast, a very preliminary study was conducted using thiobacilli.

The attachment of thiobacilli to silica and pyrite particles was investigated. The concentration of solids and the size of the solid particles were varied to enable investigation into their effects on the bacteria. Finally, experiments were conducted to study the effect of varying impeller speed and impeller type on the rate of biooxidation.

6.2 RESULTS AND DISCUSSION

6.2.1 Attachment of bacteria and shake flask growth

Experiments were conducted in shake flasks and in the stirred tank to determine the attachment of thiobacilli to the silica and the pyrite. Attachment was determined by enumerating the free bacteria in solution before and after agitation with the solid particles. It is important to note that due to the difficulty encountered in enumerating thiobacilli by microscopic counting the results presented here may not be a true representation.

Suspensions of thiobacilli were placed in shake flasks with silica and pyrite particles. The volume fraction of solids used was 0.05. The shake flasks were placed in the shaker for 2 hours. The results are shown in Table 6.2.1.

The results indicate that thiobacilli attach more readily to pyrite than to silica particles during shake flask agitation.

Table 6.2.1 The attachment of thiobacilli to a volume fraction of 0.05 of silica and pyrite particles after 2 hours in shake flasks.

particle type	number of free thiobacilli per cm^3 before agitation	number of free thiobacilli per cm^3 after agitation	attachment of thiobacilli in percent
silica	$2 * 10^8$	$1.6 * 10^8$	20
pyrite	$2 * 10^8$	$4.4 * 10^7$	78

Furthermore it was observed, by redox potential measurement, that pyrite completely inhibited growth in shake flask culture whilst the presence of silica at the same concentration did not affect the growth. DiSpirito *et al.* (1981) reported inhibitory effects of pyrite and glass beads in a concentration range of 0.1 to 5% (mass/volume).

Thiobacilli were subjected to agitation with particles at a volume fraction of 0.05 in the 1 dm^3 stirred tank for two hours. The amount of free thiobacilli were enumerated before and after agitation. The results are shown in Table 6.2.2.

Table 6.2.2 The attachment of thiobacilli to a volume fraction of 0.05 particles during agitation in the stirred tank at 772 rpm

type of particle	number of free thiobacilli per cm^3 before agitation	number of free thiobacilli per cm^3 after agitation	attachment of thiobacilli in percent
silica	$2 * 10^8$	$1.6 * 10^8$	10
pyrite	$2 * 10^8$	$1 * 10^8$	50

Thiobacilli appear to attach more readily to pyrite particles than to silica particles during agitation in a stirred tank. The level of adsorption of thiobacilli to silica particles is low compared to that reported by DiSpirito *et al.* (1983)

who reported that after one hour sorption of bacteria to glass beads was complete.

6.2.2 The effect of the concentration of silica in 1 dm^3 STR

Thiobacilli were agitated in the stirred tank for a period of two hours at an impeller speed of 772 rpm and volume fractions of silica varying from 0.05 to 0.20. Samples of thiobacilli were taken before and after agitation. Fresh 9K media (Silverman and Lundgren, 1959) was added to the samples. The thiobacilli samples were grown in shake flasks in the absence of solid particles. The redox potential of the sample leach solutions was measured for a period of up to 120 hours. The sample taken before agitation was used as a control sample. The growth of thiobacilli as determined by Eh measurement is characterised by three stages. Initially a lag period is observed, this is followed by a sharp increase in the Eh which indicates the rate of cell growth. Finally a maximum Eh is reached indicating that the thiobacilli are fully active. The results of the experiments are shown in Figure 6.2.1.

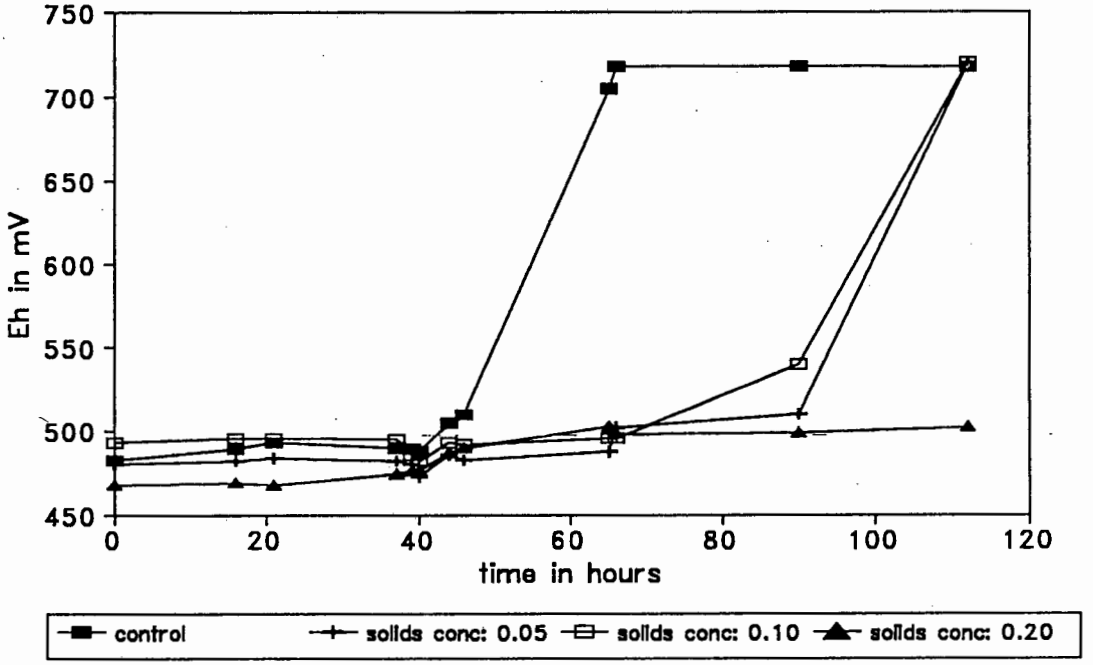

Figure 6.2.1 The rate of biooxidation of thiobacilli on 9K media in the absence of solids, subsequent to agitation at an impeller speed of 772 rpm , as a function of volume fraction of solids (silica particles of mean size 53 μm)

It can be seen from Figure 6.2.1 that the agitation of thiobacilli in the presence of silica caused an increase in the lag period before growth occurred. This indicates that there is some detrimental effect due to agitation with silica, however the thiobacilli recover. The recovery of the thiobacilli agitated with a volume fraction of 0.20 was not observed in the time period monitored.

6.3.3 The effect of silica particle size

Tests were carried out in the stirred tank at an impeller speed of 772 rpm and a volume fraction of silica of 0.05 with thiobacilli. The silica particle size varied from 53 μm to 255 μm. Samples were taken before and after agitation. The growth of the thiobacilli samples was monitored in shake flask culture, in the absence of solids, subsequent to the tests.

The results of these tests are shown in Figure 6.2.2.

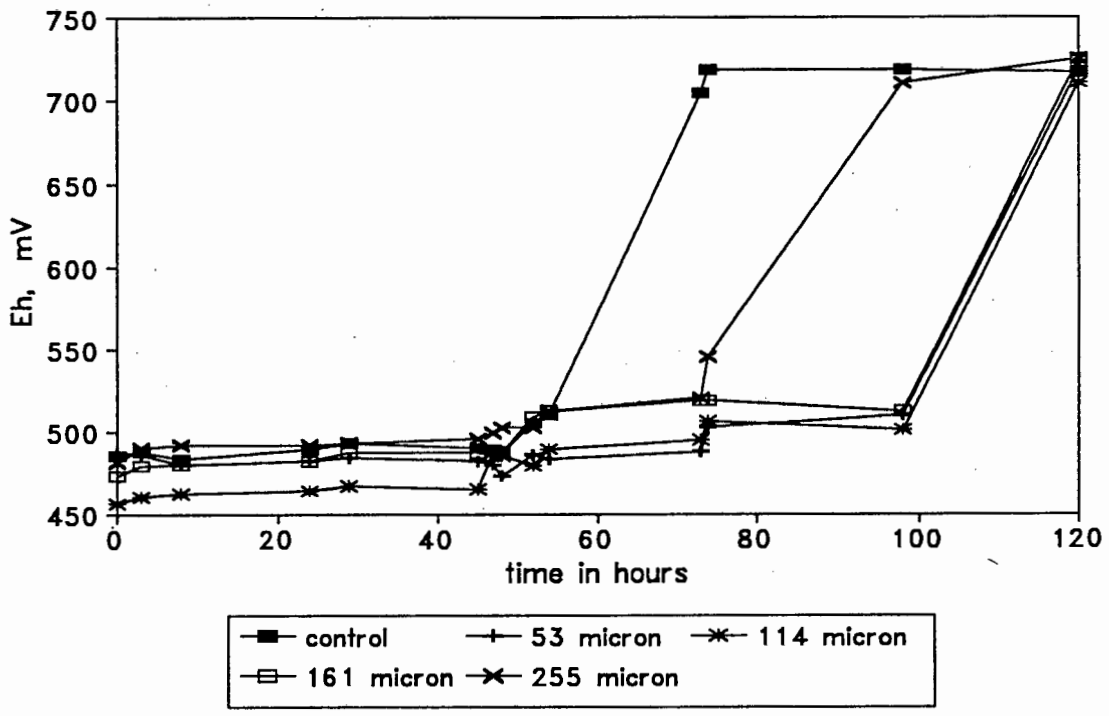

Figure 6.2.2 The rate of biooxidation of thiobacilli subsequent to agitation at a volume fraction of solids of 0.05 and at an impeller speed of 772 rpm, as a function of size of silica particle

Subsequent to a lag of 48 hours, the control sample reached maximum Eh in about 60 hours in shake flask culture, as observed for the solids loading experiments. Lag periods of 98 hours were observed for the growth of bacteria after agitation with 0.05 volume fraction of silica particles of mean diameters 53 μm, 114 μm and 161 μm. A shorter lag period of 74 hours was observed with the bacteria which had been agitated in the presence of particles of mean diameter 255 μm. The shorter lag period observed with the larger particles may be connected to the surface area concentration for attachment of thiobacilli.

6.2.4 The effect of the concentration of pyrite

Experiments were conducted using pyrite particles at volume fractions in the range 0.05 tp 0.10. The thiobacilli were agitated with the particles in the small stirred tank at an impeller speed of 772 rpm for two hours. Samples were taken before and after agitation. The growth of the thiobacilli in shake flask culture, in the absence of solids, subsequent to agitation in the stirred tank was monitored. In an attempt to account for the dilution in the sample inoculi due to attachment of thiobacilli to the pyrite during the agitation, the Eh of a diluted control sample was monitored.

The results are shown in Figure 6.2.3

The control sample reached maximum metabolic rate rapidly with no apparent lag period and reaching maximum Eh within 20 hours. The diluted control sample, although not shown in Figure 6.2.3, began to grow 2 hours after the undiluted control. The samples which had been subjected to agitation with 0.05 and 0.10 volume fractions of pyrite (mean diameter 55 μm) at 772 rpm showed a lag in metabolic rate of about 20 hours and had obtained maximum Eh within 45 hours. The 20 volume percent sample did not reach maximum Eh value until 60 hours.

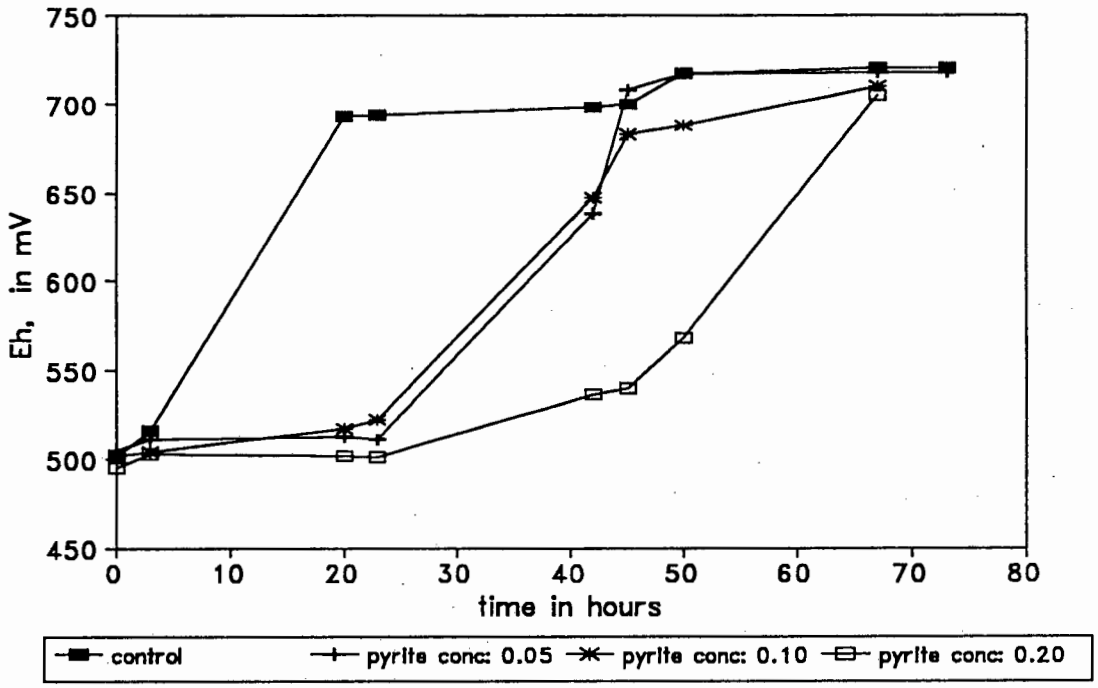

Figure 6.2.3 The rate of biooxidation of thiobacilli subsequent to agitation at an impeller speed of 772 rpm, as a function of the concentration of pyrite

The adsorption of thiobacilli to the particles and subsequent dilution of the sample inoculi may be responsible for the results obtained. Experiments were not conducted to investigate the effect of concentration of solids on the amount of attachment. The accuracy of the dilution of the control sample was hindered by the difficulties encountered in enumerating thiobacilli.

The concentration of pyrite was relatively high in these experiments, due to concentration being expressed in volume fractions of total volume. Usually pyrite loading is quoted in terms of mass by volume percentage. Volume fractions of 0.05, 0.10 and 0.20 represent mass by volume values of 24%, 48% and 96%. Concentrations of solids of above 20% mass by volume have been reported to cause decreased oxidation rates by Gormely and Branion (1989) and Torma *et al.* (1970).

6.2.5 The effect of pyrite particle size

A set of experiments were carried out with thiobacilli in the stirred tank at a volume fraction of pyrite of 0.20 and an impeller speed of 772 rpm with particles ranging in size from 41 μm to 80 μm. Samples were taken before and after agitation. The shake flask growth of the samples, in the absence of solids, was monitored by Eh measurement.

The results are shown in Figure 6.2.4.

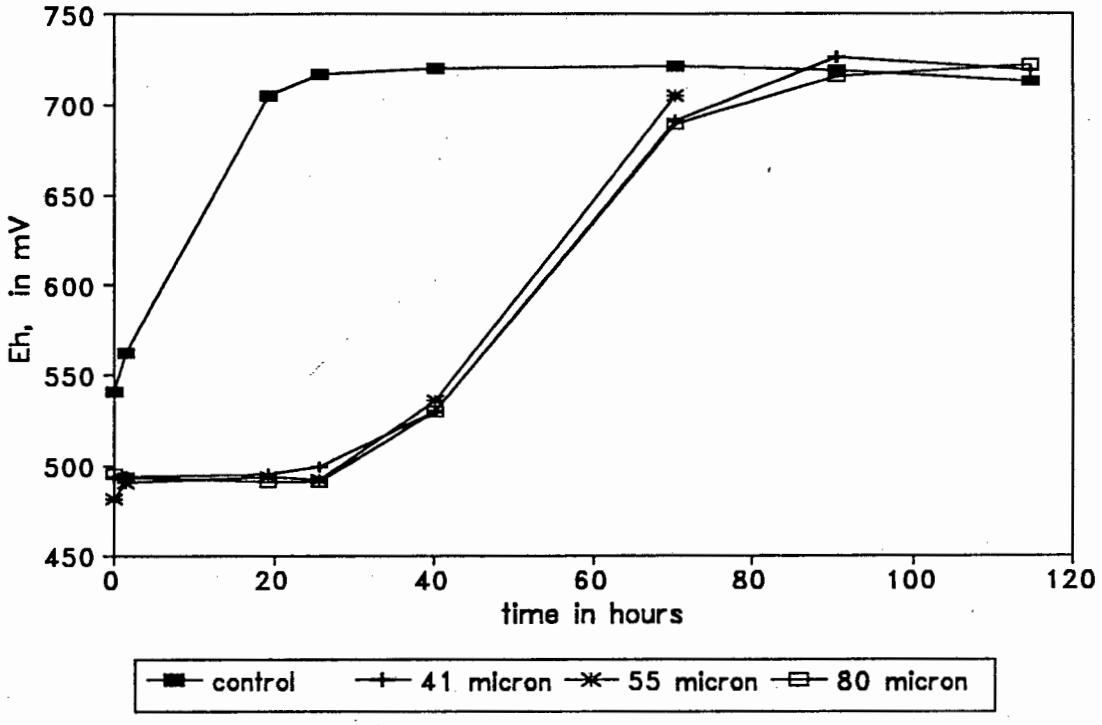

Figure 6.2.4 The rate of biooxidation of thiobacilli after agitation at a volume fraction of solids of 0.20 and an impeller speed of 772 rpm, as a function of the size of pyrite particle

The samples all showed the same lag time of about 40 hours.

6.2.6 The effect of impeller speed

The rate of biooxidation of thiobacilli was investigated at 400 rpm, 772 rpm and 1090 rpm at a volume fraction of pyrite (55 μm) of 0.20. The growth of samples taken before and after agitation, in shake flasks was monitored by Eh measurement.

The results are shown in Figure 6.2.5.

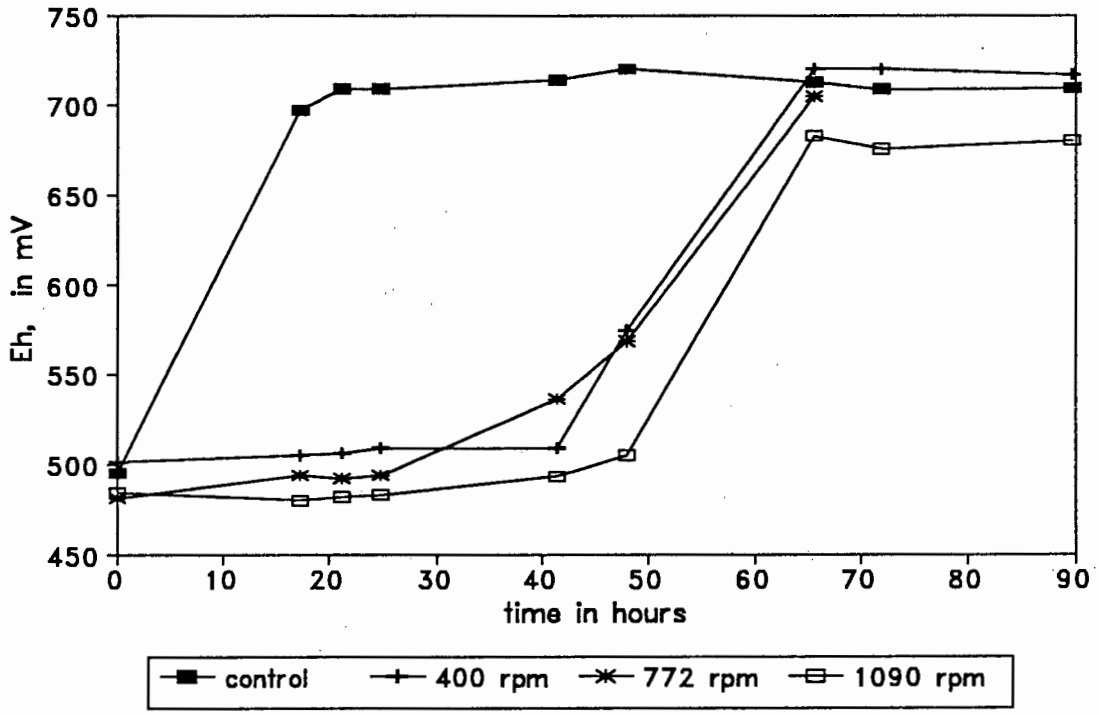

Figure 6.2.5 The rate of biooxidation of thiobacilli after agitation at a volume fraction of pyrite of 0.20 as a function of impeller speed

The lag period observed for the samples were similar, about 48 hours. The highest speed investigated was 1090 rpm (3.2 m sec^{-1}). This was considerably lower than the impeller tip speed of 5.3 m sec^{-1} reported to be inhibitory to biooxidation rate by Hackl *et al.* (1989). Higher impeller tip speeds (not attainable in this apparatus) are required to validate the observations of Hackl.

6.2.7 The effect of the concentration of low sulphur pyrite on the growth of thiobacilli in 4 dm^3 stirred tanks

The experiments carried out in the 1 dm^3 stirred tank were based on the measurement of the rate of biooxidation of thiobacilli in shake flasks, in the

absence of solids, after pretreatment with solids. This is not a representative scenario in terms of industrial processes. This set of experiments was used to examine the particle effects on growth of thiobacilli during subjection to agitation in the presence of particulates.

Thiobacilli inoculi were grown on 4K media (Silverman and Lundgren, 1959) in 4 dm^3 stirred tanks with Rushton turbines at an impeller speed of 350 rpm (equivalent tip speed of 1.4 m s^{-1}). The concentrations of pyrite used were 0%, 10%, 20% and 30%, on a mass by volume basis. The growth of the thiobacilli was monitored daily by Eh measurement over a period of 16 days. The pH of the thiobacilli solutions was kept between 1.6 and 1.9. The temperature remained constant at 35°C.

The results are shown in Figure 6.2.6.

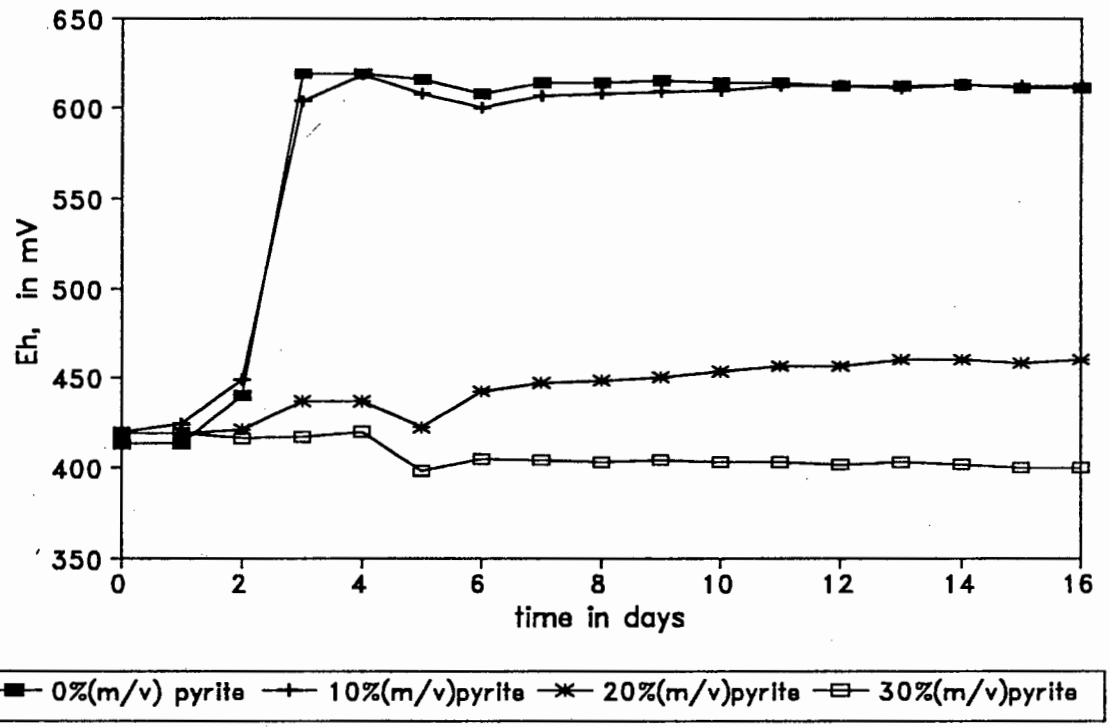

Figure 6.2.6 The effect of concentration (mass/volume basis) of low sulphur pyrite on the biooxidation rate of thiobacilli at an impeller speed of 350 rpm

The concentrations of solids employed were constrained in the range typical of biooxidation processes. Low sulphur pyrite (1.5% S) was used to ensure that oxygen limitation did not occur (Bailey and Hansford, 1993).

The tank maintained at a concentration of solids of 10% (m/v) behaved in the same manner as the tank which contained no solids. This indicated that the concentration of 10% (m/v) was not inhibitory. The redox potential of the stirred tank containing 20% (m/v) solids did not reach the maximum value of the 0 and 10% tanks in the time span investigated. The slow increase may indicate that the bacteria were still viable. This negative effect on biooxidation rate on increasing the concentration of solids to 20% and above has been reported by Gormely and Branion (1989) and Torma *et al.* (1970). The tank containing 30% (m/v) solids showed no change in biooxidation rate.

The oxygen utilization rate and dissolved oxygen concentrations in the tanks were measured on day 4 of the experiment and the results are shown in Figure 6.2.7. The oxygen flow was turned off at 10 seconds and the decrease in dissolved oxygen illustrated the oxygen consumption of the system. The oxygen flow was then turned on again at 320 seconds.

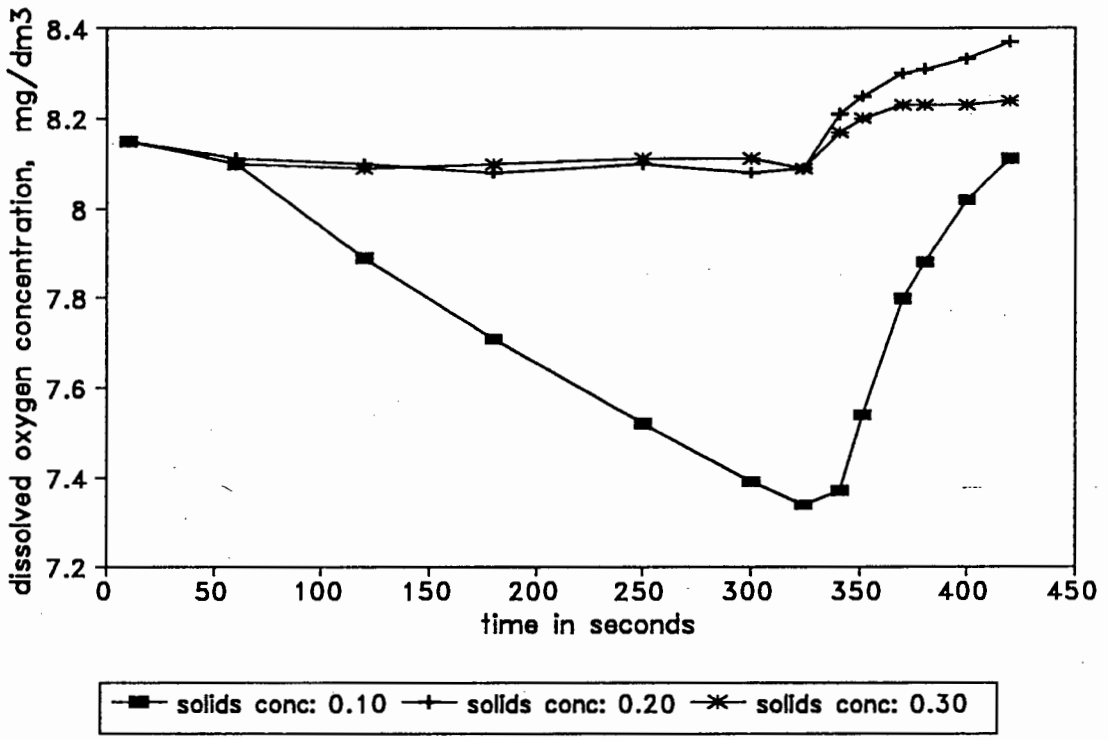

Figure 6.2.7 The effect of the concentration of pyrite (mass/volume) on dissolved oxygen levels in the 4 dm^3 stirred tanks at 350 rpm

As shown in Figure 6.2.7, the tanks containing 20 and 30% (m/v) solids did not consume oxygen, whereas the 10% solids tank showed an oxygen utilization rate of 0.925 moles O_2 dm^{-3} hr^{-1}. This confirms the negative effect of high concentrations of solids on the thiobacilli.

6.2.8 The effect of impeller speed and impeller type on biooxidation rate at 10% (m/v) concentration of solids

Experiments were carried out in the 4 dm^3 stirred tanks to investigate the effect of impeller speed and impeller type on the growth of thiobacilli. The two speeds investigated were 350 rpm (1.4 m s^{-1}) and 630 rpm (2.6 m s^{-1}). Rushton turbines were used to agitate two tanks, one at a speed of 350 rpm and the second at a speed of 630 rpm. Similarly, axial impellers were used to agitate two tanks at speeds of 350 rpm and 630 rpm. Thiobacilli inoculi were grown in the stirred tanks on 4 K media and at a concentration of pyrite of 10% (m/v). The pH was kept between 1.6 and 1.9 and the temperature was kept constant at 35°C. Growth of the thiobacilli was monitored by Eh measurement.

The results are shown in Figure 6.2.8.

The results show that the use of either the Rushton or the axial impeller at an impeller speed of 350 rpm did not inhibit the growth of thiobacilli. A considerable lag period was observed in the growth of the thiobacilli agitated by an axial impeller at an impeller speed of 630 rpm, however the rate did increase after day 14. There appeared to be no activity in the tank agitated by a Rushton turbine at an impeller speed of 630 rpm.

This type of experiment was carried out by Hackl *et al.* (1989) and similar results were obtained, however the impeller speeds that were used in their study were 3.3 m s^{-1} and 5.3 m s^{-1}. These speeds were thus considerably higher than those used in this study.

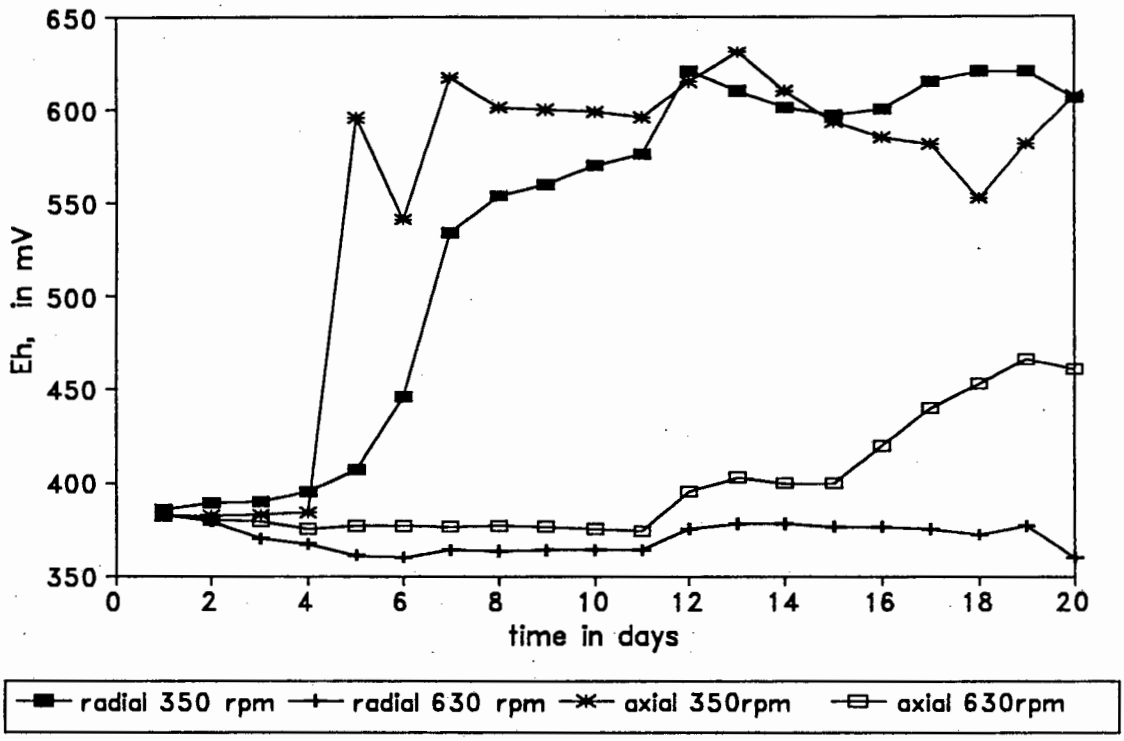

Figure 6.2.8 The effect of impeller speed and impeller type on the biooxidation of high sulphur ore (48% S) by thiobacilli at a concentration of pyrite of 10% (m/v)

6.3 CONCLUSIONS

The experiments reported in this section were of a very preliminary nature.

These experiments allowed some interesting observations to be made, however due to the preliminary nature of the experiments it was not possible to draw any conclusions.

The following observations are noteworthy.

- Subjecting thiobacilli to agitation in the presence of silica increases the lag time in subsequent shake flask culture in 9K media without solid particles.

- Subjecting thiobacilli to agitation with pyrite particles increases the lag time in subsequent shake flask culture in solid-free 9K media. The lag time was observed to be independent of both the size of pyrite particle and the impeller speeds used in the agitation experiments.

- Concentrations of low sulphur containing pyrite ores of 20% and 30% (mass/volume) in batch culture were observed to inhibit growth of thiobacilli.

- Radial flow at low speed did not cause detrimental effects to the thiobacilli, but at high speed radial flow seemed to inhibit growth at a concentration of 10% (m/v) pyrite in stirred tanks.

- Axial flow at low speed did not cause detrimental effects. The growth of thiobacilli using an axial impeller at high speed was slow.

CHAPTER 7
CONCLUSIONS AND RECOMMENDATIONS

7.1 CONCLUSIONS

7.1.1 Introduction

The aim of this research project was to investigate whether the presence of particulates caused cell disruption. In addition the effects of the physical parameters of the solid particles on cell viability were studied.

Chapters 4 and 5 presented the results of investigations into the disruption of Bakers' yeast on agitation in the presence of particulates. Chapter 6 included results of very preliminary investigations into the effect of particulates on the metabolism of thiobacilli.

7.1.2 Loss of yeast cell viability on agitation with particulates

The primary question to be answered was whether cell disruption occurred upon agitation with particulates. The cell disruption of yeast in a stirred tank without solids was monitored. This was compared to the cell disruption obtained upon agitation with particulates (Section 4.3.4). The presence of particulates was found to cause cell disruption.

7.1.3 Maximum release of soluble protein

The disruption of yeast in the French Press resulted in a higher degree of total soluble protein release than disruption in the stirred tank.

7.1.4 Validity of first order rate equation to describe cell disruption

A first order rate equation was used to describe the disruption of yeast. Due to the high degree of fit of the data (correlation coefficients of 0.99 and above) and the reported use of first order kinetics to describe cell disruption in bead mills and cell damage in stirred tank bioreactors, it was concluded that the use of first order kinetics is valid for the description of cell disruption.

7.1.5 Dependency of cell disruption rate constant on solid particle parameters

The effects of the concentration of solids, impeller speed, particle size, particle density, particle shape and the concentration of yeast on the cell disruption of Bakers' yeast are reported in Chapter 4. Increases in the concentration of solids, impeller speed and particle size each caused an increase in the rate of disruption. A marginal increase in the disruption rate constant with increased particle density was observed. The reasons for the increases in disruption rate constant may include increased collision frequency upon higher concentrations of solids and increased particle kinetic energy upon increased particle size. An increase in the concentration of yeast caused a decrease in the disruption rate. This may be attributed to a protective effect of increased viscosity.

7.1.6 Effect of particle parameters on the maximum extent of disruption

The maximum extent of disruption of yeast cells was found to be independent of the solids concentration in the range of volume fractions of 0.05 to 0.40. The maximum extent of disruption increased with increasing impeller speed up to a speed of 772 rpm and thereafter remained constant. A significant increase in the maximum extent of disruption was observed when the size of the particles used increased from 114 μm to 304 μm. The effects of particle density and the concentration of yeast on the maximum extent of disruption were found to be insignificant over the range tested.

7.1.7 Release of wall-associated proteins

The release of the wall-associated protein, invertase, was found to be greater by disruption of yeast in the stirred tank than in the French Press. This result was in direct contrast to the release of total soluble protein, which was greater by disruption in the French Press. On this basis, it may be plausible to suggest that the disruption mechanisms in the French Press result in complete rupture of the cells, whilst damage to the cell wall is predominant in the stirred tank.

The rate constant of release of invertase was observed to be greater than the rate constant of total soluble protein at low impeller speeds (115 rpm to 200 rpm) and at a volume fraction of solids of 0.05. This indicates that at these

operating conditions cell damage is limited to the cell wall, where invertase is located.

7.1.8 Validity of using mathematical models to describe disruption rate dependency on particle parameters

The effects of particle parameters on cell disruption rate constants were shown in Chapter 4. The modelling of these effects, using mathematical models, was reported in Chapter 5. Although mathematical models do not include mechanistic considerations, their use allows simple approximations to describe the disruption rate constant dependency on particle parameters. Data obtained from bead mill literature has been included. A power law model was found to fit the dependency of the disruption rate constant on the concentration of solids. The modelling of the effects of impeller speed and particle size to mathematical models was not successful, indicating that the mechanisms of disruption cannot be ignored in these cases. This analysis did not contribute further to the understanding of the process of cell disruption.

7.1.9 Dependency of disruption rate constant on the power input

The disruption rate constant was found to be dependent on the impeller power input. It was found that the disruption rate constant increased with an increase in impeller power input, independent of the cause of increase of power input.

7.1.10 Dependency of extent of disruption on the energy requirement

A dependency of the extent of disruption on the energy requirement was observed.

7.1.11 Dependency of maximum extent of disruption on the degree of suspension of solids

The maximum extent of disruption was observed to be dependent on the degree of suspension of solids. It was found that the maximum extent of disruption was low when a significant amount of the solids were not suspended.

7.2 RECOMMENDATIONS

This research project has resulted in the following recommendations. The recommendations are directed towards the operation of the stirred tank for cell disruption.

i. The disruption of cells may be described by a first order rate equation.
ii. Significant soluble protein release (94% of total) from Bakers' yeast suspensions (dry mass concentrations 50 kg m^{-3} to 60 kg m^{-3}) may be achieved in a 1 dm^3 stirred tank using silica particles of mean diameter 1245 μm at a volume fraction of solids of 0.40 and an impeller tip speed of 3 m s^{-1}.
iii. The wall associated enzyme, invertase, may be released from yeast in the 1 dm^3 tank at operating conditions of an impeller tip speed of 2.2 m s^{-1} and a volume fraction of solids of 0.20 (silica, mean diameter 1245 μm)
iv Significant soluble protein release (94% of total) may be obtained from yeast in the stirred tank at a volume fraction of 1245 μm silica of 0.20 and an impeller speed of 772 rpm with an energy input of 0.008 kW hrs.
v A minimum impeller speed of 772 rpm is recommended for use with particles of 1245 μm for adequate suspension of solids. It was found that inadequate suspension of solids resulted in low extents of disruption.

7.3 AREAS FOR FURTHER RESEARCH

The effects of particulates on the degree of disruption of yeast has been reported in this dissertation. In addition, preliminary investigations into the effect of particulates on the metabolism of thiobacilli during and after agitation have been reported. From this study the following areas of further investigation emerged.

i. Investigation is required into the mechanisms of cell disruption. Applying mechanistic models to the dependency of the disruption rate constant on particle parameters may result in valid descriptive models. Having successfully modelled these effects, a combined function of the parametric effects should be studied.
ii The general trend established in this project illustrating the effect of increased power input on the disruption rate should be investigated in terms of combined operating parameters.

iii The use of the 1 dm^3 system as a cell disruption process should be validated by investigating soluble protein release from other microorganisms.

iv In addition to the effect of agitation in the presence of particulates on cell disruption, the effect of the particulates on the substrate utilization rate, product formation rate and growth rate of the cells should be investigated. These investigations will preferably include the effect of particulates on different microorganisms. Microorganisms utilized in industrial processes, in which solid substrates are present, should be used in further studies.

REFERENCES

Abu-Reesh,I. and Kargi,F. "Biological responses of hybridoma cells to hydrodynamic shear in an agitated bioreactor," *Enzyme Microb. Technol.* **13**, p.913-919, (November 1991)

Allen,E.J., Scragg,A.H. and Pugh,K., "Cell suspension culture of *Picrasma quassioides* : the development of a rapidly growing, shear resistant cell line capable of quassin formation," *J.Plant Physiol.* **132**, 176-183,(1988)

Andrews,G.F. and Tien,C., "Bacterial film growth in adsorbent surfaces," *A.I.Ch.E.J*, **27**, 396-403,(3 May 1981)

Andrews,B.A., Huang,R.-B. and Asenjo,J.A., "Differential product release from yeast cells by selective enzymatic lysis," In: **Separations in Biotechnology, volume 2**, ed. Pyle,D.L., p.21-28, (1990)

Atkinson,B., Black,G.M., Lewis,P.J.S. and Pinches,A., "Biological particles of given size, shape, and density for use in biological reactors," *Biotechnol. Bioeng.*, **21**, p.193-200,(1979)

Atkinson,B., and Fowler,H.W., "The significance of microbial film in fermenters," Chap. 6. In: **Advances in Biochemical Engineering., 3**, p.221-277,(1974)

Atlas,R.M., "Organization and Structure of microorganisms," Chapter 4 in **Microbiology - fundamentals and applications**, ed.Atlas,R.M., MacMillan Publishing, New York, p.100, (1984)

Bailey,J.L., "Miscellaneous analytical methods," Chapter 11 in **Techniques in Protein Chemistry**, Elsevier Publish. Co., p.340-352, (1967)

Bailey,J.E., and Ollis,D.F., **Biochemical Engineering Fundamentals**, eds. Carberry,J.J., Fair,J.R., Peters,M.S., Schowalter,W.R., Wei,J., 2nd edition, published by McGraw-Hill, (1986)

Barrett,J., Hughes,M.N., Karavaiko,G.I. and Spencer,P.A., **Metal extraction by bacterial oxidation of minerals**, series ed: Dr. J.Burgess, consulting ed: Ellis Horwood, published by Ellis Horwood Lmtd, England, (1993)

Beyer,M., Ebner,H.G. and Klein,J., "Influence of pulp density and bioreactor design on microbial desulphurization of coal," *Applied Microbiol. and Biotech.*, **24**, p.342-346, (1986)

Black,G.M., Webb,C. and Atkinson,B., "Practical reactor systems for yeast cell immobilization using biomass support particles," *Biotechnol. Bioeng.*, **26**, 134-141,(1984)

Brierley,M.R. and Steel,R., "Agitation-aeration in submerged fermentation," *Appl. Microbiol.*, **7**, 57-61,(1959)

Bronnenmeier,R., Markl,H., "Hydrodynamic stress capacity of microorganisms," *Biotechnol. Bioeng.*, **24**, 553-578, (1982)

Bryers,J.D. and Characklis,W.G., "Processes governing primary biofilm formation," *Biotechnol. Bioeng.*, **24**, p.2451-2476,(1982)

Calderbank,P.H. and Moo-Young,M.B., "The prediction of power consumption in the agitation of non-newtonian fluids," *Trans. Inst. Chem. Eng.*, **37**, 26-33,(1959)

Cherry,R.S., and Kwon,K-Y., "Transient Shear Stresses on a Suspension Cell in Turbulence," *Biotechnol. Bioeng.*, **36**, p.563-571, (September 1990)

Cherry,R.S. and Papoutsakis,E.T., "Physical Mechanisms of Cell Damage in Microcarrier Cell Culture Bioreactors," *Biotechnol. Bioeng.*, **32**, p.1001-1014, (October 1988)

Cherry,R.S. and Papoutsakis,E.T., "Modelling of contact-inhibited animal cell growth on flat surfaces and spheres," *Biotechnol. Bioeng.*, **33**, p.300-305, (1989)

Croughan,M.S., Hamel,J-F. and Wang,D.I.C., "Hydrodynamic Effects in Microcarrier Cultures," *Biotechnol. Bioeng.*, **29**, p.130-141, (January 1987)

Croughan,M.S., Hamel,J-F.P. and Wang,D.I.C., "Effects of Microcarrier Concentration in Animal Cell Culture," *Biotechnol. Bioeng.*, **32**, p.975-982, (October 1988)

Croughan,M.S. and Wang,D.I.C., "Growth and Death in Overagitated Microcarrier Cell Cultures," *Biotechnol. Bioeng.* **33**, p.731-744, (1989a)

Croughan,M.S., Sayre,E.S., Wang,D.I.C., "Viscous reduction of turbulent damage in animal cell culture," *Biotechnol. Bioeng.*, **33**, p.862-872, (1989b)

Cumming,R.H., Tuffnell,J., Street,G., "*Bacillus amyloloquefaciens* on the growth phase in batch culture," *Biotechnol. Bioeng.*, **27**, 887-889, (1985)

Currie,J.A., Dunnill,P, and Lilly,M.D., "Release of Protein from Bakers'Yeast (*Saccharomyces cerevisiae*) by Disruption in an Industrial Agitator Mill," *Biotechnol. Bioeng.*, **14**, p.725-736, (1972)

Davies,J.J., "Velocities and Stresses in Turbulent Flows," Chap. 1. In: **Turbulence Phenomena**. Academic Press, London, p.62-68, (1972)

DiSpirito,A.A., Dugan,P.R. and Tuovinen,O.H., "Inhibitory effects of particulate materials in growing cultures of *Thiobacillus ferrooxidans*," *Biotechnol. Bioeng.*, **23**, p.2761-2769, (1981)

DiSpirito,A.A., Dugan,P.R. and Tuovinen,O.H., "Sorption of *Thiobacillus ferrooxidans* to particulate material," *Biotechnol. Bioeng.*, **25**, p.1163-1168, (1983)

Doulah,M.S., Hammond,T.H. and Brookman,J.S.G., "A Hydrodynamic Mechanism for the Disintegration of *Saccharomyces cerevisiae* in an Industrial Homogenizer,". *Biotechnol. Bioeng.*, **17**, p.845-858, (1975)

Dunlop,E.H. and Ye,S.J., "Micromixing in fermentors: metabolic changes in *Saccharomyces cerevisiae* and their relationship to fluid turbulence,". *Biotechnol. Bioeng.*, **36**, p.854-864, (1990)

Engler,C.R., "Disruption of Microbial Cells," Chap. 20. In: **Comprehensive Biotechnology. Vol. 2.** (Ed: Moo-Young,M) Pergamon Press, p.305-324, (1985)

Engler,C.R. and Robinson,C.W., "Disruption of *Candida utilis* Cells in High Pressure Flow Devices," *Biotechnol. Bioeng.*, **23**, p.765-780, (1981a)

Engler,C.R. and Robinson,C.W., "Effects of organism type and growth conditions on cell disruption by impingement," *Biotechnol.Lett*, **3**(2), p.83-88, (1981b)

Espejo,R.T. and Ruiz,P., "Growth of free and attached *Thiobacillus ferrooxidans* in ore suspension," *Biotechnol. Bioeng.*, **30**, p.586-592, (1987)

Follows,M., Hetherington,P.J., Dunnill,P. and Lilly,M.D., "Release of enzymes from bakers' yeast by disruption in an industrial homogenizer," *Biotechnol. Bioeng.*, **13**, p.549-560, (1971)

Fowler,J.D. and Robertson,C.R., "Metabolic behaviour of immobilized aggregates of *Escherichia coli* under conditions of varying mechanical stress," *Appl. Environ. Microbiol.*, p.93-101, (1991)

Goldstein,A. and Lampen,J.O., "ß-D-Fructofuranoside Fructohydrolase from yeast," *Methods in Enzymology*, **42** (C), p.504-511, (1975)

Gormely,L.S. and Branion,R.M.R, "Engineering design of microbiological leaching reactors," proceedings of the *International Symposium on Biohydrometallurgy*, p.499-515, (August 1991)

Gusek,T.W., Johnson,R.D., Tyn,M.T. and Kinsella,J.E., "Effect of agitational shear on growth and protease production by *Thermomonospora fusca*," *Biotechnol. Bioeng.*, **37**, p.371-374, (1991)

Hackl,R.P., Wright,F.R. and Gormely,L.S., "Bioleaching of refractory gold ores-out of the lab and into the plant," proceedings of the *International Symposium on Biohydrometallurgy*, eds. Salley,J., McCready,R.G.L. and Wichlacz,P.L., p.533-549, (August 1991)

Hamer,G., "Immobilized microbes: interfaces, gradients and physiology," *Physio.Immob. Cells*, p.15-24, (1990)

Hansford,G.S. and Bailey,A.D., "Oxygen transfer limitation of bio-oxidation at high solids concentration," proceedings of *International Biohydrometallurgy Symposium*, Jackson Hole, (August 1993)

Harris,L. and Brierly,J.A., "Biotechnology," *Mining Magazine*, p.301-303, (October 1989)

Harris,C.M., Todd,R.W., Bungard,S.J., Lovitt,R.W., Gareth Morris,J. and Kell,D.B., "Dielectric permittivity of microbial suspensions at radio frequencies: a novel method for the real-time estimation of microbial biomass,". *Enzyme Microb. Technol.*, 9, p.181-186, (1987)

Harrison,S.T.L., "The extraction and purification of poly-B-hydroxybutyrate from *Alcaligenes eutrophus*," *Doctor of Philosophy in Chemical Engineering Thesis*, Cambridge University., (1990)

Harrison,S.T.L., "Bacterial cell disruption: A key unit operation in the recovery of intracellular products." *Biotechnol. Advs.*, **9**, p.217-240, (1991)

Harrison,S.T.L., Chase,H.A. and Dennis,J.S., "The lysis of gram-negative *Alcaligenes eutrophus* by enzymes from *Cytophaga*," *Bio/technology*, **5**(2), p.115-120, (1991)

Hetherington,P.J., Follows,M., Dunnill,P. and Lilly,M.D., "Release of protein from Bakers' yeast (*Saccharomyces cerevisiae*) by disruption in an industrial homogeniser," *Trans. Instn. Chem. Engrs.*, **49**, p.142-148, (1971)

Hooker,B.S., Lee,J.M. and An,G., "Response of plant tissue culture to a high shear environment," *Enzyme Microb. Technol.*, **11**, p.484-490, (1989)

Hooker,B.S., Lee,J.M. and An,G., "Cultivation of plant cells in a stirred vessel: effect of impeller design," *Biotechnol. Bioeng.*, **35**, p.296-304, (1990)

Hunter,J.B., and Asenjo,J.A., "Kinetics of enzymatic lysis and disruption of yeast cells: 1. evaluation of two lytic systems with different properties," *Biotechnol. Bioeng.*, **30**, p.471-480, (1987)

Hunter,J.B. and Asenjo,J.A., "A structured mechanistic model of the kinetics of enzymatic lysis and disruption of yeast cells," *Biotechnol. Bioeng.*, **31**, p.929-943, (1988)

Kawase,Y. and Moo-Young,M., "Hydrodynamics in bubble column reactors with fermentation broths having a yield stress," *Applied Microbiol. and Biotech.*, **30**, p.596-603, (1989)

Kawase,Y. and Moo-Young,M., "Mathematical models for design of bioreactors: applications of Kolmogoroff's theory of isotropic turbulence," *Chem. Eng. J.*, **43**, p.B19-B41, (1990)

Keshavarz-Moore,E., Hoare,M. and Dunnill,P., "Biochemical engineering aspects of cell disruption," Chap. 3. In: **Separations for Biotechnology.**, (Eds: Verrall,MS; Hudson,MJ) Ellis Horwood Ltd, p.62-79,(1987)

Kula,M-R. and Schutte,H., "Purification of proteins and the disruption of microbial cells," *Biotechnol. Prog.*, **3**, p.31-42, (1987)

Lakhotia,S. and Papoutsakis,E.T., "Agitation induced cell injury in microcarrier cultures. Protective effect of viscosity is agitation intensity dependent: experiments and modeling," *Biotechnol. Bioeng.*, **39**, p.95-107, (1992)

Lee,C-H., Tsang,S.K., Urakabe,R. and Rha,C.K., "Disintegration of Dried Yeast Cells and its Effect on Protein Extractability, Sedimentation Property, and Viscosity of the Cell Suspension," *Biotechnol. Bioeng.*, **21**, p.1-17, (1979)

Lee,G.M., Huard,T.K., Kaminski,M.S. and Palsson,B.O., "Effect of mechanical agitation on *Hybridoma* cell growth," *Biotechnol.Lett.*, **10**(9), p.625-628, (1988)

Li,D. and Ganczarczyk,J.J., "Structure of activated sludge flocs," *Biotechnol. Bioeng.*, **35**, p.57-65, (1990)

Lilly,M.D., Ison,A., Shamlou,P.A., "The influence of the physical environment in fermenters on antibiotic production by microorganisms," In: **Harvesting Biotechnology for the 21st Century**, Eds. Ladisch,M.R., Bose,A., *American Chemical Society*, 219-222, (1992)

Limon-Lason,J., Hoare,M., Orsborn,C.B., Doyle,D.J., Dunnill,P., "Reactor properties of a high-speed bead mill for microbial cell rupture," *Biotechnol. Bioeng.*, **21**, p.745-774, (1979)

Lindstrom,E.B., Gunneriusson,E. and Tuovinen,O.H., "Bacterial oxidation of refractory sulfide ores for gold recovery," *Critical Reviews in Biotechnology*, **12**, p.133-155, (1992)

Liu,M.S., Branion,R.M.R. and Duncan,D.W., "The effects of ferrous iron, dissolved oxygen, and inert solids concentrations on the growth of *Thiobacillus ferrooxidans*," *Can. J. Chem. Eng.*, **66**, p.445-451, (1988)

Logan,B.E. and Dettmer,J.W., "Increased Mass Transfer to Microorganisms with Fluid Motion," *Biotechnol. Bioeng.*, **35**, p.1135-1144, (1990)

Logan,B.E. and Hunt,J.R., "Bioflocculation as a microbial response to substrate limitations," *Biotechnol. Bioeng.*, **31**, p.91-101, (1988)

Lovitt,R.W., Walter,R.P., Morris,J.G. and Kell,D.B., "Conductimetric assessment of the biomass content in suspensions of immobilised (gel-entrapped) microorganisms," *Applied Microbiol. and Biotech.*, **23**, p.168-173, (1986)

Lowry,O.H., Rosebrough,N.J., Farr,A.L. and Randall,R.J., *Journal of Biological Chemistry*, **193**, p.265-275, (1951)

Lynch, A.J.: **Mineral crushing and Grinding circuits**, ed. Forssberg, K.S.E., publisher Elsevier, p.98, (1985)

Maiorella,B., Dorin,G., Carion,A. and Harano,D., "Crossflow microfiltration of animal cells," *Biotechnol. Bioeng.*, **37**, 121-126, (1991)

Marffy,F. and Kula,M-R., "Enzyme yields from cells of brewer's yeast disrupted by treatment in a horizontal disintegrator," *Biotechnol. Bioeng.*, **16**, p.623-634, (1974)

Meadows,P.S., "The attachment of bacteria to solid surfaces," *Arch. Mikrobiol.*, **75**, p.374-381, (1971)

Mersmann,A., Schneider,G., Volt,H. and Wenzig,E., "Selection and design of aerobic bioreactors," *Chem. Eng. Technol.*, **13**, p.357-370, (1990)

Metzner,A.B., Feehs,R.H., Ramos,H.L., Otto,R.E. and Tuthill,J.D., "Agitation of viscous newtonian and non-newtonian fluids," *A.I.Ch.E.J.*, 7, p.3-9, (1961)

Metzner,A.B. and Otto,R.E., "Agitation of non-newtonian fluids," *A.I.Ch.E.J.*, **3**(1), p.3-10, (1957)

Mills,D.B., Bar,R. and Kirwan,D.J., "Effect of solids on oxygen transfer in agitated three-phase systems," *A.I.Ch.E.J.*, **33**(9), p. 1542-1549, (1987)

Mittelman,M.W., Nivens,D.E., Low,C. and White,D.C., "Differential adhesion, activity and carbohydrate: protein ratios of *Pseudomomnas atlantica* monocultures attaching to stainless steel in a linear shear gradient," *Microb. Ecol.*, **19**, p.269-278, (1990)

Mogren,H., Lindblom,M. and Hedenskog,G., "Mechanical disintegration of microorganisms in an industrial homogenizer," *Biotechnol. Bioeng.*, **16**, p.261-274, (1974)

Moo-Young,M. and Chisti,Y., "Considerations for designing bioreactors for shear-sensitive culture," *Bio/technology*, p.1291-1296, (November 1988)

Myerson,A.S. and Kline,P., "The adsorption of *Thiobacillus ferrooxidans* on solid particles," *Biotechnol. Bioeng.*, **25**, p.1669-1676, (1983)

Nagata,S. (Ed.) : **Mixing, Principles and applications.** 1st ed., **Vol. 1**. Kodansha Ltd, Tokyo.(1975)

Ngian,K-F. and Martin,W.R.B., "Bed expansion characteristics of liquid fluidised particles with attached microbial growth," *Biotechnol. Bioeng.*, **22**, p.1843-1856, (1980)

Nienow,A.W. and Miles,D., "Impeller power numbers in closed vessels," *Ind. Eng. Chem. Process Des. Develop.*, **10**(1), p.41-43, (1971)

Nienow,A.W., "New agitators versus Rushton turbines: a critical comparison of transport phenomena," conference proceedings of *Harnessing Biotechnology for the 21st Century*, eds. Ladisch,M.R. and Bose,A., p.193-196, (1992)

Nikolov,L. and Karamanev,D., "Experimental study of the inverse fluidized bed biofilm reactor," *Can.J.Chem.Eng.*, **65**, p.214-217, (1987)

Nikov,I. and Delmas,H., "Mechanism of solid-liquid mass transfer and shear stress in three-phase fluidized beds," *Chem. Engng. Sci.*, **47**(3), p.673-681, (1992)

Oguz,H., Brehm,A. and Deckwer,W.D., "Gas/liquid mass transfer in sparged agitated slurries," *Chem. Engng. Sci.*, **42**(7), p.1815-1822, (1987)

Oldshue,J.Y., **Fluid Mixing Technology**, McGraw-Hill, New York, 1983

Ozbas,T. and Kutsal,T., "Effects of agitation and aeration rates on riboflavin fermentation by *Ashbya gossypii*", *Biotechnol. Appl. Biochem.*, **13**, p.97-105, (1991)

Peillex,J-P., Fardeau,M-L., Boussand,R., Navarro,J-M. and Belaich,J-P., "Growth of *Methanococcus thermolithotrophicus* in batch and continuos culture on H_2 and CO_2 :influence of agitation," *Applied Microbiol. and Biotech.*, **29**, p.560-564, (1988)

Peterson,G.L., "Review of the Folin Phenol protein quantitation method of Lowry, Roseborough, Farr and Randall," *Analytical Biochemistry*, **100**, p.201-220, (1979)

Pinches,A., "Bacterial leaching of an arsenic-bearing sulfide concentrate," in *Leaching and Reduction in Hydrometallurgy*, ed. Burkin,A.R., p.28, (1975)

Poncelet,D. and Neufield,R.J., "Shear breakage of nylon membrane microcapsules in a turbine reactor," *Biotechnol. Bioeng.*, **33**, p.95-103, (1989)

Prud'homme and Shaqfeh,E., "Effect of elasticity of mixing torque requirements for rushton turbine impellers," *A.I.Ch.E.J.*, **30**(3), p.485-486, (1984)

Pryor,E.J., "Mineral processing - secondary crushing" Chapter 4 in: **Mineral Processing**, 3rd Edition, publisher Applied Science Publishers Lmtd, London, p.63-66, 1978

Rao (1966), in: **Mineral Crushing and Grinding Circuits**, ed. Forssberg, K.S.E., publisher Elsevier, p.98, (1985)

Rehacek,J. and Schaefer,J., "Disintegration of microorganisms in an industrial horizontal mill of novel design," *Biotechnol. Bioeng.*, **19**, p.1523-1534, (1977)

Reuss,M., Josic,D., Popovic,M. and Bronn,W.K., "Viscosity of Yeast suspensions," *Eur. J. Appl. Microbiol.*, **8**, p.167-175, (1979)

Reuss,M., "Influence of mechanical stress on the growth of *Rhizopus nigricans* in stirred bioreactors," *Chem. Eng. Technol.*, **11**, p.178-187, (1988)

Rittmann,B.E., "The effect of shear stress on biofilm loss rate," *Biotechnol. Bioeng.*, **24**, p.501-506, (1982)

Robertson,B. and Ulbrecht,J.J., "Measurement of shear rate on an agitator in a fermentation broth," *Biotechnol. Proc* (Eds: Ho,CS; Oldshue, JY), p.31-35, (1987)

Roy,P. and Mishra,A.K., "Factors affecting oxidation of pyrite by *Thiobacillus ferrooxidans*," *Indian Journal of Experimental Biology*, **19**, p.728-732, (1981)

Rushton,J.H, Costich,E.W. and Everett,H.J., *Chem. Eng. Prog.*, **46**, p467, (1950)

Schutte,H., Kraume-Flugel,R., Kula,M-R., "Scale-up of mechanical cell disintegration - influence of stirrer geometry on residence time distribution and cell disintegration in a 20l high-speed ball mill," *Ger. Chem. Eng.*, **9**, p.149-156, (1986)

Schutte,H., Kroner,K.H., Hustedt,H., Kula,M-R., "Experiences with a 20 litre industrial bead mill for the disruption of microorganisms," *Enzyme Microb. Technol.*, **5**, p.143-148, (1983)

Schutte,H. and Kula,M-R., "Analytical disruption of microorganisms in a mixer mill," *Enzyme Microb. Technol.*, **10**, p.552-558, (1988)

Scragg,A.H., Allan,E.J., Leckie,F., "Effect of shear on the viability of plant cell suspensions," *Enzyme Microb. Technol.*, **10**, p.361-367, (1988)

Shieh,W.K., "Suggested kinetic model for the fluidised-bed biofilm reactor," *Biotechnol. Bioeng.*, **22**, p.667-676, (1980)

Silverman,M.P. and Lundgren,D.G., "Studies on the chemotrophic iron bacterium *Ferrobacillus ferrooxidans*," *J. Bacteriology*, **77**, p.642-646, (1959)

Silverman,M.P. and Lundgren,D.G., "Studies on the chemotrophic iron bacterium *Ferrobacillus ferrooxidans*," *J. Bacteriology*, **78**, p.326-331, (1959)

Skowlund,C.T., "Effect of biofilm growth on steady-state biofilm models," *Biotechnol. Bioeng.*, **35**, p.502-510, (1990)

Smith,J.J., Lilly,M.D., Fox,R.I., "The effect of agitation on the morphology and penicillin production of *Penicillium chrysogenum*," *Biotechnol. Bioeng.*, **35**, p.1011-1023, (1990)

Smith,P.K., Krohn,R.I., Hermanson,G.T., Mallia,A.K., Gartner,F.H., Provenzano,M.D., Fujimoto,E.K., Goeke,N.M., Olson,B.J. and Klenk,D.C., "Measurement of protein using Bicinchoninic acid," *Analytical Biochemistry*, **150**, p.76-85, (1985)

Spietel,G.E., DiGiano,F.A., "Biofilm shearing under dynamic conditions," *ASCE J. Environ. Engng.*, **113**(1-3), p.464-475, (1987)

Stathopoulos,N.A. and Hellums,J.D., "Shear stress effects on human embryonic kidney cells *in vitro*," *Biotechnol. Bioeng.*, **27**, p.1021-1026, (1985)

van Suijdam;J.C. and Metz,B., "Influence of engineering variables upon the morphology of filamentous molds," *Biotechnol. Bioeng.*, **23**, p.111-148, (1981)

Thomasset,B., Gontier,E., Sangwan-Norreel,B.S., Barbotin,J.N., "Influence of stress conditions (*ie.* immobilization) on growth, viability and alkaloid contents of *Coffea arabica* and *Datura innoxia* cells," *Physio.Immob. Cells.*, p.597-602, (1990)

Toma,M.K., Ruklisha,M.P., Vanags,J.J., Zeltina,M.O., Leite,M.P., Galinina,N.I., Viesturs,U.E., Tengerdy,R.P., "Inhibition of microbial growth and metabolism by excess turbulence," *Biotechnol. Bioeng.*, **38**, p.552-556, (1991)

Torma,A.E., Walden,C.C. and Branion,R.M.R, "Microbiological leaching of a zinc sulfide concentrate," *Biotechnol. Bioeng.*, **12**, p.501-517, (1970)

Torma,A.E., Walden,C.C., Duncan,D.W. and Branion,R.M.R., "The effect of carbon dioxide and particle surface area on the microbiological leaching of a zinc sulfide concentrate," *Biotechnol. Bioeng.*, **14**, p.777, (1972)

Torma,A.E., "The role of *Thiobacillus ferrooxidans* in hydrometallurgical processes," *Advances in Biochemical Engineering*, **6**, p.1-37, (1977)

Umbrecht,W.W., **Modern microbiology**, 1st ed. Vol. **1**. (Series Eds: Emerson,R., Kennedy,D., Park,R.B., Beadle,G.W., Whitaker,D.M., A series of books in biology.) W.H.Freeman and company, San Francisco. 507 pages.(1962)

Vanags,J.J., Rikmanis,M.A., Ushkans,E.J., Viesturs,U.E., "Stirring characteristics in bioreactors," *A.I.Ch.E.J.*, **36**(9), p.1361-1369, (1990)

Vand,V, "Viscosity of solutions and suspensions" *J. Phys. Coll. Chem.*, **52**, p.277, (1948)

Wanner,O. and Gujer,W., "Multispecies biofilm model," *Biotechnol. Bioeng.*, **28**, p.314-328, (1986)

Weisman,J., Efferding,L.E., "Suspension of slurries by mechanical mixers," *A.I.Ch.E.J.*, **6**, (3), 419-426, (September, 1960)

Whitton,M.J. and Nienow,A.W., "Scale up correlations for gas holdup and mass transfer coefficients in stirred tank reactors," proceedings of *3rd International Conference on Bioreactor and Bioprocess Fluid Dynamics*, ed. A.W.Nienow, p.135-149, (1993)

Yu,M. and Bajpai,R., "Role of mixing in stirred tanks," *Biotechnol. Bioeng. Symp.*, (17), p.673-681, (1986)

APPENDIX 1

1. DETERMINATION OF PROTEIN CONCENTRATION BY LOWRY METHOD

The Folin phenol reagent of Folin and Ciocalteu contains an active constituent called phosphomolybdic-tungstic mixed acid. Proteins reduce the mixed acid to produce one or more of several reduced species which are characteristically blue in colour. The Folin-Ciocalteu reagent is only stable in acid solution, however the reduction only occurs at alkaline pH, therefore mixing of the copper-protein solution and the reagent must be rapid so that reduction occurs before the reagent is broken down.

Reagents

Reagent A : Dissolve 100 g Na_2CO_3 in 1 litre (final volume) 0.5 N NaOH.

Reagent B : Dissolve 1 g $CuSO_4.5H_2O$ in 100 ml (final volume) distilled water.

Reagent C : Dissolve 2 g potassium tartrate in 100 ml (final volume) distilled water.

Reagent D : Dissolve 0.3 g bovine serum albumin (Sigma Chemical Co., catalogue no. A4378) in 1 dm^3 (final volume) distilled water.

Reagent E : Add 5 ml of 2 N Folin-Phenol reagent (Sigma Chemical Co., catalogue no. F9252) to 50 ml distilled water and mix thoroughly.

Method

All standards and samples must be done in triplicate.

1) Pipette 0, 0.1, 0.2, 0.3, 0.4, 0.5, 0.6, 0.7, 0.8, 0.9 and 1 ml bovine serume albumin solution (Reagent D) in test tubes for the standard protein curve. Each concentration is done in triplicate.
2) Supernatants of cell samples must be used. Pipette 0.1 ml of appropriately diluted sample into test tubes.
3) Bring the total volume of all test tubes to 1 ml with distilled water.
4) Mix together 15 ml reagent A, 0.75 ml reagent B and 0.75 ml reagent C.
5) Add 1 ml of the above mixture to each test tube and mix thoroughly.
6) Incubate tubes for 15 minutes at room temperature.

7) Rapidly add 3 ml of reagent E to each tube and mix immediately. Addition and mixing of each tube should be completed before proceeding and should be done as rapidly as possible.
8) Incubate the sample in a dark place at room temperature for 45 minutes.
9) Determine the absorbance of each sample at 660nm. Absorbances should be determined as soon as possible after incubation.
10) The colour remains constant about 45 minutes to 1 hour after incubation.

The variation between readings in an assay is usually less than 3% of the mean value and always less than 5%. Figure A1 illustrates a typical standard protein curve of protein concentration versus absorbance at 660 nm. The correlation coefficient of the straight line is 0.997. The equation of the curve is:

absorbance = 0.035 + 3.054 * protein concentration (mg/ml) Eqn. A1

The average error between readings of this curve is 1.24%.

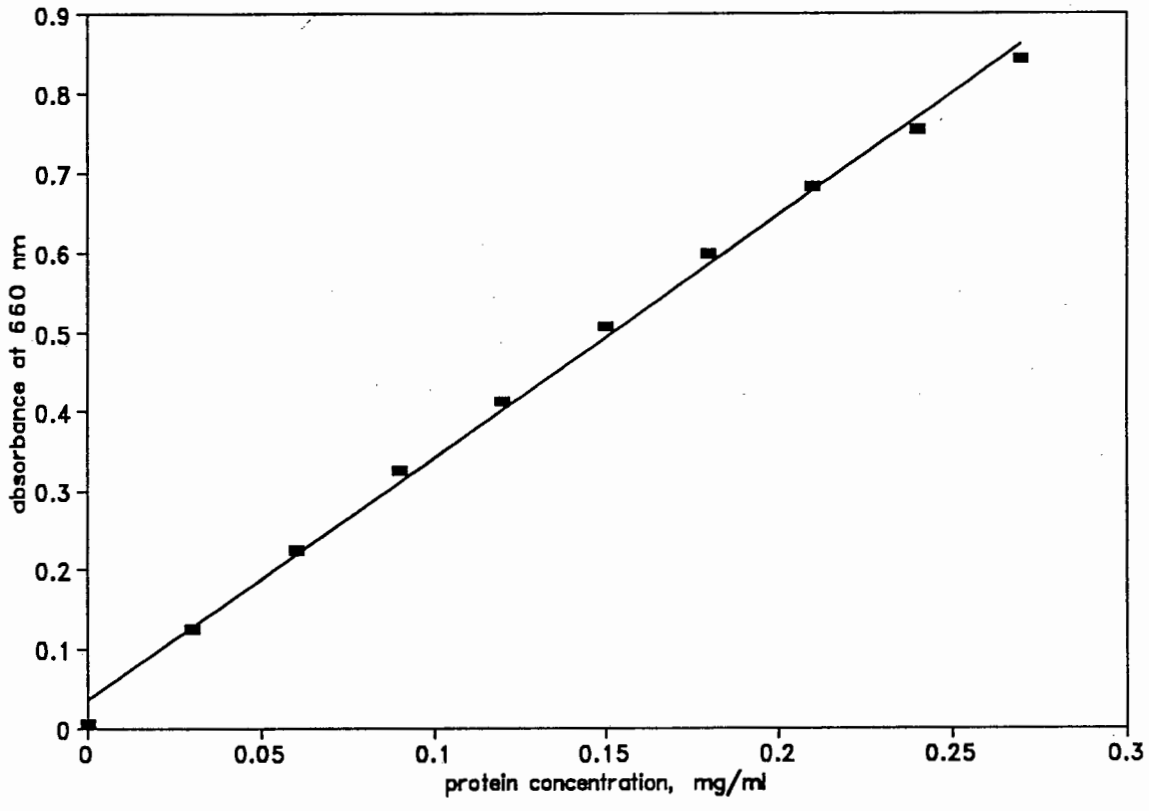

Figure A1 Standard curve of protein concentration versus absorbance at 660 nm

2. DETERMINATION OF INVERTASE ACTIVITY IN THE SAMPLE SUPERNATANT

External invertase or ß-D-Fructofuranoside Fructohydrolase is a wall-associated enzyme found in the mannoprotein layer of yeast cell walls (Hunter and Asenjo, 1988). The most common colorimetric method of determining the activity is based on the enzymic hydrolysis of sucrose to glucose and fructose (Goldstein and Lampen, 1975).

Reagents

Sodium acetate buffer 0.2 M pH 4.9

Dissolve 1.944 g of sodium acetate in 120 ml distilled water.

Dilute 1.836 ml of glacial acetic acid (17.4 M) to 160 ml with distilled water.

Mix 35 ml acetic acid solution and 105 ml sodium acetate and adjust pH to 4.9.

Potassium phosphate buffer 0.5 M pH 7.0

Dissolve 21.76 g KH_2PO_4 in 320 ml distilled water.

Dissolve 14 g K_2HPO_4 in 160 ml distilled water.

Mix 30 ml of K_2HPO_4 and 20 ml of KH_2PO_4 and adjust pH to 7.

Sucrose solution

Dissolve 1.7112 g of sucrose in 10 ml distilled water.

Invertase standard solutions

Dissolve 0.0277 g invertase (Sigma Chemical Co., catalogue no. I9253) in 10 ml distilled water. Dilutions were performed to obtain solutions containing 1, 2, 3, 4 and 5 units ml^{-1}.

Glucose kit solution 1 (Boehringer Mannheim GmbH Diagnostica, catalogue no. 124036)

glucose standard solution 9.1 mg/ 100 ml, equivalent to 0.505 mmol l^{-1}.

Glucose kit solution 2 (Boehringer Mannheim GmbH Diagnostica, catalogue no. 124036)

phosphate buffer	100 mmol l^{-1}	pH 7.0.
peroxidase	> 0.8 units ml^{-1}.	

glucose oxidase	> 10 units ml^{-1}.
ABTS	1.0 mg ml^{-1}.

Method

Each standard and sample to be done in triplicate test tubes.

1) Pipette 0.5 ml sodium acetate buffer into each test tube.
2) Pipette 0.2 ml enzyme standards and sample supernatants, appropriately diluted, into tubes.
3) To start reaction, add 0.25 ml sucrose solution and start stopwatch. Place test tubes in 30°C water bath for five to ten minutes (determined accurately).
4) Remove from water bath and add 1.0 ml potassium phosphate buffer to each test tube to stop the reaction. Place tubes in 100°C water bath for 3 minutes. Record reaction time which is the time taken from the addition of sucrose to placement in the boiling water bath.
5) When tubes have cooled, the glucose content must be analysed.
6) Pipette 0.2 ml glucose standard (kit solution 1) and distilled water (blank sample) into test tubes.
7) Pipette 0.2 ml enzyme standards and samples into test tubes.
8) Rapidly add 5.0 ml kit solution 2 and mix immediately. Incubate for 25 to 50 minutes in a dark place at room temperature. Measure the absorbances of the enzyme standards, samples and glucose standard against the distilled water (blank) at 620 nm.
9) If glucose concentration exceeds 5 g dm^{-3}, repeat assay with diluted sample.
10) Calculate the glucose concentrations of the samples using the following calculation:

$$c \text{ (mg/ 100 ml)} = 100 * A_{sample}/A_{standard} \qquad \text{Eqn. A2}$$

$$c \text{ (mmol } l^{-1}) = 5.55 * A_{sample}/A_{standard} \qquad \text{Eqn. A3}$$

11) Using the standard enzyme samples readings, construct a standard curve of glucose concentration as a function of enzyme activity and determine the sample enzyme activities from this basis.

The variation between readings within the enzyme assay is always less than 5% of the mean value of the readings. See Appendix 4 for calculation of variation. Figure A2 illustrates a typical standard enzyme assay curve of glucose concentration (mg/ 100 ml) versus invertase concentration (μmole/min/ml). The correlation coefficient of the curve is 0.996 and the function of the curve is:

glucose concentration (mg/ 100ml) = 165*invertase concentration (μmole/min/ml) - 6.84

Eqn. A4

The average variation of the readings in this curve is 3.63%.

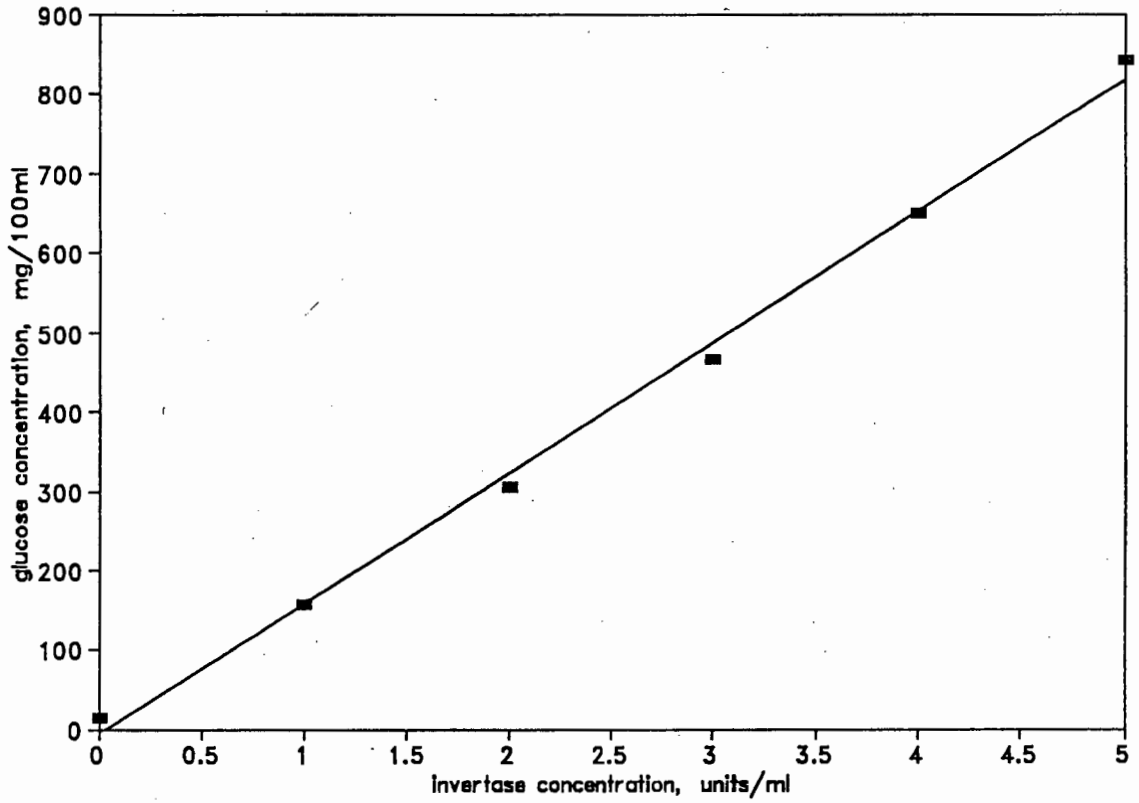

Figure A2 Invertase standard curve of glucose concentration versus enzyme concentration

APPENDIX 2

MEDIA AND BUFFER SOLUTIONS

1. Phosphate buffered saline (PBS)

NaCl	8.0 kg m^{-3}
KCl	0.2 kg m^{-3}
KH_2PO_4	0.2 kg m^{-3}
Na_2HPO_4	2.254 kg m^{-3}

2. 9 K media

$(NH_4)_2SO_4$	3.0 kg m^{-3}
K_2HPO_4	0.5 kg m^{-3}
KCl	0.1 kg m^{-3}
$MgSO_4.7H_2O$	0.5 kg m^{-3}
$Ca(NO_3)_2$	0.01 kg m^{-3}

distilled water adjusted to pH 1.8 tp 1.9 with concentrated H_2SO_4

$FeSO_4.7H_2O$	44.8 kg m^{-3}

3. 4 K media

salts as for 9 K media

$FeSO_4.7H_2O$	19.8 kg m^{-3}

APPENDIX 3

This appendix includes a sample table illustrating the calculation procedure for obtaining the disruption rate constant, k, and the extent of disruption, R_i, from the raw absorbamce data. Furthermore the values of protein release used to formulate each graph in Chapter 4 are tabulated. Finally the variations within single experiments and between different experiments is included.

impeller speed 772 rpm
20 volume % sand loading dilutions: 0-4mins: 1/10, 6-120mins: 1/110
yeast conc. = 49.76 g/l Rm = 487.2 mg protein/g cell

time in minutes	absorbance at 660 nm			average absorbance	protein conc. off std. curve mg/ml	*dilution factor	mg protein/ g cell	mg prot/g cell corrected for zero, R	R/Rm*100 = percent disruption	extent Rm/(Rm-R) = Y	Ri = ln Y	470 RI/(RI-R)	ln YI
0.000	0.082	0.089	0.085	0.085	0.013	0.127	2.562	0.000	0.000	1.000	0.000	1.000	0.000
0.500	0.266	0.210	0.217	0.231	0.065	0.646	12.976	10.414	2.138	1.022	0.022	1.023	0.022
1.000	0.319	0.342	0.331	0.331	0.100	1.000	20.101	17.539	3.600	1.037	0.037	1.039	0.038
1.500	0.424	0.418	0.430	0.424	0.133	1.332	26.774	24.212	4.970	1.052	0.051	1.054	0.053
2.000	0.489	0.510	0.526	0.508	0.163	1.632	32.803	30.241	6.207	1.066	0.064	1.069	0.067
3.000	0.676	0.696	0.707	0.694	0.229	2.292	46.053	43.491	8.927	1.098	0.094	1.102	0.097
4.000	0.843	0.848	0.862	0.851	0.265	2.651	57.301	54.739	11.235	1.127	0.119	1.132	0.124
6.000	0.149	0.152	0.153	0.151	0.036	3.985	80.083	77.521	15.912	1.189	0.173	1.198	0.180
8.000	0.181	0.190	0.198	0.190	0.050	5.485	110.229	107.667	22.099	1.284	0.250	1.297	0.260
10.000	0.212	0.217	0.215	0.215	0.059	6.483	129.889	127.328	26.135	1.354	0.303	1.372	0.316
60.000	0.487	0.506	0.562	0.526	0.169	18.633	374.464	371.903	76.335	4.226	1.441	4.791	1.567
120.000	0.630	0.620	0.618	0.623	0.204	22.429	450.747	448.185	91.992	12.487	2.525	21.545	3.070

protein results for speed experiments

speed in rpm	115	150	200	250	300	360	540	772	1090
time in minutes	R mg protein/ g cell								
0.000	0.000	0.000	0.000	0.000	0.000	0.000	0.000	0.000	0.000
1.000	0.915	0.706	0.749	1.827	1.635	3.000	12.000	17.500	17.000
2.000	0.979	1.477	1.379	2.577	3.052	6.000	23.000	30.200	30.000
4.000	1.044	1.670	1.560	5.840	7.369	13.000	39.000	54.700	60.000
6.000	1.044	1.788	2.780	9.327	10.527	18.000	70.000	77.500	75.000
8.000	1.129	2.344	2.940	11.125	14.463	23.000	90.000	107.600	101.000
10.000	2.027	2.440	4.021	13.279	17.687	27.000	101.000	127.300	119.000
30.000								251.000	
45.000								310.000	
60.000	3.822	9.150	42.832	77.835	108.990	153.000	315.000	371.900	360.000
120.000	8.892	16.213	74.140	125.488	178.740	221.000	368.000	448.100	449.000

protein results for solids experiments

solids loading volume percent	5	10	20	30	40
time in minutes	R mg protein/ g cell				
0.000	0.000	0.000	0.000	0.0000	0.000
1.000	3.000	4.000	17.500	32.5000	82.568
2.000	3.000	7.000	30.2000	50.8000	128.295
4.000	6.000	13.000	54.7000	108.4000	211.016
6.000	8.000	20.000	77.5000	182.8000	267.144
8.000	9.000	25.000	107.6000	196.1000	330.314
10.000	11.000	30.000	127.3000	248.4000	356.582
60.000	42.000	154.000	371.9000	418.6000	465.027
120.000	107.000	282.000	448.1000	449.400	474.000

protein results for size experiments

size range	59-222	106-247	180-383	185-501	560-973	510-1027	526-1027	861-1761
geometric mean particle size microns	114.400	161.600	255.620	304.400	703.000	691.930	735.000	1245.600
time in min	R mg protein/ g cell							
0.000	0.000	0.000	0.000	0.000	0.000	0.000	0.000	0.000
1.000	0.677	0.277	2.939	11.149	17.530	14.153	15.150	14.000
2.000	0.977	0.194	7.441	21.884	26.743	27.392	29.021	26.000
4.000	1.604	2.822	13.885	40.337	50.518	48.985	52.309	48.000
6.000	1.754	3.873	20.706	56.632	79.795	74.884	78.490	74.000
8.000	1.905	6.861	26.179	83.061	99.501	98.223	104.670	96.000
10.000	1.930	8.573	30.439	115.036	127.371	102.395	124.939	136.000
60.000	2.331	45.954	136.424	285.764	360.052	366.100	362.304	342.000
120.000	15.340	82.390	234.940	346.409	374.025	428.227	369.290	410.000

protein results for density experiments

particle type	carbon	silica	chromite
particle density kg/m3	1640.000	2700.000	4500.000
time in minutes	R mg protein/ g cell		
0.000	0.000	0.000	0.000
1.000	8.662	9.564	17.986
2.000	17.665	15.486	31.953
4.000	32.458	27.652	49.270
6.000	41.375	49.481	80.107
8.000	57.764	59.825	100.301
10.000	75.089	78.533	112.854
60.000	293.778	325.876	345.409
120.000	386.959	390.668	435.539

protein results for yeast concentration experiments

yeast concentration g/l	10.200	20.200	55.400	108.000	130.000
time in minutes	R mg protein/g cell				
0.000	0.000	0.000	0.000	0.000	0.000
1.000	20.085	19.624	14.100	10.919	20.113
2.000	35.244	34.714	26.215	19.617	28.104
4.000	63.415	62.391	48.302	35.059	37.465
6.000	96.764	86.616	74.500	59.384	44.772
8.000	119.629	101.030	96.156	72.811	63.106
10.000	144.641	124.173	138.201	96.288	98.302
60.000	322.505	247.398	342.309	327.408	313.074
120.000	351.812	283.465	410.270	397.863	389.107

variation within a standard protein assay

protein concentration mg/ml	absorbance at 660 nm			average absorbance, a	standard deviation, s	variation in percent s/a *100
0.030	0.125	0.124	0.130	0.126	0.0026	2.060
0.060	0.220	0.225	0.230	0.225	0.0041	1.820
0.090	0.318	0.330	0.328	0.325	0.0052	1.600
0.120	0.414	0.415	0.411	0.413	0.0017	0.410
0.150	0.509	0.510	0.502	0.507	0.0036	0.710
0.180	0.582	0.593	0.619	0.598	0.0155	2.590
0.210	0.673	0.672	0.697	0.681	0.0116	1.700
0.240	0.757	0.741	0.760	0.753	0.0083	0.010
0.270	0.844	0.843	0.839	0.842	0.0022	0.260
					average variation	1.24

variation between standard protein assays performed on different days in a period of 9 months

number of standard tests	protein conc. mg/ml	mean of absorbance readings, x	standard deviation, s	variation in percent s/x *100
8	0.030	0.125	0.012	9.470
8	0.060	0.222	0.023	10.180
8	0.090	0.312	0.033	10.430
8	0.120	0.395	0.043	10.840
8	0.150	0.482	0.056	11.560
7	0.180	0.578	0.054	9.270
6	0.210	0.668	0.058	8.650
7	0.240	0.725	0.087	11.930
7	0.270	0.805	0.092	11.480
			average variation	10.42

variation between standard runs at 772 rpm and 20% loading over 9 month period

number of tests	time of sample	average protein conc., x	standard deviation, s	variation in percent s/x *100
13	1.000	0.014	0.0015	11.140
13	2.000	0.026	0.0022	8.600
13	4.000	0.047	0.0063	13.380
13	6.000	0.069	0.0067	9.670
13	8.000	0.091	0.0092	10.210
13	10.000	0.114	0.0132	11.570
11	60.000	0.332	0.0259	7.800
8	120.000	0.399	0.0299	7.500
			average variation	9.980

variation between different french press experiments

number of tests	number of passes in french press	average protein conc., x	standard deviation, s	variation in percent s/x *100
8	1	0.267	0.041	15.350
9	2	0.435	0.055	12.600
8	3	0.470	0.030	6.430
10	4	0.505	0.044	8.730
			average variation	10.780

APPENDIX 4

The release of invertase is tabulated in this appendix. An example of the calculational table used for obtaining the enzyme release constant is given. The variations within and between experiments are reported.

Impeller speed 250 rpm Em = 2070 units invertase/g cell
yeast conc. = 50.79 g/l

time in min	absorbance at 620 nm			average absorbance	glucose concentration mg/100ml	glucose concentration mmol/l	invertase concentration off std. curve mmol/l (micromole/ml)	*dilution factor	inv. conc./ time of reaction mmol/l/min =micromole/ml /min=units/ml	invertase conc. in units/ g cell	invertase conc. corrected for zero, E	Em/(Em-E) = F	ln F
0.000	0.347	0.327	0.300	0.325	116.997	6.493	0.300	3.301	0.280	5.508	0.000	1.000	0.000
1.000	0.573	0.623	0.561	0.586	211.051	11.713	0.674	9.818	0.815	16.048	10.541	1.005	0.005
2.000	0.673	0.674	0.608	0.652	234.835	13.033	1.020	11.216	0.950	18.714	13.207	1.006	0.006
4.000	0.961	0.985	0.988	0.966	356.036	19.760	1.760	19.357	1.640	32.298	26.790	1.013	0.013
6.000	1.338	1.462	1.185	1.336	481.081	26.700	2.323	27.756	2.352	46.312	40.805	1.020	0.020
8.000	0.945	0.977	0.827	0.916	330.210	18.327	1.602	33.842	2.851	56.134	50.626	1.025	0.025
10.000	1.116	1.126	1.126	1.124	405.045	22.480	2.059	43.236	3.664	72.146	66.638	1.033	0.033
60.000	1.561	1.750	1.982	1.771	638.198	35.420	3.483	212.443	18.004	354.472	348.965	1.203	0.185
120.000	3.100	3.140	2.556	2.932	1056.577	58.640	6.037	366.262	31.210	614.498	608.990	1.417	0.348

enzyme release for speed experiments at 20 volume percent solids

speed in rpm	115	150	200	250	300	350	772
time in minutes	enzyme release, E, micromole/min/g cell (units/g cell)						
0.000	0.000	0.000	0.000	0.000	0.000	0.000	0.000
1.000	5.450	5.473	6.676	10.541	4.486	7.264	37.795
2.000	8.560	9.284	8.277	13.207	9.426	9.787	82.542
4.000	15.440	13.297	9.730	26.790	23.368	20.208	180.831
6.000	17.647	17.149	14.174	40.805	29.085	30.436	240.861
8.000	16.947	23.530	19.220	50.626	38.936	43.599	340.640
10.000	25.679	24.924	36.108	66.638	55.138	56.575	493.948
60.000	49.689	100.586	325.370	348.965	334.431	470.264	1585.836
120.000	79.157	189.217	568.930	608.990	704.907	700.864	2070.000

enzyme release for solids loading experiments at 772 rpm

solids loading volume percent	5	10	20
time in minutes	enzyme release, E, micromoles/min/g cell (units/g cell)		
0.000	0.000	0.000	0.000
1.000	3.284	3.710	37.795
2.000	4.364	12.397	82.542
4.000	8.097	22.754	180.861
6.000	14.934	46.962	240.861
8.000	24.547	57.139	340.640
10.000	43.008	95.833	493.948
60.000	301.091	819.089	1585.836
120.000	410.000	1122.354	2070.021

enzyme release from french press experiment

number of passes in french press	E units/g cell
0	0.000
1	1405.04
2	1511.674
3	1563.199
4	1568.229

variation between readings within an enzyme assay standard curve

invertase concentration units/ml	absorbance at 620 nm			average absorbance, a	standard deviation, s	variation in percent s/x *100
0	0.042	0.048	0.046	0.045	0.002	5.500
1	0.465	0.498	0.496	0.486	0.019	3.810
2	0.938	0.928	0.973	0.946	0.019	2.040
3	0.127	0.131	0.136	0.131	0.004	2.810
4	0.190	0.189	0.170	0.183	0.009	5.030
5	0.230	0.237	0.245	0.237	0.006	2.590
					average variation	3.630

variation between standard enzyme assay curves on different days over 5 months

number of tests	starting enzyme conc. units/ml	average value measured, e units/ml	standard deviation, s	variation in percent s/e *100
6	1.000	1.201	0.128	10.660
6	2.000	2.359	0.218	9.240
6	3.000	3.190	0.352	11.040
6	4.000	4.182	0.708	16.930
6	5.000	5.281	0.901	17.060
			average variation	12.990

APPENDIX 5

The data obtained from the *T. ferrooxidans* experiments are tabulated in this appendix.

silica loading at 772 rpm in rig

solids loading volume percent	control (not agitated)	5.000	10.000	20.000
time in hours	ratio of Fe3+ to Fe2+, EH im mV			
0.000	483.000	480.000	493.000	468.000
16.000	489.000	482.000	496.000	469.000
21.000	493.000	484.000	496.000	468.000
37.000	490.000	482.000	495.000	474.000
39.000	489.000	480.000	486.000	476.000
40.000	488.000	473.000	482.000	476.000
44.000	505.000	486.000	493.000	487.000
46.000	510.000	483.000	492.000	490.000
65.000	704.000	486.000	496.000	503.000
68.000	716.000	502.000	496.000	498.000
90.000	716.000	510.000	540.000	499.000
112.000	717.000	719.000	720.000	502.000

silica particle size in rig

geometric mean particle size in microns	control (not agitated)	53.000	116.000	165.000	212.000
time in hours	ratio of Fe3+ to Fe2+, EH im mV				
0.000	485.000	487.000	456.000	473.000	481.000
3.000	488.000	486.000	480.000	479.000	490.000
8.000	483.000	480.000	482.000	480.000	492.000
24.000	489.000	482.000	484.000	482.000	492.000
29.000	493.000	484.000	487.000	487.000	493.000
45.000	490.000	482.000	485.000	487.000	496.000
47.000	489.000	480.000	487.000	485.000	499.000
48.000	488.000	473.000	485.000	487.000	502.000
52.000	505.000	486.000	479.000	509.000	502.000
54.000	510.000	483.000	489.000	512.000	512.000
73.000	704.000	486.000	495.000	519.000	520.000
74.000	716.000	502.000	506.000	519.000	545.000
98.000	718.000	510.000	501.000	512.000	710.000
120.000	717.000	719.000	710.000	725.000	725.000

pyrite solids loading data in rig

solids loading volume percent	control (not agitated)	5.000	10.000	20.000
time in hours	ratio of Fe3+ to Fe2+, EH im mV			
0.000	501.000	506.000	502.000	495.000
3.000	516.000	511.000	504.000	503.000
20.000	693.000	512.000	517.000	502.000
23.000	694.000	511.000	522.000	501.000
42.000	696.000	636.000	647.000	536.000
45.000	700.000	708.000	683.000	540.000
50.000	717.000	717.000	688.000	566.000
67.000	720.000	716.000	719.000	705.000
73.000	720.000	716.000		

pyrite particle size in rig

geometric mean particle size in microns	control (not agitated)	12.000	53.000	116.000
time in hours	ratio of Fe3+ to Fe2+, EH im mV			
0.000	541.000	493.000	481.000	495.000
1.000	558.000	494.000	490.000	493.000
19.000	707.000	495.000	494.000	491.000
26.000	716.000	499.000	492.000	491.000
40.000	717.000	530.000	536.000	530.000
70.000	720.000	691.000	705.000	689.000
91.000	715.000	728.000		716.000
115.000	720.000	719.000		722.000

speed data at 20 volume percent pyrite

impeller speed im rpm (m/sec)	control (not agitated)	400.000 (1.1)	772.000 (2.2)	1090.000 (3.1)
time in hours	ratio of Fe3+ to Fe2+, EH im mV			
0.000	495.000	501.000	481.000	484.000
17.000	697.000	505.000	494.000	480.000
21.000	709.000	506.000	492.000	482.000
25.000	709.000	509.000	494.000	483.000
41.000	714.000	509.000	536.000	493.000
48.000	720.000	574.000	568.000	505.000
66.000	713.000	720.000	705.000	683.000
72.000	709.000	720.000		676.000
90.000	710.000	717.000		681.000

low sulphur pyrite solids loading at 350 rpm in four liter tanks

solids loading mass/volume percent	0.000	10.000	20.000	30.000
time in days	ratio of Fe3+ to Fe2+, EH im mV			
0.000	413.000	420.000	419.000	419.000
1.000	413.000	424.000	419.000	419.000
2.000	440.000	449.000	421.000	416.000
3.000	619.000	604.000	437.000	417.000
4.000	619.000	618.000	437.000	420.000
5.000	616.000	608.000	422.000	398.000
6.000	608.000	600.000	442.000	405.000
7.000	614.000	607.000	447.000	404.000
8.000	614.000	608.000	448.000	403.000
9.000	615.000	609.000	450.000	404.000
10.000	614.000	610.000	453.000	403.000
11.000	614.000	612.000	456.000	403.000
12.000	612.000	612.000	456.000	402.000
13.000	612.000	611.000	460.000	403.000
14.000	613.000	613.000	460.000	402.000
15.000	611.000	612.000	458.000	400.000
16.000	611.000	612.000	460.000	400.000

dissolved oxygen data taken on day 4 for loading experiments

solids loading mass/volume %	10.000	20.000	30.000
	dissolved oxygen concentration, mg O2/l		
time in seconds			
10.000	8.150	8.150	8.150
60.000	8.100	8.110	8.100
120.000	7.890	8.100	8.090
180.000	7.710	8.080	8.100
250.000	7.520	8.100	8.110
300.000	7.390	8.080	8.110
324.000	7.340	8.090	8.090
341.000	7.370	8.210	8.170
351.000	7.540	8.250	8.200
370.000	7.800	8.300	8.230
380.000	7.880	8.310	8.230
400.000	8.020	8.330	8.230
420.000	8.110	8.370	8.240

speed data in four liter stirred tanks

impeller speed in rpm (m/sec)	350.000 (1.4)	630.000 (2.6)	350.000 (1.4)	630.000 (2.6)
impeller type	radial (Rushton)	radial (Rushton)	axial	axial
time in days	ratio of Fe3+ to Fe2+, EH im mV			
1.000	386.000	383.000	382.000	382.000
2.000	389.000	379.000	382.000	380.000
3.000	390.000	370.000	383.000	379.000
4.000	395.000	367.000	384.000	375.000
5.000	407.000	361.000	596.000	377.000
6.000	446.000	360.000	541.000	377.000
7.000	534.000	364.000	617.000	376.000
8.000	554.000	363.000	601.000	377.000
9.000	560.000	364.000	600.000	376.000
10.000	570.000	364.000	599.000	375.000
11.000	576.000	364.000	596.000	374.000
12.000	621.000	375.000	615.000	395.000
13.000	610.000	378.000	631.000	403.000
14.000	601.000	378.000	610.000	400.000
15.000	597.000	376.000	593.000	400.000
16.000	600.000	376.000	585.000	420.000
17.000	615.000	375.000	581.000	440.000
18.000	620.000	372.000	552.000	453.000
19.000	620.000	377.000	581.000	466.000
20.000	606.000	360.000	607.000	461.000

APPENDIX 6

This appendix includes an example table illustrating the calculation of power consumption and power numbers from the measured torques. The power consumptions obtained for each set of experiments is included. Figures illustrating the power numbers calculated from the measurement of Newtonian fluids with the torque system are included. These Newtonian fluids were used to check the validity of using the torque measurement system to calculate the power consumption.

An example of calculation of power and power number from torque measurement of a Newtonian fluid of known viscosity:
torque is measured by converting the mass lifted from a balance, due to the liquid torque, to a force

60 % sucrose
density = 1283.98 kg/m3
viscosity = .05847 Pa s

impeller speed in rpm	impeller speed, N in rps	mass lifted from balance in kg	force =mass*g(9.81m/sec2) in N	torque, M =force*distance from fulcrum, in Nm	power, P =2*pi*N*M in W	power number =P/(dens*N3*D5)	reynolds number =dens*D2*N/visc
0.000	0.000	0.000	0.000	0.000	0.000		
129.600	2.160	0.001	0.011	0.001	0.007	1.183	138.314
252.900	4.215	0.014	0.132	0.006	0.168	3.813	269.905
430.500	7.175	0.040	0.396	0.019	0.857	3.933	459.446
521.100	8.685	0.059	0.581	0.028	1.521	3.939	556.138
627.500	10.458	0.092	0.905	0.043	2.856	4.235	669.692
721.300	12.022	0.127	1.244	0.060	4.510	4.403	789.799
836.800	13.947	0.168	1.645	0.079	6.920	4.327	893.065

power data

speed rpm	power in W	solids volume fraction	power in W	density of particles kg/m3	power in W	biomass concentration g/dm3	power in W
200.00	0.04	0.05	3.85	1600.00	3.69	20.00	5.24
250.00	0.16	0.10	4.05	2700.00	4.86	55.00	4.41
300.00	0.22	0.20	4.46	4500.00	6.77	102.00	6.00
360.00	0.58	0.30	5.47			130.00	5.44
540.00	0.96	0.40	6.48				
772.00	4.41						
1090.00	5.86						

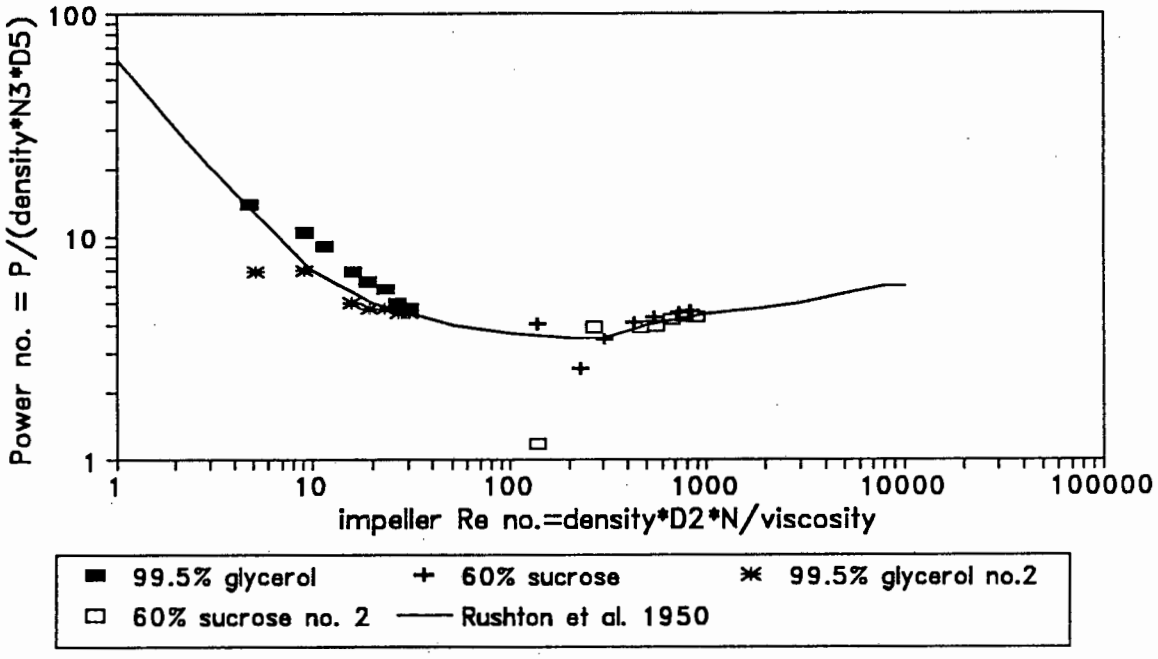

Figure A3 The power number as a function of impeller Reynolds' number for Newtonian fluids of high viscosity

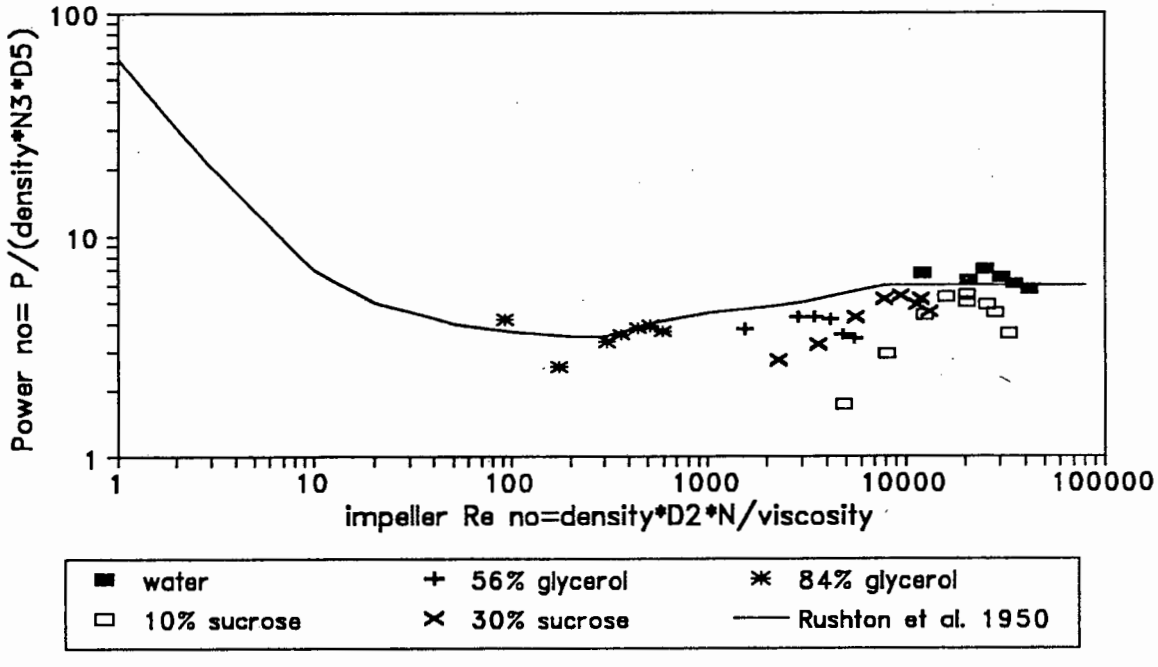

Figure A4 The power number as a function of the impeller Reynolds' number for Newtonian fluids of low viscosity

APPENDIX 7

This appendix includes the size analyses tables obtained from Malvern analyses of the size fractions of silica, pyrite and chromite particles used. Figures A5 and A6 illustrate the size distributions of the silica particles.

size analyses of silica, pyrite and chromite

SILICA

Malvern analyser
screen fraction: 25-250 microns
geometric mean = 114 micron

upper size microns	mass % in range	upper size microns	mass % in range	upper size microns	mass % in range	upper size microns	mass % in range	upper size microns	mass % in range	upper size microns	mass % in range	
564.0	0.4	254.0	1.7	114.0	5.1	51.3	1.2	23.1	0.1	10.4	0.0	D90
524.0	0.4	236.0	2.7	106.0	4.6	47.7	0.6	21.4	0.1	9.6	0.0	222.12 micron
488.0	0.4	219.0	3.6	98.6	4.2	44.4	0.5	19.9	0.0	9.0	0.0	
454.0	0.4	204.0	4.3	91.7	3.8	41.2	0.4	18.5	0.0	8.3	0.0	D10
422.0	0.5	190.0	4.9	85.3	3.5	38.4	0.4	17.2	0.0	7.8	0.1	58.81 micron
392.0	0.5	176.0	5.4	79.3	3.2	35.7	0.4	16.0	0.0	7.2	0.1	
365.0	0.5	164.0	5.7	73.8	2.9	33.2	0.4	14.9	0.0	6.7	0.1	D50
339.0	0.6	153.0	5.9	68.6	2.6	30.8	0.3	13.9	0.0	6.2	0.1	125.9 micron
315.0	0.5	142.0	5.9	63.8	2.3	28.7	0.3	12.9	0.0	5.8	0.1	
293.0	0.7	132.0	5.8	59.3	2.0	26.7	0.2	12.0	0.0			
273.0	1.1	123.0	5.5	55.2	1.6	24.8	0.2	11.2	0.0			

Malvern analyser
screen fraction:45-250 micron
geometric mean = 161 micron

upper size microns	mass % in range	upper size microns	mass % in range	upper size microns	mass % in range	upper size microns	mass % in range	upper size microns	mass % in range	upper size microns	mass % in range	
564.0	0.3	254.0	4.4	114.0	1.1	51.3	0.4	23.1	0.0	10.4	0.0	D90
524.0	0.3	236.0	7.0	106.0	0.6	47.7	0.1	21.4	0.0	9.6	0.0	246.72 micron
488.0	0.4	219.0	9.0	98.6	0.3	44.4	0.0	19.9	0.0	9.0	0.0	
454.0	0.4	204.0	10.2	91.7	0.1	41.2	0.0	18.5	0.0	8.3	0.0	D10
422.0	0.5	190.0	10.7	85.3	0.0	38.4	0.0	17.2	0.0	7.8	0.0	125.67 micron
392.0	0.6	176.0	10.6	79.3	0.0	35.7	0.0	16.0	0.0	7.2	0.0	
365.0	0.7	164.0	9.9	73.8	0.1	33.2	0.0	14.9	0.0	6.7	0.0	D50
339.0	0.8	153.0	8.8	68.6	0.3	30.8	0.0	13.9	0.0	6.2	0.0	176.24 micron
315.0	0.9	142.0	7.2	63.8	0.6	28.7	0.0	12.9	0.0	5.8	0.0	
293.0	1.2	132.0	5.2	59.3	0.7	26.7	0.0	12.0	0.0			
273.0	2.3	123.0	3.0	55.2	0.8	24.8	0.0	11.2	0.0			

Malvern analyser
screen fraction: 180-250 micron
geometric mean = 256 micron

upper size microns	mass % in range	upper size microns	mass % in range	upper size microns	mass % in range	upper size microns	mass % in range	upper size microns	mass % in range	upper size microns	mass % in range	
564.0	0.7	254.0	10.8	114.0	0.4	51.3	0.0	23.1	0.0	10.4	0.0	D90
524.0	0.8	236.0	11.0	106.0	0.6	47.7	0.0	21.4	0.0	9.6	0.0	362.52 micron
488.0	1.2	219.0	10.7	98.6	0.7	44.4	0.0	19.9	0.0	9.0	0.0	
454.0	1.8	204.0	9.8	91.7	0.7	41.2	0.0	18.5	0.0	8.3	0.0	D10
422.0	2.3	190.0	8.8	85.3	0.6	38.4	0.0	17.2	0.0	7.8	0.0	180.48 micron
392.0	3.1	176.0	2.3	79.3	0.5	35.7	0.0	16.0	0.0	7.2	0.0	
365.0	4.0	164.0	1.2	73.8	0.4	33.2	0.0	14.9	0.0	6.7	0.0	D50
339.0	5.2	153.0	0.2	68.6	0.2	30.8	0.0	13.9	0.0	6.2	0.0	241.15 micron
315.0	6.6	142.0	0.0	63.8	0.0	28.7	0.0	12.9	0.0	5.8	0.0	
293.0	7.8	132.0	0.0	59.3	0.0	26.7	0.0	12.0	0.0			
273.0	9.3	123.0	0.0	55.2	0.0	24.8	0.0	11.2	0.0			

screen fraction: 250-850 micron
geometric mean = 304.4 micron

size microns	cumulative % below size	size microns	cumulative % below size	size microns	cumulative % below size	
1750.00	100.00	250.00	31.98	37.00	0.06	D90
1470.00	100.00	210.00	17.17	31.00	0.06	500.9 micron
1230.00	100.00	180.00	8.61	26.00	0.05	
1030.00	100.00	150.00	3.37	22.00	0.03	D10
870.00	99.29	125.00	1.36	18.00	0.02	184.88 micron
730.00	97.45	105.00	0.72	15.00	0.01	
610.00	94.92	90.00	0.46	13.00	0.00	D50
510.00	90.86	75.00	0.26	11.00	0.00	296.8 micron
430.00	83.33	60.00	0.12	9.00	0.00	
360.00	69.87	50.00	0.08			
300.00	51.23	43.00	0.07			

laser diffraction anlyser
screened fraction: 500-850
geometric mean - 703 micron

size microns	cumulative % below size	size microns	cumulative % below size	size microns	cumulative % below size	
1750.00	100.00	250.00	0.00	37.00	0.00	D90
1470.00	100.00	210.00	0.00	31.00	0.00	973.88 micron
1230.00	100.00	180.00	0.00	26.00	0.00	
1030.00	95.65	150.00	0.00	22.00	0.00	D10
870.00	79.55	125.00	0.00	18.00	0.00	508.18 micron
730.00	54.33	105.00	0.00	15.00	0.00	
610.00	28.39	90.00	0.00	13.00	0.00	D50
510.00	10.19	75.00	0.00	11.00	0.00	709.98 micron
430.00	1.99	60.00	0.00	9.00	0.00	
360.00	0.00	50.00	0.00			
300.00	0.00	43.00	0.00			

laser diffraction analyser
screened fraction: 500-1000 micron
geometric mean = 735 micron

size microns	cumulative % below size	size microns	cumulative % below size	size microns	cumulative % below size	
1750.00	100.00	250.00	0.00	37.00	0.00	D90
1470.00	100.00	210.00	0.00	31.00	0.00	1026.79 micron
1230.00	100.00	180.00	0.00	26.00	0.00	
1030.00	90.38	150.00	0.00	22.00	0.00	D10
870.00	71.23	125.00	0.00	18.00	0.00	526.45 micron
730.00	45.97	105.00	0.00	15.00	0.00	
610.00	22.60	90.00	0.00	13.00	0.00	D50
510.00	7.52	75.00	0.00	11.00	0.00	752.35 micron
430.00	1.28	60.00	0.00	9.00	0.00	
360.00	0.00	50.00	0.00			
300.00	0.00	43.00	0.00			

Malvern analyser
screened size: 500-1800
geometric mean size = 1245.6 micron

upper size microns	mass % in range	upper size microns	mass % in range	upper size microns	mass % in range	
1880.0	22.6	370.0	0.1	73.0	0.0	D90
1622.0	21.3	320.0	0.2	63.0	0.0	1761.65 micron
1400.0	19.1	275.0	0.2	54.3	0.0	
1207.0	15.4	238.0	0.1	46.8	0.0	D10
1042.0	10.7	205.0	0.0	40.5	0.0	881.46 micron
898.0	5.6	177.0	0.0	34.8	0.0	
775.0	3.1	153.0	0.0	30.2	0.0	D50
668.0	1.4	132.0	0.0	26.0	0.0	1338.45 micron
577.0	0.3	114.0	0.0	22.3	0.0	
498.0	0.0	98.2	0.0	19.3	0.0	
430.0	0.0	84.7	0.0			

laser diffraction analyser
screened fraction:250-1000
geometric mean = 722

size microns	cumulative % below size	size microns	cumulative % below size	size microns	cumulative % below size	
1750.00	100.00	250.00	1.73	37.00	0.00	D90
1470.00	100.00	210.00	0.87	31.00	0.00	1026.79 micron
1230.00	91.34	180.00	0.35	26.00	0.00	
1030.00	73.98	150.00	0.15	22.00	0.00	D10
870.00	51.14	125.00	0.09	18.00	0.00	510 micron
730.00	29.85	105.00	0.06	15.00	0.00	
610.00	15.87	90.00	0.04	13.00	0.00	D50
510.00	9.50	75.00	0.03	11.00	0.00	750 micron
430.00	7.00	60.00	0.00	9.00	0.00	
360.00	5.14	50.00	0.00			
300.00	3.21	43.00	0.00			

pyrite before sieving

upper size microns	mass % in range	upper size microns	mass % in range	upper size microns	mass % in range	upper size microns	mass % in range	upper size microns	mass % in range	upper size microns	mass % in range	
564	0.0	254.0	0.7	114.0	2.3	51.3	3.3	23.1	1.6	10.4	0.6	D90
524	0.0	236.0	0.8	106.0	2.5	47.7	2.0	21.4	1.4	9.6	0.6	151.75 micron
488	0.0	219.0	0.9	98.6	2.7	44.4	2.8	19.9	1.3	9.0	0.6	
454	0.1	204.0	1.1	91.7	2.9	41.2	2.7	18.5	1.2	8.3	0.6	D10
422	0.1	190.0	1.2	85.3	3.1	38.4	2.5	17.2	1.0	7.8	0.7	11.23 micron
392	0.2	176.0	1.4	79.3	3.3	35.7	2.4	16.0	1.0	7.2	0.8	
365	0.2	164.0	1.5	73.8	3.4	33.2	2.3	14.9	0.9	6.7	0.8	D50
339	0.3	153.0	1.7	68.6	3.6	30.8	2.2	13.9	0.8	6.2	0.8	53.76 micron
315	0.4	142.0	1.9	63.8	3.7	28.7	2.1	12.9	0.7	5.8	0.7	
293	0.5	132.0	2.0	59.3	3.7	26.7	2.0	12.0	0.7			
273	0.6	123.0	2.2	55.2	3.5	24.8	1.8	11.2	0.6			

screened fraction: <45 micron
geometric mean size = 12 micron

upper size microns	mass % in range	upper size microns	mass % in range	upper size microns	mass % in range	upper size microns	mass % in range	upper size microns	mass % in range	upper size microns	mass % in range	
118.0	0.5	53.3	4.3	24.0	2.8	10.8	1.2	4.8	0.5	2.2	0.1	D90
110.0	0.6	49.5	4.7	22.3	2.8	10.0	1.0	4.5	0.4	2.0	0.1	151.75 micron
102.0	0.7	46.1	4.9	20.7	2.7	9.3	0.9	4.2	0.4	1.9	0.1	
95.2	0.9	42.8	5.0	19.3	2.5	8.7	0.8	3.9	0.4	1.8	0.1	D10
88.6	1.1	39.8	4.8	17.9	2.3	8.1	0.7	3.6	0.3	1.6	0.1	11.23 micron
82.4	1.4	37.0	4.4	16.7	2.0	7.5	0.7	3.4	0.3	1.5	0.1	
76.6	1.8	34.4	4.0	15.5	1.9	7.0	0.6	3.1	0.3	1.4	0.1	D50
71.2	2.2	32.0	3.5	14.4	1.7	6.5	0.6	2.9	0.3	1.3	0.1	53.76 micron
66.2	2.7	29.8	3.1	13.4	1.6	6.0	0.8	2.7	0.2	1.2	0.1	
61.6	3.2	27.7	2.9	12.5	1.5	5.6	0.5	2.5	0.2			
57.3	3.8	25.8	2.8	11.6	1.3	5.2	0.5	2.3	0.2			

screened fraction: 45-75 micron
geometric mean size = 58 micron

upper size microns	mass % in range	upper size microns	mass % in range	upper size microns	mass % in range	upper size microns	mass % in range	upper size microns	mass % in range	upper size microns	mass % in range	
188.0	0.0	84.5	9.0	38.0	1.9	17.1	0.4	7.7	0.2	3.5	0.1	D90
175.0	0.0	78.6	9.7	35.4	1.6	15.9	0.3	7.2	0.1	3.2	0.0	95.31 micron
163.0	0.0	73.1	9.9	32.9	1.4	14.8	0.2	6.7	0.1	3.0	0.0	
151.0	0.0	68.0	9.5	30.6	1.2	13.7	0.2	6.2	0.1	2.8	0.0	D10
141.0	0.0	63.2	7.6	28.4	1.0	12.8	0.1	5.8	0.1	2.6	0.0	31.94 micron
131.0	0.0	58.8	4.8	26.4	0.8	11.9	0.1	5.4	0.1	2.4	0.0	
122.0	0.9	54.7	3.7	24.6	0.7	11.1	0.1	5.0	0.1	2.2	0.0	D50
113.0	2.7	50.8	2.9	22.9	0.6	10.3	0.1	4.6	0.1	2.1	0.0	68.3 micron
105.0	4.5	47.3	2.4	21.3	0.6	9.6	0.1	4.3	0.1	1.9	0.0	
97.8	6.2	44.0	2.2	19.8	0.6	8.9	0.2	4.0	0.1			
90.9	7.8	40.9	2.1	18.4	0.5	8.3	0.2	3.7	0.1			

screened fraction: 75-180 micron
geometric mean size = 116 micron

upper size microns	mass % in range	upper size microns	mass % in range	upper size microns	mass % in range	upper size microns	mass % in range	upper size microns	mass % in range	upper size microns	mass % in range	
564.0	0.1	254.0	0.5	114.0	7.0	51.3	1.2	23.1	0.3	10.4	0.1	D90
524.0	0.1	236.0	0.9	106.0	6.7	47.7	1.3	21.4	0.2	9.6	0.1	172.4 micron
488.0	0.1	219.0	1.4	98.6	5.9	44.4	1.3	19.9	0.2	9.0	0.1	
454.0	0.1	204.0	2.0	91.7	4.9	41.2	1.4	18.5	0.2	8.3	0.1	D10
422.0	0.1	190.0	2.7	85.3	4.1	38.4	1.4	17.2	0.3	7.8	0.1	37.31 micron
392.0	0.1	176.0	3.5	79.3	3.6	35.7	1.4	16.0	0.3	7.2	0.1	
365.0	0.1	164.0	4.4	73.8	3.3	33.2	1.2	14.9	0.3	6.7	0.2	D50
339.0	0.1	153.0	5.2	68.6	2.8	30.8	0.9	13.9	0.2	6.2	0.2	103.79 micron
315.0	0.2	142.0	5.9	63.8	2.2	28.7	0.6	12.9	0.2	5.8	0.1	
293.0	0.2	132.0	6.4	59.3	1.6	26.7	0.5	12.0	0.2			
273.0	0.3	123.0	6.7	55.2	1.3	24.8	0.3	11.2	0.1			

chromite
laser diffraction analyser
screened fraction: 500-850 micron
geometric mean = 349 micron

size microns	cumulative % below size	size microns	cumulative % below size	size microns	cumulative % below size	
1750.00	100.00	250.00	15.02	37.00	0.02	D90
1470.00	100.00	210.00	5.58	31.00	0.01	533.24 micron
1230.00	100.00	180.00	1.91	26.00	0.01	
1030.00	100.00	150.00	0.68	22.00	0.00	D10
870.00	100.00	125.00	0.47	18.00	0.00	228.72 micron
730.00	100.00	105.00	0.34	15.00	0.00	
610.00	96.98	90.00	0.20	13.00	0.00	D50
510.00	87.89	75.00	0.09	11.00	0.00	352.23 micron
430.00	72.92	60.00	0.04	9.00	0.00	
360.00	52.73	50.00	0.04			
300.00	31.65	43.00	0.03			

crushed silica, laser diffraction
screened fraction:500-850 micron
geometric mean = 366 micron

size microns	cumulative % below size	size microns	cumulative % below size	size microns	cumulative % below size	
1750.00	100.00	250.00	13.01	37.00	0.01	D90
1470.00	100.00	210.00	5.08	31.00	0.00	569.08 micron
1230.00	100.00	180.00	2.00	26.00	0.00	
1030.00	100.00	150.00	0.85	22.00	0.00	D10
870.00	100.00	125.00	0.54	18.00	0.00	234.82 micron
730.00	99.69	105.00	0.34	15.00	0.00	
610.00	94.65	90.00	0.20	13.00	0.00	D50
510.00	83.29	75.00	0.09	11.00	0.00	370.83 micron
430.00	66.94	60.00	0.04	9.00	0.00	
360.00	46.90	50.00	0.02			
300.00	27.49	43.00	0.02			

activated carbon, laser diffraction analyser
screened fraction: 500-850
geometric mean = 353.5 micron

size microns	cumulative % below size	size microns	cumulative % below size	size microns	cumulative % below size	
1750.00	100.00	250.00	14.13	37.00	0.01	D90
1470.00	100.00	210.00	5.22	31.00	0.01	541.02 micron
1230.00	100.00	180.00	1.82	26.00	0.00	
1030.00	100.00	150.00	0.68	22.00	0.00	D10
870.00	100.00	125.00	0.48	18.00	0.00	231.45 micron
730.00	100.00	105.00	0.33	15.00	0.00	
610.00	96.61	90.00	0.19	13.00	0.00	D50
510.00	87.03	75.00	0.07	11.00	0.00	356.76 micron
430.00	71.59	60.00	0.03	9.00	0.00	
360.00	51.13	50.00	0.02			
300.00	30.22	43.00	0.02			

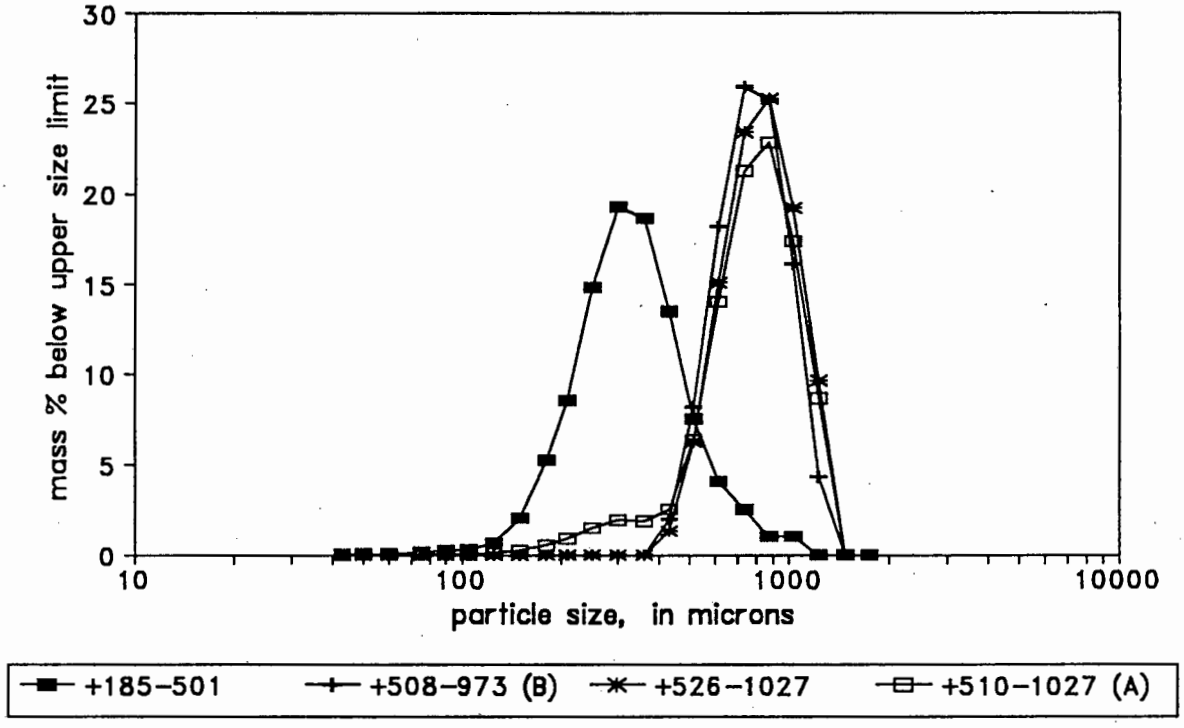

Figure A5 Size distributions of the following silica particle fractions: +185-501, +508-974, +526-1027, +510-1027.

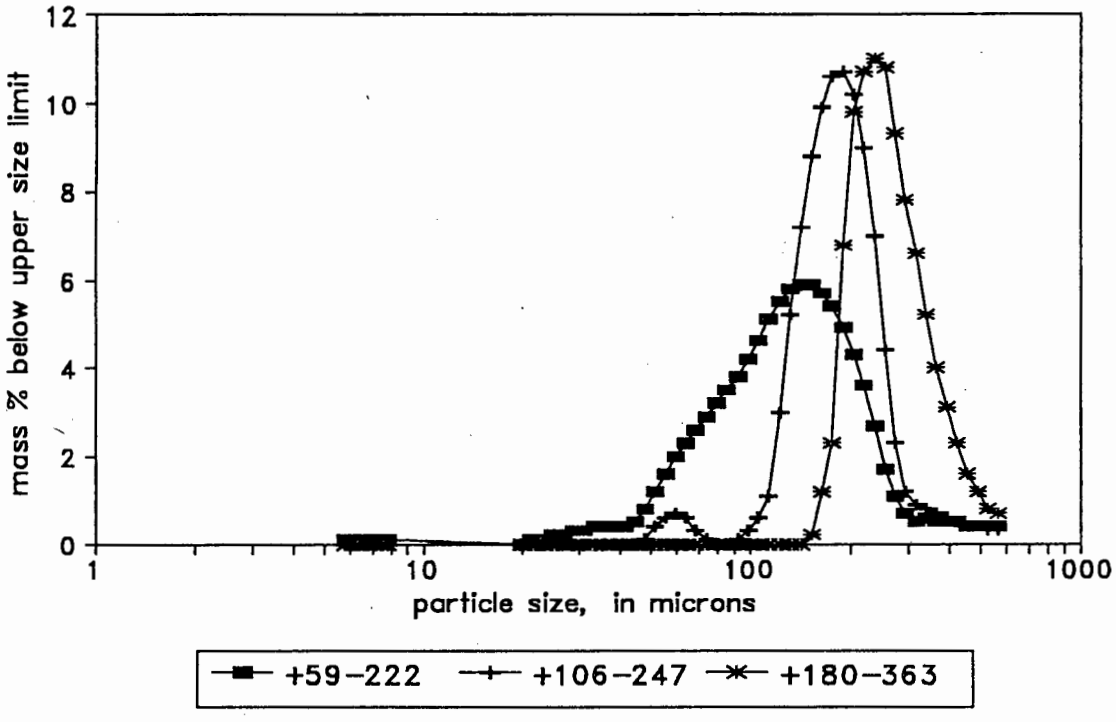

Figure A6 Size distributions of the following silica particle fractions: +59-222, +126-247, +180-363.

APPENDIX 8

This appendix includes a sample calculation of the Weissman and Efferding (1960) method of height of solids suspension as well as the table of calculations for different speeds.

1. Sample calculation

i) terminal settling velocity, v_{ts}

$$v_{ts} = g\, d_p^2\, (\rho_p - \rho)/(18\, \mu_l)$$
$$= 9.81\ (0.001245)^2\ (1700)/(18*0.001)$$
$$= 1.436\ m\ s^{-1} \qquad \text{Eqn. A5}$$

ii) pulp volume, Vm

$$V_m = f(Z') = (\pi\, T^2/4)\ (Z' + C)$$
$$= (\pi\ 0.108^2/4)\ (Z' + 0.033)$$
$$= 0.00916\ (Z' + 0.033) \qquad \text{Eqn. A6}$$

iii) volume fraction of solids, ϕ

$$\phi = S/(\rho_p\, V_m)$$
$$= (0.405/2700)/\ [0.00916\ (Z' + 0.033)]$$
$$= 0.01637\ (Z' + 0.033) \qquad \text{Eqn. A7}$$

iv) density of slurry, ρ_{sl}

$$\rho_{sl} = 0.01637\ (Z' + 0.033)\ 2700 + [1 - 0.01637\ (Z' + 0.033)]\ 1000 \qquad \text{Eqn. A8}$$

v) Substitution of equations A5, A6, A7 and A8 into Eqn. 5.5.7 results in a function of Z' only.

slurry visc = 0.02
liq visc = 0.0025
calculation of Z' for speed data

Z'	f(Z') for 772	f(Z') for 1090	f(Z') for 540	f(Z') for 380	f(Z') for 3	f(Z') for 250	f(Z') for 200
5E-06	-0.954	-1.019	-0.767	-0.486	-0.264	-0.197	0.116
0.005	-0.854	-0.919	-0.667	-0.385	-0.164	-0.097	0.217
0.010	-0.760	-0.826	-0.573	-0.292	-0.070	-0.003	0.310
0.020	-0.588	-0.653	-0.401	-0.119	0.103	0.169	0.483
0.040	-0.280	-0.345	-0.093	0.189	0.411	0.477	0.791
0.045	-0.208	-0.273	-0.021	0.261	0.482	0.549	0.863
0.050	-0.138	-0.203	0.049	0.331	0.552	0.619	0.933
0.060	-0.002	-0.067	0.185	0.467	0.689	0.755	1.069
0.065	0.065	-0.001	0.252	0.533	0.755	0.822	1.135
0.070	0.130	0.065	0.317	0.599	0.820	0.887	1.201
0.080	0.258	0.193	0.445	0.727	0.949	1.015	1.329